



Durham E-Theses

Analysts of meson-meson production

Ozmutlu, E. N.

How to cite:

Ozmutlu, E. N. (1978) *Analysts of meson-meson production*, Durham theses, Durham University.
Available at Durham E-Theses Online: <http://etheses.dur.ac.uk/8302/>

Use policy

The full-text may be used and/or reproduced, and given to third parties in any format or medium, without prior permission or charge, for personal research or study, educational, or not-for-profit purposes provided that:

- a full bibliographic reference is made to the original source
- a [link](#) is made to the metadata record in Durham E-Theses
- the full-text is not changed in any way

The full-text must not be sold in any format or medium without the formal permission of the copyright holders.

Please consult the [full Durham E-Theses policy](#) for further details.

ANALYSIS OF MESON-MESON PRODUCTION

THESIS SUBMITTED TO
THE UNIVERSITY OF DURHAM

BY

E. N. OZMUTLU, B.Sc., M.Sc.

FOR
THE DEGREE OF DOCTOR OF PHILOSOPHY

DEPARTMENT OF PHYSICS
UNIVERSITY OF DURHAM

SEPTEMBER 1978

The copyright of this thesis rests with the author.
No quotation from it should be published without
his prior written consent and information derived
from it should be acknowledged.



CONTENTS

	<u>Page</u>	
Abstract	i	
Acknowledgements	iii	
Chapter I	Introduction	1
	1.1 Survey of Meson Spectroscopy	6
	1.2 $J^{PC} = 0^{++}$ Mesons	14
	1.3 Summaries of the Other Chapters	17
Chapter II	Data and Formalism	19
	2.1 Survey of $\pi\pi$ and $K\bar{K}$ Production	19
	2.2 Observables and Amplitudes	23
	2.3 Properties and Formalism of One-Pion-Exchange Amplitudes	27
	2.4 Exchanges and Amplitudes	33
Chapter III	S^* , ϵ Problem	43
	3.1 Early History of the S^*	43
	3.2 Poles and the Dynamical Structure of the S^*	45
	3.3 $\pi\pi \rightarrow \pi\bar{\pi}(K\bar{K})$ Coupled Channel Analysis in the S^* Region	59

		<u>Page</u>
Chapter IV	Analysis of the $\pi^- p \rightarrow (K^- K^0) p$ Reaction	69
	4.1 Introduction	69
	4.2 Amplitude Analysis in the A_2 Mass Region	70
	4.3 Amplitude Analysis in the ρ Meson Region	79
	4.4 Amplitudes As a Function of $M_{K\bar{K}}$	86
	4.5 Conclusions	90
Chapter V	Analysis of $\pi^- p \rightarrow (K^+ K^-) n$ $\pi^+ n \rightarrow (K^+ K^-) p$ Reactions	94
	5.1 Introduction	94
	5.2 D Wave Studies	97
	5.3 Threshold Region Analysis	111
	5.4 $\pi\pi \rightarrow K\bar{K}$ Phase Shift Analysis	120
	5.5 Conclusions	130
Chapter VI	Classification of $J^{PC} = 0^{++}$ Mesons	133
Chapter VII	Conclusions	140
Appendix I	Moments in Terms of Density Matrix Elements	145
Appendix II	S-Matrix, State Normalization, Phase Space, Cross Section, Partial Wave Expansion	149
Appendix III	The π Coupling at the Nucleon Vertex	152
Appendix IV	Phase Space Calculation	155
Appendix V	$\pi\pi \rightarrow \pi\pi (K\bar{K})$ Scattering	158

		<u>Page</u>
Appendix VI	Density Matrix Elements In Terms of Di-Meson Production Amplitudes	161
Appendix VII	Classification of Phase Shift Solutions	162
Appendix VIII	The Effect of the K^+, K^- and K^0, \bar{K}^0 Mass Difference	164
References		168

ABSTRACT

We study properties of mesons, which decay into the $(\pi\pi)$ and $(K\bar{K})$ channels, using high-statistics (meson-meson) production data for reactions of the type

$$\pi N \longrightarrow (\pi\pi) N$$

$$\pi N \longrightarrow (K\bar{K}) N$$

with a primary interest in the $J^{PC} = 0^{++}$ mesons.

We first investigate the properties of the S^* and find that it is a normal Breit-Wigner resonance. We also present evidence for a broad elastic $\pi\pi$ resonance, the ϵ meson. We propose forms of parametrization of the coupled channel $(\pi\pi, K\bar{K})$ $I = 0$ S wave to investigate the nature of the S^* and ϵ . We see that it is not possible to explain these mesons simply as $(q\bar{q})$ states and that forces in the $(qq\bar{q}\bar{q})$ sector are also important.

We analyse recent (K^-K^0) production data and find evidence for a new $I = 1, 0^{++}$ meson, the $\delta'(1300)$. This (K^-K^0) analysis also gives evidence for the spin 4, $A_2(1900)$ state, illuminates the A_2 and g production mechanisms and determines the $g \longrightarrow K\bar{K}$ branching ratio. We discuss the identification of the $\delta(970)$ and $\delta'(1300)$ and find the most natural answer is that, besides the conventional $(q\bar{q})$ nonet, there is a low lying $(qq\bar{q}\bar{q})$ nonet of 0^{++} mesons.



Using high-statistics (K^+K^-) production data, together with the results of the (K^-K^0) analysis, we are able to investigate $I = 0$ ($K\bar{K}$) states. We first study the resonant D wave (f, f', A_2). Then using $I = 0$ D wave as a reference wave we carry out a $\pi\pi \rightarrow K\bar{K}$ phase shift analysis.

ACKNOWLEDGEMENTS

I am very grateful to Dr. Alan D. Martin for his invaluable support in every stage of this work. I also thank Prof. Euan J. Squires and Drs. Penny Estabrooks, Tokuzo Shimada and Mike Pennington for helpful discussions. The financial support of the Government of the Republic of Turkey is also gratefully acknowledged.

CHAPTER 1

Introduction

Today we know a great deal about the micro-world of elementary particles. The interactions among these particles can be classified into four groups; strong, electromagnetic, weak and gravitational forces. Our present knowledge is not enough to understand the nature fully but a huge amount of information has been accumulated during the past few years. This information can be used to obtain a better understanding of nature. The existence of four different forces might indicate that their underlying dynamics had different origins. On the other hand all these interactions could be different manifestations of a single dynamical form. On this point, a great deal of progress has been made towards the unification of electromagnetic and weak interactions and possibly also strong interactions, based on Gauge Theories.

A big problem in this type of work is the gaps in our knowledge of these interactions. When we try to unify these forces, we have to look at limited experimental information, and usually at the end we have to predict some results rather than obtain confirmation from well-

known observations. So the obvious job of getting more information about these interactions individually must be done both experimentally and theoretically. In this thesis we study some of the problems concerning strong interactions using recently available high statistics di-meson production data.

The main feature of strong interactions is the conservation of some quantum numbers. Hadrons, the particles which can interact strongly, can be labelled by these conserved quantities. These quantum numbers are the isospin, baryon number, and strangeness. The charge independence of strong interactions has led us to the idea of isospin. In a world that only strong interactions exist, it is not possible to distinguish proton from neutron or positive charged pion from π^0 or π^- . This is best explained by the existence of a symmetry in the theory. We can think of proton and neutron as two different states of a single particle, called nucleon. Similarly π^+ , π^0 , π^- are the three different states of a pion. There is a very close analogue of the angular momentum; one can assign a quantum number to the nucleon $I = \frac{1}{2}$ and represent proton by $I_3 = +\frac{1}{2}$ and neutron by $I_3 = -\frac{1}{2}$. We call this quantity isospin. We can assign isospin to all observed hadrons. In this scheme charge independence of strong interactions means an invariance under rotations in the "isospin space". This invariance implies the isospin conservation under strong interactions. Baryon number is assigned $B = \pm 1$ for spin-

half hadrons (baryons) and $B = 0$ for integer-spin hadrons (mesons). Sum of baryon numbers of an initial and a final state, related by strong interactions, are equal. The properties of the K mesons and hyperons have implied the existence of another conserved quantum number. These "strange" particles are produced in pairs by strong interactions and decay into hadrons by weak interactions. This indicates that strange particles have an extra property which is conserved by strong interactions and violated by weak. So we assign $S = +1$ for the kaons and Λ^0, Σ and $S = 0$ for proton, neutron and pions. If we define the hyper-charge as

$$Y = B + S,$$

we observe some regularities among the isospin and hyper-charge of the hadrons.

Having introduced the isospin, we have already proposed a classification scheme for hadrons. We have allocated particles on the different representations of the group, $SU(2)$. Gell-Mann and Nishijima⁽¹⁾ have classified hadrons in terms of a larger group $SU(3)$ combining isospin and hypercharge. Discovery of Ψ and Υ particles in recent years has led us to extend $SU(3)$ to $SU(n)$ by introducing new additive quantum numbers e.g. charm, beauty ... The smallest non-trivial representation of $SU(n)$ has (n) dimension, and all the other representations of $SU(n)$ can be constructed as products of this smallest representation and its conjugate one. This observation has been interpreted as if this smallest multiplet has contained (n)

elementary objects, from which all the hadrons could be constructed. These basic building blocks are called quarks. The number of different "flavour" of quarks is at least four and probably more.

The quark model can classify baryons and mesons successfully. But the symmetry is broken by the mass splitting observed within multiplets. The deep dynamical basis of the model is still unknown. Quarks have not been observed as free particles yet. This suggests that the quarks are confined inside hadrons by some yet unknown mechanisms. In the recent years attention has focussed on developing a quark dynamics consistent with the absence of free quarks. The main problem of this theory is the explanation of the confining forces. In the past years, existence of quarks was in doubt, because of the lack of free quarks. However, the deep inelastic electron-proton scattering has shown that proton is not a single, solid object but it has a certain substructure. Detailed analysis of the data is consistent with the existence of quarks "inside" the hadrons.

The discovery of Ψ and χ family and the charmed mesons in the last three years, has given more evidence to support the quark model. All the observed properties of these particles can be explained by introducing the new "charmed quark". The theoretical basis is provided by Quantum-Chromodynamics, a non-Abelian gauge theory of strong interactions in which flavourful and colourful quarks interact via exchange of an octet of colourful, massless vector

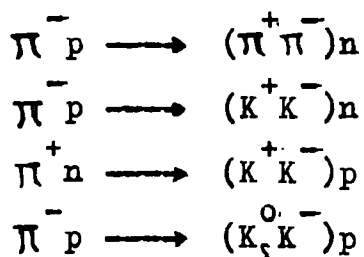
gluons⁽²⁾. The theory is

$$\left[\begin{array}{c} \text{SU}(3) \\ \text{colour} \end{array} \right] \otimes \left[\begin{array}{c} \text{SU}(n) \\ \text{flavour} \end{array} \right]$$

where $n = 4$ with u, d, s and c quarks. Only colour singlet states are supposed to exist in nature. Although the real world is "colourless", the colour degree of freedom manifests itself in various ways⁽³⁾. We can apply the ideas of QCD to the old hadrons as well as the new ones. But the small masses of the old hadrons and their many open channels make the spectroscopic calculations difficult.

The problems of performing experiments which can produce mesonic resonances have caused difficulties in studying the meson side of the scheme. However, the colliding beams of $e^+ - e^-$, $p\bar{p}$ annihilation and the high statistics meson production experiments, which have become available recently, provide a rich source of information about mesons. Since the symmetry rules can lead us to understand the dynamical structure of hadrons, it is very important to study the problems of particle classification. This type of work will be the main check of the $SU(4)$ and the other higher symmetries proposed for hadron dynamics.

In this thesis we study some of the mesons using the data for the reactions



We shall pay particular attention to mesons with quantum numbers $J^{PC} = 0^{++}$.

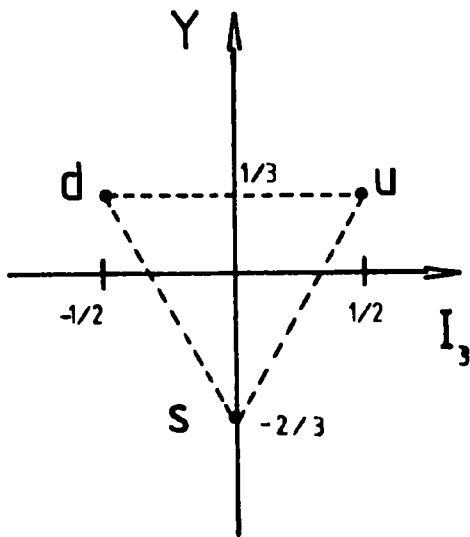
1.1 Survey of Meson Spectroscopy

The L-excitation quark model has provided a very economical description of the hadron spectroscopy^(4,5).

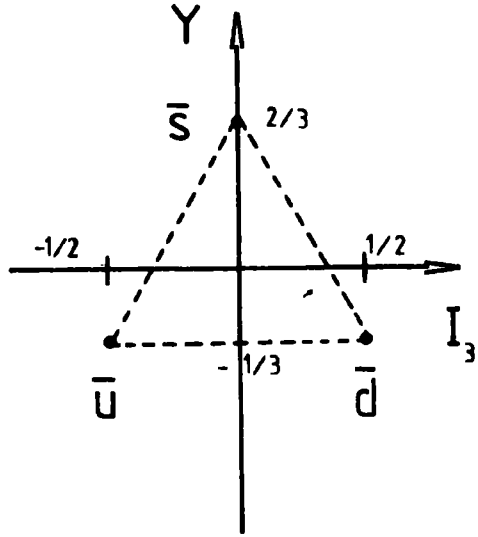
In the model, we assume existence of three different "flavours" of quarks, u, d, s, which are the main building blocks of the "conventional particles". Since we study the "old particles" in this thesis, we limit our discussion to three classical quarks for the sake of simplicity. We give the quantum numbers of the quarks in Table 1.1.

Type	I	I_3	S	B	Y	$Q=I_3+Y/2$
u(p)	1/2	1/2	0	1/3	1/3	2/3
d(n)	1/2	-1/2	0	1/3	1/3	-1/3
s(λ)	0	0	-1	1/3	-2/3	-1/3

Table 1.1: The quantum numbers of the classical quarks, where $Y = B + S$. We show both names of quarks, which are commonly used.



(Quarks)



(Antiquarks)

Figure 1.1: 3 and $\bar{3}$ representations of $SU(3)$. 3 contains quarks while $\bar{3}$ contains anti-quarks.

Quarks belong to the 3 representation of $SU(3)$ and anti-quarks belong to $\bar{3}$ (Fig. 1.1). Mesons are quark-anti-quark states and baryons are three quark states. Quarks have spin half and can undergo orbital excitations. If we take product of

$$\begin{aligned}
 3 \otimes \bar{3} &= 8 \oplus 1 \\
 3 \otimes 3 \otimes 3 &= 10 \oplus 8 \oplus 8 \oplus 1
 \end{aligned}
 \tag{1.1}$$

this agrees with the observation that mesons occur in 8 and 1 representations, but baryons in 10 , 8 and 1 . Including the spin ($SU(2)$) we are led to consider the non-relativistic orbital excitation quark model based on

$$SU(6) \otimes O(3)
 \tag{1.2}$$

where the rotation group $O(3)$ arises from orbital motion.

The parity of an orbital state of angular momentum L , is

$$P = (-)^{L+1} \quad \text{for mesons} \quad (1.3)$$

$$P = (-)^L \quad \text{for baryons} \quad (1.4)$$

and the total angular momentum is

$$\vec{J} = \vec{L} + \vec{S} \quad (1.5)$$

where \vec{S} is the total of the spin of quarks. $S = 0, 1$ for mesons and $1/2, 3/2$ for baryons. Quarks are fermions and so for a $q\bar{q}$ pair, the C-parity of the neutral, $Y = 0$ members should be

$$C = (-)^{L+S} \quad (1.6)$$

Using (1.3) and (1.6)

$$PC = (-)^{S+1} \quad (1.7)$$

If we define the natural and unnatural parity for mesons such

$$P = (-)^J \quad \text{Natural Parity} \quad (1.8)$$

$$P = (-)^{J+1} \quad \text{Unnatural Parity} \quad (1.9)$$

natural parity mesons must have $S = 1$, since $J = L \pm 1$. So their PC must be positive. Hence the states which have the quantum numbers

$$J^{PC} = 0^{+-}, 1^{+-}, 2^{+-}, 3^{+-} \dots \quad (1.10)$$

are not allowed for $q-\bar{q}$ pair. The only other mesonic state which is forbidden in the quark model has

$$J^{PC} = 0^{--}. \quad (1.11)$$

It would have to have $L = S$ because of its zero spin, but then by eg. (1.6) its C should be positive.

We show the predicted $SU(3)$ nonets together with the corresponding observed mesons in Table 1.2. Only the $J^{PC} = 0^{-+}, 1^{--}, 2^{++}$ nonets are completely filled with well-established mesons. For all the other nonets we have problems; either members of the nonets are missing or are not well-established, or their properties are not well known. The situation for the baryon spectrum is much better. This is not surprising since baryons are more directly accessible experimentally. For instance baryon resonances may be observed in formation experiments (see Figure 1.2) whereas the lack of mesonic targets prevents such experiments in the case of mesons.^{†)} Meson states are, in general, studied by production experiments (see for example, Figure 1.3). This type of experiment can suffer

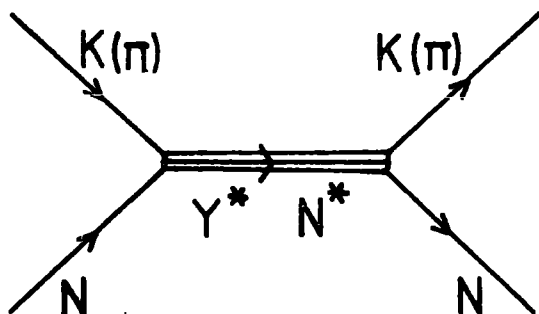


Figure 1.2

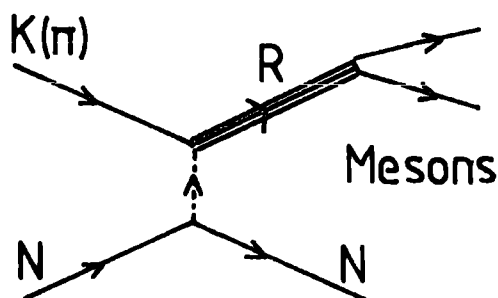


Figure 1.3

†)

$J^{PC} = 1^{--}$ meson states can be found directly in e^+e^- colliding beam experiments, and $p\bar{p}$ annihilation reactions can, in principle, be regarded as formation experiments.

L	S	J ^{PC}	SU(3) Nonet			
			I = 1/2	I = 1	I = 0	I = 0
0	0	0 ⁻⁺	K(495)	π(139)	η(550)	η'(960)
	1	1 ⁻⁻	K*(890)	ρ(770)	ω(780)	φ(1020)
1	0	1 ^{+ -}	Q _B (1355)?	B(1235)	?	?
	1	2 ⁺⁺	K*(1420)	A ₂ (1320)	ρ(1270)	ρ'(1510)
	1	1 ⁺⁺	Q _A (1340)?	A ₁ (1100)?	D(1285)	E?
	1	0 ⁺⁺	κ(1450)?	δ(970)	S*(980)	ε(1200)?
2	0	2 ⁻⁺	?	A ₃ (1640)?	?	?
	1	3 ⁻⁻	K*(1780)	ρ(1680)	ω(1675)	?
	1	2 ⁻⁻	?	Z?	?	?
	1	1 ⁻⁻	K*(1650)?	ρ'(1600)?	?	?
3	0	3 ^{+ -}	?	?	?	?
	1	4 ⁺⁺	K*(2100)?	A ₂ (1900)	h(2040)	?
	1	3 ⁺⁺	?	?	?	?
	1	2 ⁺⁺	?	?	?	?

Table 1.2: A possible assignment of meson states. We do not show the radial excitation states which would normally arise in any inter-quark potential model. For example the ρ'(1600) which are put in L = 2, S = 1 state, can also be allocated to a L = 0 radial excitation state.

from lack of statistics since the "meson cloud" around the nucleon is diffuse. Even when enough statistics are available, we have to overcome additional problems to perform partial wave analysis. We need a dynamical production model to remove the unwanted baryon. Since quantum number restrictions are stringent for meson systems, for observing unnatural parity meson resonances one needs at least three final state non-strange mesons. The analysis of such three meson states is complicated both theoretically and experimentally.

So far we have assumed that the mesons are quark-anti-quark states. In theory there is no reason why mesons cannot be $(qq\bar{q}\bar{q})$, $(qqq\bar{q}\bar{q})$... states. The recently developed models of hadron dynamics, based on QCD, have explored the possibility of such states. Moreover meson states can be constructed only with gluons without any quarks ^(6,7,8). For instance Jaffe and Johnson have predicted a much richer meson spectrum with small masses, using a coloured-quark-gluon model based on a semi-classical approximation to the M.I.T. bag model ^(6,7). In particular they have classified the observed $J^{PC} = 0^{++}$ mesons as $(qq\bar{q}\bar{q})$ states. They have claimed that there might be gluonic hadrons (usually called glueballs) with $J^{PC} = 0^{++}$, 2^{++} mass around 960 MeV, 0^{-+} , 1^{-+} , 2^{-+} mass about 1290 MeV, 0^{+-} , 1^{++} , 2^{+-} , 3^{++} with mass 1460 MeV, 0^{++} , 2^{++} mass 1590 MeV. These should be flavour and colour singlets. These glueballs would be relatively narrow since their coupling

to normal hadrons violates the OZI rule. If they exist, they might be a relatively important component in the decay of the new hadrons. The new mesons decay by annihilation into glue which could resonate before converting into classical quarks. These gluonic hadrons must obey the decay systematic of SU(3) flavour singlets. Robson has also predicted a rich spectrum of glueballs, suggesting a model in which glueballs can be constructed from building blocks (gluons), in analogy with the simple quark model⁽⁸⁾. He identified the $S^*(980)$ as a glueball.

Let us turn to the other alternative that mesons are multiquark states, such as constructed from two quarks and two anti-quarks ($qq\bar{q}\bar{q}$). According to Jaffe and Johnson's predictions, the mesons made up as ($qq\bar{q}\bar{q}$) states are expected to be very broad since a ($qq\bar{q}\bar{q}$) state could simply "fall apart" into two ($q\bar{q}$) mesons. Jaffe has claimed that the $J^{PC} = 0^{++}$ mesons (ϵ , S^* , δ , κ) are the ($qq\bar{q}\bar{q}$) states not the ($q\bar{q}$), $L = 1$, $S = 1$ states of the classical quark model⁽⁷⁾. It is difficult to interpret the known properties of 0^{++} mesons as the members of ($q\bar{q}$) $L = 1$, $S = 1$ nonet, but as we do not have enough information about these mesons it is hard to select one of these two alternative interpretations. This is a very crucial area of the meson spectroscopy, in particular equally possible existence of glueballs and ($q\bar{q}$), ($qq\bar{q}\bar{q}$) states prevents us to go further without having enough information about these mesons. However recently observed ($K\bar{K}$)S-wave enhancement at $M_{K\bar{K}} \sim 1.3$ GeV might provide a clue⁽⁹⁾. There is uncertainty about its

isospin. An Argonne group has claimed from K^+K^- production data that it has $I = 0$ ⁽¹⁰⁾, whereas a Notre-Dame group has assigned $I = 1$ from a study of $K_S^0K_S^0$ production data⁽⁹⁾. In this thesis we shall present strong evidence to show that there is a $I = 1$ ($K\bar{K}$) resonance with $M \approx 1.3$ GeV. Let us call it δ' . The existence of $\delta'(1300)$, in addition to the $I = 1$ $\delta(970)$, supports Jaffe's prediction of having two entire nonets of 0^{++} mesons, one of which contains $(qq\bar{q}\bar{q})$ mesons, while the other covers $(q\bar{q})$ mesons⁽⁷⁾. It will be very important to observe the other members of the second 0^{++} nonet.

Jaffe and Johnson have predicted the existence of other $(qq\bar{q}\bar{q})$ multiplets, with masses below 1.6 GeV. For example $J^{PC} = 0^{++}$ 1, 8, 27 SU(3) multiplets at 1116 MeV, 1^{++} 1, 8 at 1176 MeV, 1^{++} 8, 8, 10, $\bar{10}$ at 1223 MeV, 0^{++} 1, 8 at 1418 MeV, 1^{++} 1, 8, 27 at 1451 MeV. They have noted that large widths of these states have made it difficult to observe them. They also claimed existence of $(q\bar{q})$ states having quantum numbers which classical quark model has forbidden, namely the states in (1.10).

In contrast to the very rich spectrum of meson states predicted by such theoretical models, the experimental meson spectrum is very poor. It is important to obtain as much experimental information as possible about the meson spectrum, in particular about the problematical 0^{++} states. Here we use available high statistics spectrometer data to shed light on these problems.

1.2 $J^{PC} = 0^{++}$ Mesons

We list the known 0^{++} mesons in Table 1.3, showing their observed decay modes together with some of the processes in which we observe them. We put question marks after uncertain mass or width values.

Apart from the well-established $J^{PC} = 0^{-+}, 1^{--}, 2^{++}$ nonets, only the 0^{++} nonet has candidates for all its members. Since the quantum numbers of the 0^{++} mesons allow them to decay into two 0^{-+} meson states, many of their decay channels are experimentally accessible. They are

Meson	I^G	Mass (MeV)	Width (MeV)	Seen Decay Modes	Reactions
δ	1^-	970	50	$\pi^- \eta, K^- K^0$ $K^+ K^-$	$K^- p \rightarrow (\eta \pi^-) \Sigma^+$ $\pi^- p \rightarrow (K^+ K^-) n$
δ'	1^-	1300	220	$K^- K_S^0, K_S^0 K_S^0$ $K^+ K^-$	$\pi^- p \rightarrow (K^- K_S^0) p$ $\pi^- p \rightarrow (K^+ K^-) n$
κ	$1/2$	1450?	large?	$K \pi$	$K^\pm p \rightarrow (K^\pm \pi^+) n$ $K^\pm p \rightarrow (K \pi)^\pm p$
S^*	0^+	980?	90?	$\pi \pi, K^+ K^-$ $K_S^0 K_S^0$	$\pi^- p \rightarrow (\pi^+ \pi^-) n$ $\pi^- p \rightarrow (K^+ K^-) n$
ϵ	0^+	1200?	large?	$\pi^+ \pi^-$	$\pi^- p \rightarrow (\pi^+ \pi^-) n$

Table 1.3: The known 0^{++} mesons

interesting states to study for many reasons. They provide a useful testing ground for dynamical models. Also the decay of these S-wave states are suitable for studying

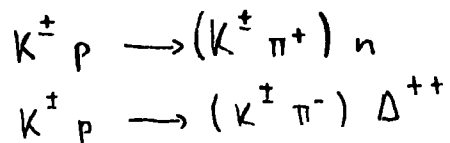
symmetry breaking effects without kinematical complications⁽¹¹⁾. They provide information on the spin-orbit splitting in the quark-antiquark interaction through comparison with the $J^{PC} = 2^{++}$, and 1^{++} states. A comparison of the decay rates of the three different nonets ($J^{PC} = 0^{++}, 1^{++}, 2^{++}$) with same quark-anti-quark relative orbital angular momentum is important for higher symmetry schemes⁽¹²⁾. We know that ω, ϕ and f, f' are ideally mixed, while η is mainly in octet and η' in singlet. When we have an established 0^{++} nonet, it will be very interesting to study its mixing properties and the extent to which its decays are governed by OZI rule. $I = 0, 0^{++}$ mesons, having vacuum quantum numbers, can be not the $(q\bar{q})$ states, but constructed by some peculiar dynamical effects, for instance they might be dilatons⁽⁵⁾. However, perhaps the most important reason to study the 0^{++} states is to clarify whether or not there exist low lying $(qq\bar{q}\bar{q})$ states and glueballs in addition to the conventional quark model, $(q\bar{q})$ states. The discovery of δ' , which we describe in previous section, has already opened this question up and made this subject a crucial area for further studies.

Although many decay channels of the 0^{++} mesons are experimentally accessible, in practice there are several problems. We generally observe these mesons as a result of phase-shift analyses. In these analyses, the $L = 0$ S-wave, being the lowest partial wave, is less constrained by the experimental observables than the higher $L = 1, 2, 3 \dots$ (P, D, F ...) waves. Moreover it is relatively suppressed

due to occurrence of $(2L + 1)$ factors in the partial wave decomposition of the cross section. With the present accuracy of experiments, it is not easy to determine such low partial wave contributions. The second challenge comes from the ambiguities inherent in phase-shift analyses. These ambiguities have nothing to do with experimental accuracy; even if we have infinitely accurate data, they will occur. More than one set of solutions can describe a given set of data and further information must be sought to select a unique solution. This means it is difficult to determine the S-wave reliably and any structure seen in a S-wave amplitude is more suspect than those for the leading partial waves.

Besides these general difficulties in determining an $L = 0$ amplitude, the 0^{++} mesons have their own problems. The $I = 1$ $\delta(970)$ is located just below the $K\bar{K}$ threshold and consequently it is not easy to determine its parameters. A similar problem occurs for $S^*(980)$. There is doubt about whether it is a resonance, or a threshold effect, namely a cusp. The situation is complicated by uncertainty in determining on which of the Riemann sheets the poles occur. In addition to this we do not observe the S^* as a peak in $\pi\pi$ S-wave but rather it is located on a broad elastic background, which has been attributed⁽¹¹⁾ to the $\mathcal{E}(1200)$ meson. Two overlapping $I = 0$ S-wave resonances (S^* , \mathcal{E}) in a two channels situation ($\pi\pi$, $K\bar{K}$) makes the problem of unambiguous identification particularly difficult.

For the $I = \frac{1}{2}$ $K(1450)$ we may look at the recent analysis of the SLAC data for the reactions



at 13 GeV/c⁽¹³⁾. They have found a structure in $(K\pi)$ S-wave at around 1.45 GeV, about 250 MeV wide, located on an elastic, slowly varying background. However none of the four solutions, that they have presented, show structure that we can unambiguously interpret as two overlapping resonances. There is definitely one resonance in $(K\pi)$ S-wave but its properties, and the nature of its background, is uncertain and we need more information to illuminate the $(K\pi)$ S-wave amplitude.

We shall study many of these problems using recently available high statistics di-meson production data. In some cases we shall emphasise the necessity of more experimental information.

1.3 Summaries of the Other Chapters

The rest of this thesis is planned as follows: we shall give a brief survey of the recent high-statistics di-meson production experiments in Chapter II. We shall also discuss the relations among observables and amplitudes, the Chew-Low formulae for one-pion-exchange (OPE) amplitudes, absorptive effects, the exchange mechanisms of the reactions which we analyse in this thesis. We study

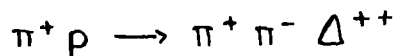
the properties of the S^* effect and its background (the ξ meson) in Chapter III. We discuss the effects of the various combinations of the S^* poles on the complex energy-squared plane and propose forms of parametrization of the coupled channel ($\pi\pi, K\bar{K}$) $I = 0, L = 0$ amplitude which allow for the presence of overlapping S^* and ξ resonances and permit a determination of their parameters. In particular we perform a coupled-channel analysis of the data for the reactions $\pi^-p \rightarrow (\pi^+n^-)n$ and $\pi^-p \rightarrow (K^+K^-)n$ to investigate the properties of the S^* and ξ . We shall present an analysis of the reaction $\pi^-p \rightarrow (K^-K^0)p$ in Chapter IV. We determine the amplitudes as functions of t in A_2 and g resonance regions and also as a function of the effective (K^-K^0) mass in the region $1.0 < M_{K^-K^0} < 2.0$ GeV. We shall study the production mechanisms and the properties of the mesons, which can decay into K^-K^0 final state. We analyse the data for the reactions $\pi^-p \rightarrow (K^+K^-)n$ and $\pi^+n \rightarrow (K^+K^-)p$ in Chapter V. Here we use the results of Chapter IV to eliminate the $I = 0, I = 1$ ambiguity. We study the $L = 2$ $K\bar{K}$ amplitudes of these reactions in detail. We calculate explicitly the effect of the mass difference of K^+, K^- and K^0, \bar{K}^0 and analyse the data with $M_{K\bar{K}} < 1.1$ GeV in terms of the S^* and δ mesons. Finally we perform an $\pi\pi \rightarrow K\bar{K}$ phase shift analysis in Chapter V. We discuss the possible classification schemes of the $J^{PC} = 0^{++}$ mesons in Chapter VI and summarise our conclusions in Chapter VII.

CHAPTER II

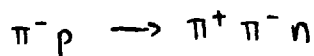
Data and Formalism

2.1 Survey of $\pi\pi$ and $K\bar{K}$ Production

The early experiments of di-meson production reactions had limited statistics. Development of spectrometers over the past few years has provided facilities to perform high-statistics di-meson production experiments. An example of such experiments has come from a Saclay group⁽¹⁴⁾. They have reported total 30000 events of $\pi^-\pi^0$ and $\pi^+\pi^-$ production in 1970. Three years later a Berkeley group has presented result of the 32100 events of



reaction⁽¹⁵⁾. In 1974 a CERN-Munich group completed a very high statistics study of reaction



(over 300000 events)⁽¹⁶⁾. The $\pi\pi \rightarrow \pi\pi$ interaction has been studied extensively using the data of these experiments. For detailed reviews of the $\pi\pi$ interactions we refer to the book by Martin, Morgan and Shaw⁽¹⁷⁾ and the CERN Report by Petersen⁽¹⁸⁾. We shall use the data of the CERN-Munich experiment to study the $S^*-\xi$ problem.

Six high statistics experiments have been carried out of ($K\bar{K}$) production in recent years. We list these experiments in Table 2.1.

<u>Group</u>	<u>Ref.</u>	<u>Reaction</u>	<u>P_{lab}(GeV/c)</u>	<u>No. of Events</u>
Argonne EMS	(47)	$\pi^- p \rightarrow K^+ K^- n$	6.0	16,000
CERN-Münich	(56)	$\pi^- p \rightarrow K^+ K^- n$	18.4	27,000 (with $t < 0.2$)
Argonne EMS	(19)	$\pi^- p \rightarrow K^+ K^- n$	6.0	110,000
		$\pi^+ n \rightarrow K^+ K^- p$	6.0	50,000
Zurich CERN Imperial Coll.)	(20)	$\pi^- p \rightarrow K_s^0 K_s^0 n$	8.9	6,400
Notre Dame Argonne)				
Geneva	(21)	$\pi^- p \rightarrow K^- K_s^0 p$	10.0	40,000

Table 2.1

Since the $K\bar{K}$ state is a particle-anti-particle state, it has the properties⁽²²⁾

$$P | K\bar{K} \rangle = (-)^L | K\bar{K} \rangle \quad (2.1)$$

$$C | K\bar{K} \rangle = (-)^L | K\bar{K} \rangle \quad (2.2)$$

$$G = (-)^{I+L} \quad (2.3)$$

where P and C are the parity and the charge conjugation operators respectively, G is the G parity, L is the spin of the $K\bar{K}$ system and I is the total isospin, it can have values

$$I = 0, 1 \quad (2.4)$$

Thus the allowed quantum numbers for $K\bar{K}$ states are

$$J^{PC} = 0^{++}, 1^{--}, 2^{++}, 3^{--} \dots \quad (2.5)$$

For a given J^{PC} , I can be 0 or 1.

The $K_S^0 K_S^0$ system can only have even values of angular momentum. For a two identical spin-zero particles, Bose statistics do not allow odd values of the angular momentum. Therefore, the $K^0 \bar{K}^0$ states, which can decay through the $K_S K_S$ state, can only have the quantum numbers

$$J^{PC} = 0^{++}, 2^{++}, 4^{++} \dots \quad (2.6)$$

The $K^0 K^-$ system has $Q = -1$ and therefore can only have $I = 1$.

The $\pi\pi$ state has the same quantum numbers of those in eq. (2.5). Since $\pi\pi$ system has $G = +$, from eq. (2.3)

$$L + I = \text{even} \quad (2.7)$$

where L, I are the spin and isospin of the $\pi\pi$ system; for the $\pi\pi$ system we can have

$$I = 0, 1, 2. \quad (2.8)$$

The equation (2.7) separates out isospin values of the $\pi\pi$ system for a given value of L . This restriction does not hold for the $K\bar{K}$ system. This means if we observe a new resonance in the $K\bar{K}$ system, it is not straightforward to assign its isospin. On this point the $K^- K^0$ system is particularly useful to determine the isospin of resonances of the $K\bar{K}$ system. Moreover, the $K_S K_S$ system, which has only

$J = \text{even}$ amplitudes, is also very valuable in sorting out the phase-shift ambiguities of the $K\bar{K}$ production.

The charge-exchange processes

$$\begin{aligned}
 \pi^- p &\longrightarrow \pi^+ \pi^- n \\
 \pi^- p &\longrightarrow K^+ K^- n \\
 \pi^+ n &\longrightarrow K^+ K^- p \\
 \pi^- p &\longrightarrow K_S^0 K_S^0 n
 \end{aligned}
 \tag{2.9}$$

have the common feature of dominance of one-pion exchange amplitudes in the forward scattering region. This feature allows us to study $\pi\pi \longrightarrow \pi\pi$ and $\pi\bar{\pi} \longrightarrow K\bar{K}$ interactions by isolating the pion exchange amplitudes. At the meson vertex $\bar{\pi}(\pi\pi)$ of the reaction

$$\pi N \longrightarrow \pi\pi N$$

G parity must be always negative. This condition allows only a small number of exchanges. Since there is no such condition for the $K\bar{K}$ system, the number of allowed exchanges is larger. The richness of allowed exchanges for the $K\bar{K}$ production complicates the isolation of the one-pion-exchange (OPE) amplitudes.

The $K\bar{K}$ production mechanism in the reaction

$$\pi^- p \longrightarrow K^- K_S^0 p \tag{2.10}$$

is different from those in (2.9). The possibility of the exchange of vacuum quantum numbers allows the exchange of pomeron, f , etc., and the pion exchange is only allowed

for the $J = \text{odd}$ amplitudes by the G parity selection rule. Therefore this reaction is not a good place to study the one-pion exchange amplitudes, however it is very useful in determining the contributions of the other exchanges in the $K\bar{K}$ production.

2.2 Observables and Amplitudes

We consider processes of the type

$$\pi N \longrightarrow (m_1 m_2) N \quad (2.11)$$

where m_i are mesons. The amplitudes describing these processes are functions of five kinematical variables. We choose these variables to be (see Fig. 2.1)

$$\begin{aligned} s &= (p_1 + p_2)^2 \\ t &= (p_2 - p_5)^2 \\ M^2 &= (p_3 + p_4)^2 \end{aligned} \quad (2.12)$$

θ, ϕ , di-meson decay angles in the $m_1 m_2$ rest frame.

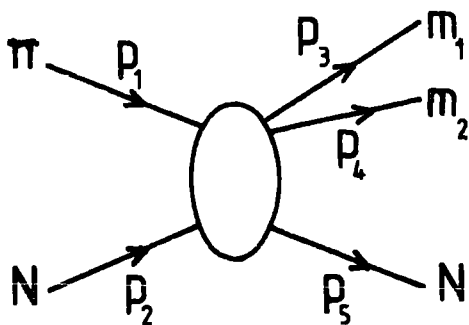


Figure 2.1: Diagram of process $\pi N \longrightarrow m_1 m_2 N$. P_i are the four-momenta of the corresponding particles.

At given incident momentum, the process can be described by four variables, namely t, M, θ and ϕ in (2.12). The decay angles θ, ϕ can be measured either in the t -channel (Gottfried-Jackson) or s -channel (helicity) frame. The specification of these two frames is shown

in Fig. 2.2.

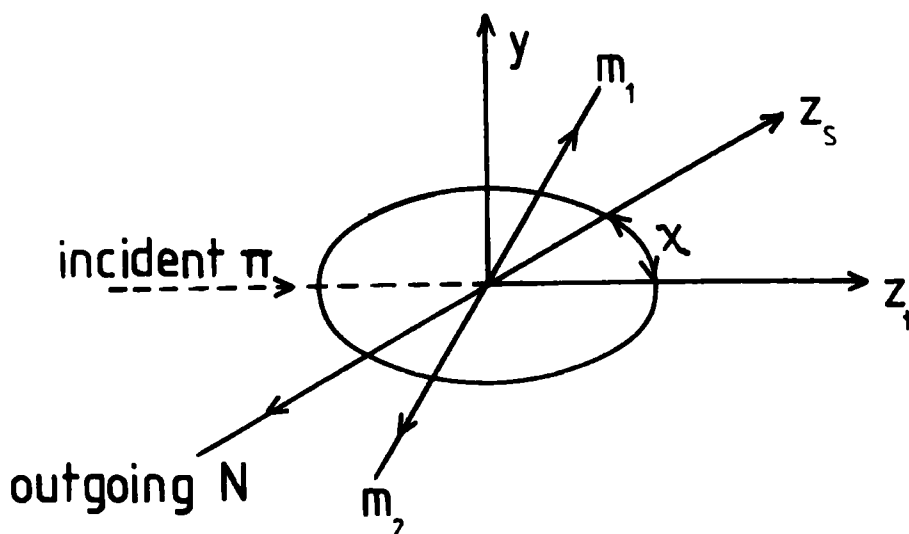


Figure 2.2: The s and t channel frames.
The two frames are related by a rotation χ about the normal to the $\pi N \rightarrow m_1 m_2 N$ reaction plane.

The experimental information consists of an intensity distribution, for a given incident momentum:

$$\frac{d\sigma}{dM dt d\Omega} = \frac{d\sigma}{dM dt} W(\theta, \phi). \quad (2.13)$$

The left-hand side of (2.13) corresponds to the number of events in the element $dM dt d\Omega$. On the right hand side first term is proportional to the number of events in the element $dM dt$ and it is the integrated intensity

$$N = 4\pi \langle I \rangle = \frac{d\sigma}{dM dt}. \quad (2.14)$$

$W(\theta, \phi)$ specifies the m_1, m_2 angular distribution. It can be expanded in terms of spherical harmonics

$$W(\theta, \phi) = \sum_{J, M} \langle Y_M^J \rangle \text{Re } Y_M^J(\theta, \phi) \quad (2.15)$$

where $\langle Y_M^J \rangle$ are the expectation values of the corresponding spherical harmonics and are called the normalised

moments. The experimental data are usually presented in the form

$$A_M^J(M, t) = N \langle Y_M^J \rangle \quad (2.16)$$

as functions of M and t . A_M^J 's are generally called the unnormalised moments.

The intensity distribution defined in eq. (2.13) may be expressed in terms of helicity amplitudes. If we restrict ourselves to the case that produced mesons have spin zero, we can define the helicity amplitudes, either in t or s -channel, as

$$H_{\lambda' \lambda}^{S, (t)}(t, M, \theta, \phi) \quad (2.17)$$

for fixed value of incident momentum. Here λ', λ denote the initial and final nucleon helicity components. The normalization of these amplitudes is such that

$$\frac{d\sigma}{dM dt d\Omega} = \frac{1}{2} \sum_{\lambda', \lambda} |H_{\lambda', \lambda}^{S, (t)}|^2 \quad (2.18)$$

To discuss the production of the di-meson system, it is convenient to decompose $H_{\lambda', \lambda}^{S, (t)}$ into a sum of $H_{\lambda', \lambda, \lambda_R}^{S, (t) L}$ amplitudes, corresponding to the production of di-meson states of spin L and helicity λ_R . Ignoring the channel label

$$H_{\lambda', \lambda}^{S, (t)}(t, M, \theta, \phi) = \sum_{L, \lambda_R} (2L+1)^{1/2} H_{\lambda', \lambda, \lambda_R}^{L, (t)}(t, M) d_{\lambda_R 0}^L(\theta, \phi) e^{i\lambda \phi} \quad (2.19)$$

Substituting into the eq. (2.18)

$$\frac{d\sigma}{dM dt d\Omega} = \frac{1}{2} \sum_{\lambda', \lambda} \sum_{L_1, \lambda_{R1}} \sum_{L_2, \lambda_{R2}} (2L_1+1)^{1/2} (2L_2+1)^{1/2} e^{i(\lambda_{R1} - \lambda_{R2})\phi} \quad (2.20)$$

$$(H_{\lambda', \lambda, \lambda_{R1}}^{L_1})^* H_{\lambda', \lambda, \lambda_{R2}}^{L_2} d_{\lambda_{R1} 0}^{L_1}(\theta, \phi) d_{\lambda_{R2} 0}^{L_2}(\theta, \phi) \quad (2.20)$$

We define the spin density matrix elements for di-meson production

$$\rho_{\lambda_{R1} \lambda_{R2}}^{L_1 L_2} = \frac{1}{2N} \sum_{\lambda' \lambda} \left(H_{\lambda' \lambda \lambda_{R1}}^{L_1} \right)^* H_{\lambda' \lambda \lambda_{R2}}^{L_2}, \quad (2.21)$$

where N is given by eq. (2.14). Using eqs. (2.15), (2.20) and (2.21) we can express the normalised moments in terms of the spin density matrix elements:

$$\langle Y_M^J \rangle = (4\pi)^{-1/2} \sum_{L_1, \lambda_{R1}} \sum_{L_2, \lambda_{R2}} \left[\frac{(2L_1+1)(2L_2+1)}{2J+1} \right]^{1/2} \langle L_1, L_2; 0, 0 | J, 0 \rangle \times$$

$$(-)^{\lambda_{R2}} \langle L_1, L_2; \lambda_{R1}, -\lambda_{R2} | J, M \rangle \text{Re} \rho_{\lambda_{R1} \lambda_{R2}}^{L_1 L_2} \quad (2.22)$$

where $\langle l_1, l_2; m_1, m_2 | j, m \rangle$ denote Clebsch-Gordan coefficients. Note that the relations (2.19)-(2.22) are equally valid in terms of either t or s -channel helicity amplitudes. The explicit expansions of eq. (2.22) are listed in Appendix I in the case $L_1, L_2 \leq 4, |\lambda_{R1}|, |\lambda_{R2}| \leq 1$. As the experimental data are given more conveniently in terms of moments, in the presence of more than one spin state of produced di-meson system, we usually do not have information direct on $\rho_{\lambda' \lambda}^{L_1 L_2}$'s. Instead we have information on linear combinations of density matrix elements.

It is useful for the description of t -channel exchanges to define the following combinations of the amplitudes (in either the t or s -channel frames)

$$H_{\lambda' \lambda \lambda_R}^{L \pm} = \frac{1}{\sqrt{2}} \left(H_{\lambda' \lambda \lambda_R}^L \mp (-)^{\lambda_R} H_{\lambda' \lambda -\lambda_R}^L \right) \quad \text{for } \lambda_R > 0$$

$$H_{\lambda' \lambda 0}^{L -} = H_{\lambda' \lambda 0}^L. \quad (2.23)$$

At high energies the amplitudes $H_{\lambda' \lambda \lambda_R}^{L+}$ and $H_{\lambda' \lambda \lambda_R}^{L-}$ describe

the production of a di-meson system by natural and unnatural parity exchange, respectively⁽²³⁾.

The t and s-channel amplitudes are related by usual crossing relations. These relations are discussed in reference (17) in full generality, here we summarise some of the results: The crossing matrices are block diagonal in terms of $H^{L^{\pm}}$ amplitudes defined in (2.23). The amplitudes with exchange of definite naturality are related among themselves by crossing. The crossing transformation on the nucleon helicities has the following properties: It is diagonal in the forward direction for the unnatural and natural parity exchanges amplitudes, i.e. flip \rightarrow flip, non-flip \rightarrow non-flip. Except very close to the forward direction, the unnatural parity exchange amplitudes transform in an anti-diagonal way for the nucleon helicity (flip \rightarrow non-flip) while the transformation continues to be approximately diagonal for the natural parity exchange amplitudes.

2.3 Properties and Formalism of One-Pion - Exchange Amplitudes

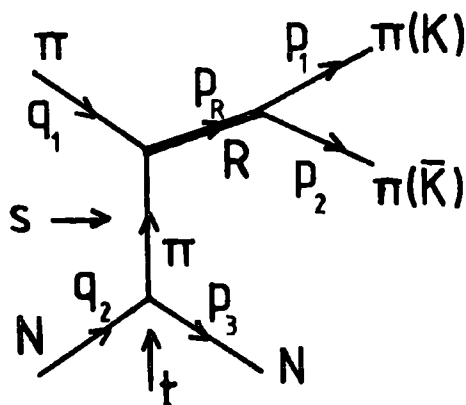
Most of our knowledge on $\pi\pi \rightarrow \pi\pi, K\bar{K}$ interactions has been obtained from studies of the one-pion-exchange (OPE) processes:

$$\begin{aligned} \pi N &\rightarrow \pi\pi N \\ \pi N &\rightarrow K\bar{K}N. \end{aligned} \tag{2.24}$$

The importance of these processes is due to the dominance of the OPE contribution. If we can isolate this contribution, the associated $\pi\pi \rightarrow \pi\pi, K\bar{K}$ amplitudes follow immediately. However there are complications. We never observe the one-pion-exchange contribution alone in the processes of the

type of (2.24). There are several other amplitudes giving contributions to the observables besides the OPE amplitudes. The amplitudes, corresponding to non-OPE exchanges can give sizeable contributions, specially in $K\bar{K}$ production processes. Therefore we have to take into account all possible exchanges and important corrections arising from absorptive effects. In order to do this we should have a dynamical model, together with high statistics data to give information on these amplitudes.

We should extrapolate the scattering region amplitudes to the pion pole, in order to determine the physical $\pi\pi \rightarrow \pi\pi(k\bar{k})$ amplitudes. Let us consider the diagram shown in Fig. 2.3. Even if we ignore all other contribu-



utions, the processes of type (2.24) cannot give directly the physical $\pi\pi \rightarrow \pi\pi(k\bar{k})$ amplitudes. Roughly speaking the physical amplitudes for the reactions in (2.24) are in the form

Figure 2.3: OPE Diagram in processes $\pi N \rightarrow \pi\pi(k\bar{k}) N$. R is a meson resonance.

$$A \sim V(N\pi N) \frac{1}{t - m_\pi^2} F(t) A(\pi\pi \rightarrow \pi\pi(k\bar{k})) \quad (2.25)$$

where $V(N\pi N)$ is the vertex function describing the bottom vertex in Fig. 2.3, $1/(t - m_\pi^2)$ is the OPE propagator, $F(t)$ is a form factor satisfying $F(m_\pi^2) = 1$, and $A(\pi\pi \rightarrow \pi\pi(k\bar{k}))$ are the physical $\pi\pi \rightarrow \pi\pi(k\bar{k})$ amplitudes. In order to determine the $A(\pi\pi \rightarrow \pi\pi(k\bar{k}))$ we

have to calculate $V(N\pi N)$ and $F(t)$. The form of the $V(N\pi N)$ vertex function can be determined using the Feynman diagram techniques. The most model independent way to determine $F(t)$ is to fit the t -dependence of Λ in the relation (2.25) bearing in mind the condition $F(m_\pi^2) = 1$. In this way we can determine the $\pi\pi \rightarrow \pi\pi(\kappa\bar{\kappa})$ amplitudes from $\pi N \rightarrow \pi\pi(\kappa\bar{\kappa})N$ OPE amplitudes up to some known kinematical factors. This extrapolation method was originally proposed by Goebel, and by Chew and Low⁽²⁴⁾, and a detailed calculation was given by Ferrari and Selleri⁽²⁵⁾. Different conventions used by the different authors prevent the use of their results directly. Therefore we review the calculation using the currently accepted convention.

We follow the convention given in the book by Pilkuhn⁽²⁶⁾. We give the definition of the S-matrix, the normalization of the states, the cross section, etc. in Appendix II.

Consider the diagram in Fig. 2.3. We define the kinematical variables such

$$\begin{aligned} s &= (q_1 + q_2)^2 \\ t &= (q_2 - p_3)^2 \\ M^2 &= (p_1 + p_2)^2 = p_R^2 \end{aligned} \quad (2.26)$$

θ, ϕ Polar angles of produced $\pi\pi(\kappa\bar{\kappa})$
in the R rest frame

We normalise the scattering matrix element T for this process so that

$$T = V(N\pi N) \frac{F(t)}{t - m_\pi^2} T(\pi\pi \rightarrow \pi\pi(\kappa\bar{\kappa})). \quad (2.27)$$

The terms on right-hand side of the eq. (2.27) are the

same as (2.25). We introduce the shorthand notation:

$$\mathcal{T} = T(\pi\pi \longrightarrow \pi\pi(k\bar{k})). \quad (2.28)$$

The S-matrix element

$$S_{\beta\alpha} = \delta_{\beta\alpha} + i(2\pi)^4 \delta^4(q_1 + q_2 - p_1 - p_2 - p_3) V(N\pi N) \frac{F(+)}{t - m_\pi^2} \mathcal{T}. \quad (2.29)$$

Using eqs. (A.II.9) and (A.II.13) we can write the cross section:

$$d\sigma = \frac{1}{2[\lambda(s; m_N^2, m_\pi^2)]^{1/2}} dLips(s; p_1, p_2, p_3) \left[V(N\pi N) \frac{F(+)}{t - m_\pi^2} \mathcal{T} \right]^2 \quad (2.30)$$

As we do not have any nucleon polarisation information, we average over the initial nucleon helicity states and sum over the final nucleon helicity states. In eq. (2.30) only $V(N\pi N)$ depends on the nucleon helicities. In Appendix III we show

$$\frac{1}{2} \sum_{\lambda_1, \lambda_2} |V(N\pi N)_{\lambda_1, \lambda_2}|^2 = -G^2 t, \quad (2.31)$$

where $G^2/4\pi \simeq 14.6$ (27).

The Lorentz-invariant phase-space element in eq.

(2.30)

$$dLips(s; p_1, p_2, p_3) = (2\pi)^4 \delta^4(q_1 + q_2 - p_1 - p_2 - p_3) (2\pi)^{-9} \prod_{i=1}^3 \frac{d^3 p_i}{2E_i} \quad (2.32)$$

can be re-written as

$$\int_{\phi} dLips(s; p_1, p_2, p_3) = \frac{dt dM^2}{(4\pi)^2 [\lambda(s; m_N^2, m_\pi^2)]^{1/2}} dLips(M^2; p_1, p_2) \quad (2.33)$$

(see Appendix IV). Substituting eqs. (2.31) and (2.33)

into eq. (2.30) we obtain

$$d\sigma = \frac{1}{2\lambda(s; m_N^2, m_\pi^2)} \frac{G^2(-t)}{(t - m_\pi^2)^2} F(+)^2 dt dM^2 \frac{1}{(4\pi)^2} \times \quad (2.34)$$

$$dLips(M^2; p_1, p_2) |\mathcal{T}|^2.$$

So far we have explicitly calculated the $N\pi N$ vertex factor and the $(\pi N \rightarrow RN)$ phase-space element. The

$$dLips(M^2; p_1, p_2) |\mathcal{T}|^2 \quad (2.35)$$

describes the subprocess

$$\pi\pi \longrightarrow R \longrightarrow \pi\pi, (k\bar{k}).$$

At this point we treat the exchanged pion as an on-shell real particle; the off-shell effects are described by the $F(t)$ factor. We show in Appendix V that

$$\int_{\Omega} dLips(M^2; p_1, p_2) |\mathcal{T}|^2 = 16\pi M\rho \sum_{L=0}^{\infty} (2L+1) |T_L(\pi\pi \rightarrow \pi\pi(k\bar{k}))|^2 \quad (2.35)$$

where \int_{Ω} represents the integration over the solid angle element $d\Omega = d\phi d\cos\theta$, $\rho = (M^2/4 - m_m^2)^{1/2}$ is the $\pi\pi(k\bar{k})$ centre of mass momentum. Recall that

$$dM^2 = 2M dM \quad (2.36)$$

and in the laboratory system (c.f. (A.II.12))

$$\lambda(s; m_N^2, m_{\pi}^2) = 4 p_{Lab}^2 m_N^2. \quad (2.37)$$

Substituting eqs: (2.35), (2.36), (2.37) into eq. (2.34), we find

$$\frac{d\sigma}{dt dM} = \frac{1}{p_{Lab}^2 m_N^2} \frac{G^2}{4\pi} \frac{-t}{(t - m_{\pi}^2)^2} F(t)^2 M^2 \rho \sum_{L=0}^{\infty} (2L+1) |T_L(\pi\pi \rightarrow \pi\pi(k\bar{k}))|^2 \quad (2.38)$$

This equation is the result that we seek. The right hand side contains only known factors except $F(t)$ and the T_L . Once we determine $F(t)$ we can obtain the $\pi\pi \rightarrow \pi\pi(k\bar{k})$ partial wave amplitudes, T_L , immediately. Note

that the eq. (2.38) is the cross-section of the $\pi N \rightarrow \pi\pi(\kappa\bar{\kappa})N$ process. For observed processes with definite charges (such as $\pi^- p \rightarrow \pi^+ \pi^- n$) we have to include the appropriate isospin Clebsch-Gordan coefficients.

The OPE amplitudes have distinctive features. They have the pole $1/(t - m_\pi^2)$, and vanish as $\sqrt{-t}$ at $t = 0$. These two factors give a characteristic t -dependence. The OPE amplitudes have the pure nucleon helicity non-flip structure and produce only helicity zero states of the $\pi\pi(\kappa\bar{\kappa})$ system in the t -channel. These properties can be proved by noticing the π has spin zero, therefore $J_3 = m$ should be zero for the $N\bar{N}$ and $\pi(\pi\pi)$, $\pi(\kappa\bar{\kappa})$ systems. So for pure OPE, only $\langle Y_{M=0}^J \rangle$ moments of produced di-meson system can be different from zero in the t -channel (see Appendix I). But experiments show non-zero $\langle Y_{M \neq 0}^J \rangle$ moments in the t -channel (16, 19, 20, 21). This indicates the existence of absorptive corrections and amplitudes produced by other exchanges.

The absorptive corrections to OPE amplitudes have been extensively studied for the reaction $\pi^- p \rightarrow \pi^+ \pi^- n$, (see reference (17) and references therein). Let us assume that only the $L = 0, \lambda_R = 0$ $H_{\lambda'\lambda_R}^L$ $\pi\pi(\kappa\bar{\kappa})$ production amplitude is produced by OPE in the t -channel. Ignoring the t_{\min} effect, by crossing we find the s -channel amplitudes

$$H_{\lambda'\lambda_0}^{L=1} \sim \frac{\sqrt{-t}}{t - m_\pi^2}, \quad H_{\lambda'\lambda_0}^{L=1} \sim \frac{-t}{t - m_\pi^2} \quad (2.39)$$

which vanish at $t = 0$. The data do not agree with this prediction. For example the ρ meson production cross-section

in $\pi^+ p \rightarrow \pi^+ \pi^- n$ does not vanish at $t = 0$. This has been explained by the absorptive corrections to the $H_{\lambda'\lambda}^{L=1}$ amplitudes which do not vanish at $t = 0$. The simplest phenomenological way to introduce such contributions is to add a constant to the $P_{\pm 1}$ amplitudes

$$H_{\lambda'\lambda}^{L=1} \sim \frac{-t}{t - m_{\pi}^2} + C. \quad (2.40)$$

The Williams model⁽²⁸⁾ or the "Poor Man Absorption" description⁽²⁹⁾ assumes $C = 1$. We can let C be a complex number⁽³⁰⁾. The authors of ref. (30) have found a solution with a small imaginary part of C . If we choose C to be a real constant, we can make some specific predictions: (i) all helicity amplitudes, for a given L , have a common phase, (ii) all amplitudes, including the predicted non-OPE amplitudes, are pure nucleon helicity flip in the s -channel (except the negligible H_{++}^S OPE amplitude), (iii) for the t -channel amplitudes

$$\frac{H_{++0}^{(+)L}}{H_{++1}^{(+)L}} = \frac{C(M)}{\sqrt{L(L+1)}}, \quad (2.41)$$

where $C(M)$ is a real function of the di-meson effective mass M , and L is the spin of the produced $\pi\bar{\pi}$ system⁽³¹⁾. Detailed fits to the experimental data have shown that $C(M)$ can be parametrized as a polynomial in M , and all these predictions are consistent with the data^(32, 33).

2.4 Exchanges and Amplitudes

In this section we discuss the allowed exchanges for the following di-meson production processes:

$$\begin{aligned}
 \pi^- p &\longrightarrow \pi^+ \pi^- n \\
 \pi^- p &\longrightarrow K_s^0 K_s^0 n \\
 \pi^- p &\longrightarrow K^+ K^- n \\
 \pi^+ n &\longrightarrow K^+ K^- p \\
 \pi^- p &\longrightarrow K_s^0 K^- p .
 \end{aligned}
 \tag{2.42}$$

In particular we want to determine the exchange contributions to the s-channel helicity amplitudes. Parity and G-parity conservation gives relations between helicity amplitudes in terms of the quantum numbers of the exchanged object⁽²³⁾. Assume the process $1 + 2 \rightarrow 3 + 4$ is mediated by the exchange of a Regge pole with intrinsic parity η , G-parity G , spin J , signature $\mathcal{S} = (-)^J$, isospin I in the t-channel $\bar{1} + 2 \rightarrow 3 + \bar{1}$, (Fig. 2.4). We can apply

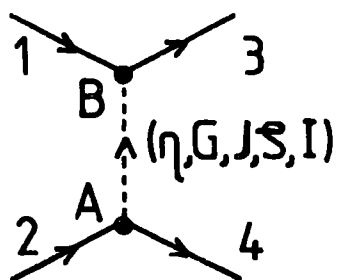


Figure 2.4

parity and G-parity conservation at vertices A and B. In terms of s-channel helicity amplitudes, the results of this procedure are⁽²³⁾:

Parity at vertex A:

$$H_{\lambda_3 \lambda_4; \lambda_1 \lambda_2}^S \approx \eta \mathcal{S} \eta_4 \eta_2 (-)^{s_4 - s_2} (-)^{\lambda_4 - \lambda_2} H_{\lambda_1 - \lambda_4; \lambda_1 - \lambda_2}^S .
 \tag{2.43}$$

Parity at vertex B:

$$H_{\lambda_3 \lambda_4; \lambda_1 \lambda_2}^S \approx \eta \mathcal{S} \eta_3 \eta_1 (-)^{s_3 - s_1} (-)^{\lambda_3 - \lambda_1} H_{-\lambda_3 \lambda_4; -\lambda_1 \lambda_2}^S .
 \tag{2.44}$$

Assuming 2 and 4 are the same type of particle, G-parity at vertex A:

$$H_{\lambda_3, \lambda_4; \lambda_1, \lambda_2}^S \simeq G \eta (-)^I (-)^{\lambda_4 - \lambda_2} H_{\lambda_3, \lambda_1; \lambda, \lambda_4}^S \quad (2.45)$$

where s_i, λ_i, η_i are the spin, helicity and intrinsic parity of particles 1, 2, 3, 4 respectively.

If we only consider production of the meson in the processes in (2.42), we can describe them by a single diagram (Figure 2.5), where R is the produced meson with

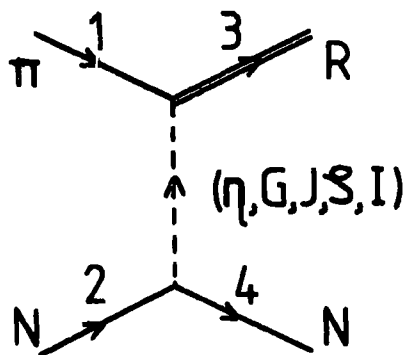


Figure 2.5

spin L , helicity λ_R , and intrinsic parity η_R . Recalling $S_\pi = 0, S_N = 1/2$, $\eta_\pi = -$, $\eta_N = +$ and fixing $\lambda_2 = +1/2$ we can re-write (2.43)-(2.45) in simpler forms:

$$H_{\lambda_R, \lambda_4; 0+}^S \simeq \eta \zeta (-)^{\lambda_4 - 1/2} H_{\lambda_R - \lambda_4; 0-}^S \quad (2.46)$$

$$H_{\lambda_R, \lambda_4; 0+}^S \simeq \eta \zeta \eta_R (-)^{L + \lambda_R + 1} H_{-\lambda_R, \lambda_4; 0+}^S \quad (2.47)$$

$$H_{\lambda_R, \lambda_4; 0+}^S \simeq G \eta (-)^I (-)^{\lambda_4 - 1/2} H_{\lambda_R+; 0, \lambda_4}^S \quad (2.48)$$

Let us consider the nucleon helicity non-flip amplitude (i.e. $\lambda_1 = +1/2$), taking $\lambda_R = 0$, from equation (2.47)

$$H_{0+; 0+}^S \simeq \eta \zeta \eta_R (-)^{L+1} H_{0+; 0+}^S$$

which gives

$$\eta \zeta = \eta_R (-)^{L+1}, \quad \eta (-)^J = -\eta_R (-)^L. \quad (2.49)$$

Recall the natural and unnatural parity definition for

mesons

$$\begin{aligned} \eta &= (-)^L \quad \text{Natural Parity} \\ \eta &= (-)^{L+1} \quad \text{Unnatural Parity.} \end{aligned}$$

Eq. (2.49) implies that a meson with natural parity in $\lambda_R=0$ state can only be produced by unnatural parity exchange and vice versa.

For any value of λ_R with $\lambda_4 = \lambda_2 = +1/2$ using (2.48)

$$H_{\lambda_R+; 0+}^S \approx G \eta (-)^I H_{\lambda_R+; 0+}^S$$

which implies that only exchanges which can satisfy the condition

$$G \eta = (-)^I \quad (2.50)$$

can give a contribution to the nucleon helicity non-flip amplitudes in the s-channel.

Now we take $\lambda_2 = +1/2$, $\lambda_4 = -1/2$, using equations (2.46) and (2.48)

$$H_{\lambda_R-; 0+}^S \approx \eta \zeta (-)^I H_{\lambda_R+; 0-}^S$$

$$H_{\lambda_R-; 0+}^S \approx G \eta (-)^{I+1} H_{\lambda_R+; 0-}^S$$

which together give

$$H_{\lambda_R-; 0+}^S = G \zeta (-)^I H_{\lambda_R-; 0+}^S$$

The last relation shows that only exchanges which can satisfy the condition

$$G = (-)^{I+J} \quad (2.51)$$

can give contribution to the nucleon helicity flip amplitudes in the s-channel.

It is useful to know the small $|t|$ behaviour of the different amplitudes, so we can identify the amplitudes by studying their small $|t|$ region structure. Near the forward direction, helicity amplitudes have characteristic behaviour described by the kinematical "half-angle factors" which express the conservation of angular momentum along the direction of motion. In the process $\pi + N(2) \rightarrow R + N(4)$

$$H_{\lambda_R \lambda_4; 0 \lambda_2}^S \sim (-t)^{|\lambda_2 - \lambda_4 + \lambda_R|/2} \quad (2.52)$$

The t-channel helicity amplitudes have similar small-t behaviour, consistent with those of s-channel amplitudes and the crossing relations⁽¹⁷⁾.

Now we discuss the exchange mechanism of the processes in (2.42) individually:

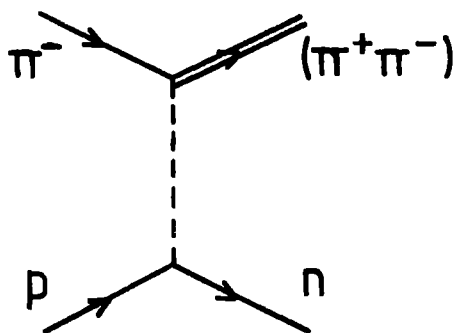
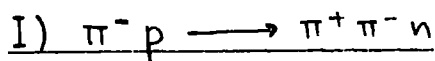


Figure 2.6

Because this is a charge exchange process, the exchanged particle (or Regge pole) has $I = 1$. The $(\pi^+ \pi^-)$ system has definite G-parity $G = +$ so at the top vertex of Fig. 2.6 $G = -$, as the pion

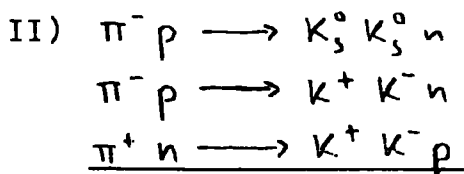
has $G = -$. Therefore only exchanges with $I^G = 1^-$ can give contribution to this process. Ignoring the low lying Regge trajectories, the only known Regge trajectories with $I^G = 1^-$ are:

$$\begin{aligned}
 \pi (I^G = 1^-, J^P = 0^-) & \text{ Unnatural Parity} \\
 A_1 (I^G = 1^-, J^P = 1^+) & \text{ Unnatural Parity} \\
 A_2 (I^G = 1^-, J^P = 2^+) & \text{ Natural Parity.} \quad (2.53)
 \end{aligned}$$

Using eq. (2.23) and eqs. (2.49)-(2.52), we summarise the possible exchanges in Table 2.2:

s-channel helicity amp.	Exchanges		Small-t behaviour
	UPE	NPE	
H_{+-0}^L	π		$\sqrt{-t}$
H_{++0}^L	A_1		C
H_{+-1}^{L-}	π		$-t$
H_{++1}^{L-}	A_1		$\sqrt{-t}$
H_{+-1}^{L+}		A_2	$-t$
H_{++1}^{L+}		A_2	$\sqrt{-t}$

Table 2.2: Regge exchange contributions to the s-channel helicity amplitudes in process $\pi^- p \rightarrow \pi^+ \pi^- n$.



These are all charge exchange processes therefore we need $I = 1$ exchange. The $(K\bar{K})$ system has $G = (-)^{L+I}$, where L is the spin of $(K\bar{K})$ system and $I = 0, 1$ is the total isospin. At the $\pi(K\bar{K})$ vertex we can have $G = +, -$ with $G = -(-)^{L+I}$. The allowed exchanges for these processes have $I^G = 1^-, 1^+$. We have listed $I^G = 1^-$ exchanges in

(2.53). The known $I^G = 1^+$ Regge trajectories are:

$$\begin{aligned}
 &B(I^G = 1^+ \quad J^P = 1^+) \quad \text{Unnatural Parity} \\
 &\mathbf{z}(I^G = 1^+ \quad J^P = 2^-) \quad \text{Unnatural Parity} \\
 &\rho(I^G = 1^+ \quad J^P = 1^-) \quad \text{Natural Parity.} \quad (2.54)
 \end{aligned}$$

The \mathbf{z} is the exchange-degenerate partner of A_1 ^(34,35).

The G-parity selection rule shows which exchanges can contribute to the amplitudes with definite L and I of the $(K\bar{K})$ system:

$$\begin{aligned}
 L = \text{even} \quad I = \text{even} \quad G = -, & (\pi, A_1, A_2) \\
 L = \text{even} \quad I = \text{odd} \quad G = +, & (B, \mathbf{z}, \rho) \\
 L = \text{odd} \quad I = \text{even} \quad G = +, & (B, \mathbf{z}, \rho) \\
 L = \text{odd} \quad I = \text{odd} \quad G = -, & (\pi, A_1, A_2). \quad (2.55)
 \end{aligned}$$

As we have explained in Section 2.1, the $K_S^0 K_S^0$ system can only have even values of L.

There is a very useful relation between amplitudes of $\pi^- p \rightarrow K^+ K^- n$ and $\pi^+ n \rightarrow K^+ K^- p$.

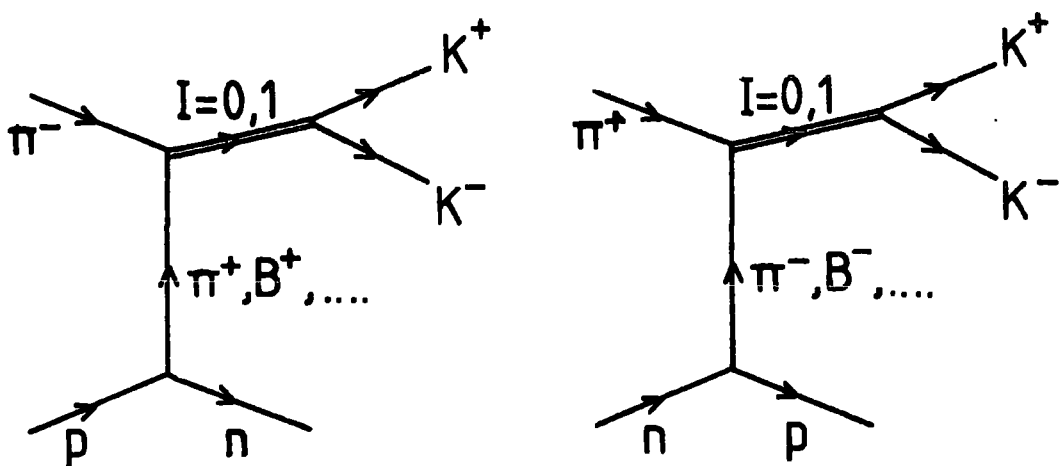


Figure 2.7

For the meson vertices of Fig. 2.7 the isospin Clebsch-Gordan coefficients give

$$\begin{aligned} \langle \pi^- \pi^+ | K \bar{K}; I=0 \rangle &= \langle \pi^+ \pi^- | K \bar{K}; I=0 \rangle \\ \langle \pi^- B^+ | K \bar{K}; I=0 \rangle &= \langle \pi^+ B^- | K \bar{K}; I=0 \rangle \end{aligned} \quad (2.56)$$

and

$$\begin{aligned} \langle \pi^- \pi^+ | K \bar{K}; I=1 \rangle &= - \langle \pi^+ \pi^- | K \bar{K}; I=1 \rangle \\ \langle \pi^- B^+ | K \bar{K}; I=1 \rangle &= - \langle \pi^+ B^- | K \bar{K}; I=1 \rangle. \end{aligned} \quad (2.57)$$

Therefore if we denote $A(\pi^- p)$ as the amplitude of the process $\pi^- p \rightarrow K^+ K^- n$, $A(\pi^+ n)$ as that for $\pi^+ n \rightarrow K^+ K^- p$ and $A(I=0)$, $A(I=1)$ as amplitudes for producing $I=0,1$ of $(K\bar{K})$ system respectively, then (2.56) and (2.57) give

$$\begin{aligned} A(\pi^- p) &= A(I=0) + A(I=1) \\ A(\pi^+ n) &= A(I=0) - A(I=1). \end{aligned} \quad (2.58)$$

Using eq. (2.23) and eqs. (2.49)-(2.52), we list in Table 2.3 the Regge exchange contributions to the s-channel helicity amplitudes for the charge-exchange processes $\pi N \rightarrow (K \bar{K}) N$:

s-channel helicity amp.	Exchanges				Small-t behaviour
	UPE		NPE		
	G=-	G=+	G=-	G=+	
H_{+-0}^L	π	B			$\sqrt{-t}$
H_{++0}^L	A_1	Z			C
H_{+-1}^{L-}	π	B			-t
H_{++1}^{L-}	A_1	Z			$\sqrt{-t}$
H_{+-1}^{L+}			A_2	ρ	-t
H_{++1}^{L+}			A_2	ρ	$\sqrt{-t}$

Table 2.3: Regge exchange contributions to the s-channel helicity amplitudes in charge-exchange $\pi N \rightarrow (K \bar{K}) N$ processes.

$$\underline{\text{III) } \pi^- p \longrightarrow K_s^0 K^- p}$$

Here we can have $I = 0$ or 1 exchange. The $(K^0 K^-)$ system has $I = 1$ and $G = (-)^{L+I}$. Therefore at the $\pi (K^0 K^-)$ vertex $G = (-)^L$, and exchanges with $I^G = 0^+, -, 1^+, -$ are allowed. We have listed the $I^G = 1^-, +$ exchanges in (2.53) and (2.54), the dominant $I^G = 0^+, -$ exchanges are:

$$\begin{aligned} \mathbb{P} (I^G = 0^+, J^P = 0^+) & \text{ Natural Parity} \\ \mathcal{F} (I^G = 0^+, J^P = 2^+) & \text{ Natural Parity} \\ \omega (I^G = 0^-, J^P = 1^-) & \text{ Natural Parity} \end{aligned} \quad (2.59)$$

where we ignore low lying η and H trajectories. The G -parity rule $G = (-)^L$ shows which exchanges can contribute to the amplitudes producing a spin L of the $(K^0 K^-)$ system:

$$\begin{aligned} L = \text{even} \quad G = + & \quad (\mathbb{P}, f) \\ L = \text{even} \quad G = + & \quad (B, \mathcal{Z}, \mathcal{F}) \\ L = \text{odd} \quad G = - & \quad (\omega) \\ L = \text{odd} \quad G = - & \quad (\pi A_1 A_2). \end{aligned} \quad (2.60)$$

Using eq. (2.23) and eqs. (2.49)-(2.52) we list in Table 2.4 the Regge exchange contributions to the s -channel helicity amplitudes in the process $\pi^- p \longrightarrow (K^0 K^-) p$. We should make some remarks about the NPE side of the Table 2.4: the pomeron is expected to couple dominantly to amplitudes with no helicity-flip at the nucleon vertex, that is H_{++1}^{L+} . Also it is a phenomenological fact that the f and ω couple dominantly to H_{++1}^{L+} , while the \mathcal{F} and A_2 couple dominantly to amplitudes with nucleon helicity-flip, i.e. H_{+-1}^{L+} (36).

L	s-channel helicity amp.	Exchanges				Small-t behaviour
		UPE		NPE		
		I=0	I=1	I=0	I=1	
even	H_{+-0}^L		B			$\sqrt{-t}$
	H_{++0}^L		Z			C
	H_{+-1}^{L-}		B			-t
	H_{++1}^{L-}		Z			$\sqrt{-t}$
	H_{+-1}^{L+}			P, f	f	-t
	H_{++1}^{L+}			P, f	f	$\sqrt{-t}$
odd	H_{+-0}^L		π			$\sqrt{-t}$
	H_{++0}^L		A_1			C
	H_{+-1}^{L-}		π			-t
	H_{++1}^{L-}		A_1			$\sqrt{-t}$
	H_{+-1}^{L+}			ω	A_2	-t
	H_{++1}^{L+}			ω	A_2	$\sqrt{-t}$

Table 2.4: Regge exchange contributions to the s-channel helicity amplitudes in the process $\pi^+ p \rightarrow (\kappa^0 \kappa^-) p$, where L is the spin of $(\kappa^0 \kappa^-)$ system.

CHAPTER III

S^{*}, ξ : Problem

3.1 Early History of the S^{*}

Historically the S^{*} effect was originally observed as a (K₁⁰K₁⁰) enhancement, rising sharply from the production threshold in the process $\pi^- p \rightarrow (K_1^0 K_1^0) n$, which has a strong OPE contribution⁽³⁷⁾. The (K⁰K⁻) system did not show such a strong enhancement⁽³⁸⁾, therefore the (K₁⁰K₁⁰) threshold peak has been identified as a resonance with $I^G_{JPC} = 0^+ 0^{++}$ produced by one-pion-exchange⁽³⁹⁾. However the resonance interpretation was not certain, since fits, in terms of complex scattering length and S^{*} Breit-Wigner resonance formulae, could describe the data equally well⁽⁴⁰⁾. A few years later, this (K₁⁰K₁⁰) enhancement was also seen in the (K⁺K⁻) state⁽⁴¹⁾. As we have observed the S^{*} effect via $\pi\pi \rightarrow S^* \rightarrow K\bar{K}$ we should also expect to see the S^{*} in $\pi\pi \rightarrow \pi\pi$ scattering. Early phase shift analyses of $\pi\pi \rightarrow \pi\pi$ scattering determined the phase of L = 0, I = 0 $\pi\pi \rightarrow \pi\pi$ amplitude ($S_{\pi\pi}^{I=0}$) complicated by the up-down ambiguity, without any information on the S^{*} (14, 42). The first evidence of the S^{*} effect in $\pi\pi \rightarrow \pi\pi$ came from a Berkeley group⁽⁴³⁾. They reported the existence of a narrow anomaly near the K \bar{K} threshold in both the mass distribution and angular distribution of the $\pi^+\pi^-$ system produced in the reaction $\pi^+ p \rightarrow (\pi^+\pi^-) \Delta^{++}$ at 7 GeV/c.

The anomaly in the $\pi^+\pi^-$ effective mass distribution shows a shoulder between 910-950 MeV, a sharp drop between 950-980 MeV and a flat region above 980 MeV. The normalised $\langle Y_0^1 \rangle$ moment has a strong drop at 980 MeV. Since $\langle Y_0^1 \rangle \sim \rho_0^1 \sim \text{Re}(PS^*)$, this anomaly indicates a rapid movement either in the S-wave or the P wave. The normalised $\langle Y_0^2 \rangle$ moment has a sharp rise at 980 MeV, which is $\sim |P|^2 / (|S|^2 + |P|^2)$, this means either the P wave is increasing or the S wave is decreasing. All these anomalies are most easily understood as a rapid variation in the $S_{\pi\pi}^{I=0}$ amplitude associated with the $K\bar{K}$ threshold. The same group analysed the $\pi\pi \rightarrow \pi\pi$ data, together with (K^+K^-) mass spectrum, assuming that the $S_{\pi\pi}^{I=0}$ amplitude could be parametrized as a resonance which couples to the $\pi\pi$ and $K\bar{K}$ channels⁽⁴⁴⁾. They found that the $S_{\pi\pi}^{I=0}$ amplitude must start at about 900 MeV with phase $\delta_s = 90^\circ$ and reach $\delta_s \approx 180^\circ$ at about 990 MeV, selecting the "down" solution as the unique one. Selection of the "down" solution as the physical one, has been confirmed by comparison with $\pi^+\pi^- \rightarrow \pi^0\pi^0$ data⁽⁴⁵⁾. The structure of the $S_{\pi\pi}^{I=0}$ amplitude, determined by the Berkeley group, has been confirmed by the results of analyses of the high statistics data for the $\pi^-\rho \rightarrow \pi^+\pi^-\nu$ process at 17.2 GeV/c^(16, 32, 33, 45).

The structure of the $S_{\pi\pi}^{I=0}$ amplitude indicates that the S^* is located on a large background, which is $\delta_s \sim 80^\circ - 90^\circ$ at around $M = 900$ MeV. Morgan extracted the S^* effect from the $S_{\pi\pi}^{I=0}$ amplitude and found a slowly rising background phase reaches 90° around $M_{\pi\pi} = 1100-1300$ MeV and is almost elastic⁽⁴⁶⁾. The structure of the

background may be interpreted as a very broad, almost elastic resonance with mass around 1100-1300 MeV, called the ξ meson.

The nature of the S^* is still uncertain, since the resonance and the scattering length descriptions can fit the $\pi\pi \rightarrow \pi\pi$ data equally well. The old $K\bar{K}$ production experiments, having limited statistics, cannot distinguish these two possibilities either. However high statistics $\pi^-p \rightarrow (K^+K^-)n$ experiments have been reported recently (47, 56). These data contain information on the full angular distribution of the produced K^+K^- pair in the threshold region and provide the opportunity to perform a coupled channel analysis of the S^* using $\pi^-p \rightarrow \pi^+\pi^-n$ and $\pi^-p \rightarrow K^+K^-n$ processes. This analysis gives information on the phase of the $L = 0, I = 0$ $\pi\pi \rightarrow K\bar{K}$ amplitude as well as its magnitude.

3.2 Poles and the Dynamical structure of the S^*

As we have discussed in previous section, the S^* effect is associated with strong anomalies in the $\pi\pi \rightarrow \pi\pi$ and $\pi\pi \rightarrow K\bar{K}$ channels. It is well known that such sizeable anomalies can arise at the threshold of an open channel only when the amplitude has poles near the threshold (48,49,50). To a good approximation we can discuss the S^* in terms of just two channels, $\pi\pi$ and $K\bar{K}$. All the phase shift analyses of the $\pi\pi \rightarrow \pi\pi$ scattering are consistent with negligible 4π inelasticity effects below the $K\bar{K}$ threshold. In this two channel approximation the amplitudes have two right-hand cuts on the complex S (total energy squared)-plane, starting from the opening points of the two channels.

Therefore we have to deal with a Riemann surface with four sheets. The poles can occur on any of the unphysical sheets and so lead to different amplitude structure. So, in order to understand the S^* , it is crucial to know how pole positions on various sheets effect the amplitudes.

The $\pi\pi \rightarrow \pi\pi$ and $\pi\pi \rightarrow K\bar{K}$ scattering can be conveniently described either via the partial wave \underline{S} matrix or the partial wave \underline{T} matrix. As we are interested in $L = 0$, we omit the subscript L from eq. (A.II.15)

$$\underline{S} = \underline{1} + 2i \underline{k}^{\frac{1}{2}} \underline{T} \underline{k}^{\frac{1}{2}} \quad (3.1)$$

where \underline{S} , \underline{k} and \underline{T} are 2×2 matrices in the channel space and

$$\underline{k}^{\frac{1}{2}} = \begin{pmatrix} k_1^{\frac{1}{2}} & 0 \\ 0 & k_2^{\frac{1}{2}} \end{pmatrix} \quad (3.2)$$

where

$$\begin{aligned} k_1 &= k_{\pi\pi} = \frac{1}{2} (S - 4 m_{\pi}^2)^{\frac{1}{2}} \\ k_2 &= k_{K\bar{K}} = \frac{1}{2} (S - 4 m_K^2)^{\frac{1}{2}} \end{aligned} \quad (3.3)$$

are the pion and kaon centre of mass momenta with $S = M_{\pi\pi}^2$ or $M_{K\bar{K}}^2$. Here we neglect the K^+, K^- and K^0, \bar{K}^0 mass difference. We shall study this effect in Chapter V. We introduce the so-called Argand amplitudes by

$$\underline{A} = \underline{k}^{\frac{1}{2}} \underline{T} \underline{k}^{\frac{1}{2}}. \quad (3.4)$$

The normalization of the A amplitudes is such that, with only a single channel open, unitarity gives

$$\text{Im}A = |A|^2 \quad (3.5)$$

The $\pi\pi \rightarrow \pi\pi$, $\pi\pi \rightarrow K\bar{K}$, $K\bar{K} \rightarrow K\bar{K}$ processes are described by

elements

$$\begin{aligned}
 S_{11} &= S(\pi\pi \rightarrow \pi\pi) \\
 S_{22} &= S(K\bar{K} \rightarrow K\bar{K}) \\
 S_{12} &= S_{21} = S(\pi\pi \rightarrow K\bar{K}).
 \end{aligned}
 \tag{3.6}$$

These S matrix elements may be expressed in terms of phases and elasticities by

$$\underline{S} = \begin{pmatrix} \eta e^{2i\delta_1} & i\sqrt{1-\eta^2} e^{i(\delta_1+\delta_2)} \\ i\sqrt{1-\eta^2} e^{i(\delta_1+\delta_2)} & \eta e^{2i\delta_2} \end{pmatrix}
 \tag{3.7}$$

which satisfy the unitarity condition

$$\underline{S} \underline{S}^\dagger = \underline{S}^\dagger \underline{S} = \underline{1}.
 \tag{3.8}$$

The corresponding A matrix can be written using eq. (3.1) and (3.4),

$$\underline{A} = \begin{pmatrix} \frac{\eta e^{2i\delta_1} - 1}{2i} & \frac{\sqrt{1-\eta^2} e^{i(\delta_1+\delta_2)}}{2} \\ \frac{\sqrt{1-\eta^2} e^{i(\delta_1+\delta_2)}}{2} & \frac{\eta e^{2i\delta_2} - 1}{2i} \end{pmatrix}.
 \tag{3.9}$$

The four Riemann sheets are shown in Fig. 3.1; where, for clarity, we show the cuts displaced just below the real axis.

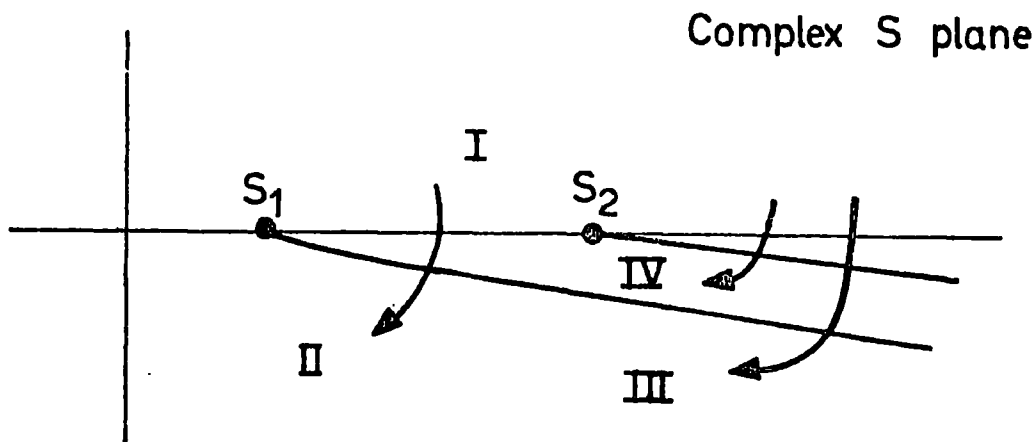


Figure 3.1: The Riemann sheets for the and KK channels. The cuts are displaced just below the real axis for clarity.

Sheets I, II, III, IV correspond to $(\text{Im}k_1, \text{Im}k_2) = ++, -+, --, +-,$ respectively. We refer to the physical sheet as sheet I; the physical amplitudes are evaluated on the upper side of the right hand cuts on this sheet.

A convenient way to guarantee the singularity structure and unitarity properties of S matrix elements is to introduce an analytic function $d(s) = d(k_1, k_2)$ with square root branch points at $k_1 = 0$ and $k_2 = 0$ ^(50, 51). Then if we put

$$S_{11} = \frac{d^{\text{II}}(s)}{d^{\text{I}}(s)} = \frac{d(-k_1, k_2)}{d(k_1, k_2)} \quad (3.10)$$

$$S_{22} = \frac{d^{\text{IV}}(s)}{d^{\text{I}}(s)} = \frac{d(k_1, -k_2)}{d(k_1, k_2)} \quad (3.11)$$

$$S_{11} S_{22} - S_{12}^2 = \frac{d^{\text{III}}(s)}{d^{\text{I}}(s)} = \frac{d(-k_1, -k_2)}{d(k_1, k_2)} \quad (3.12)$$

we find that the S_{1j} ($1, j = 1, 2$) have the correct analytic structure in the physical region. The poles of the S

matrix are caused by the zeros of $d^I(s) = d(s)$. This method can be generalised to many channel cases^(50, 51).

For equal mass particles in each channel we can map the whole four-sheeted s -surface onto a single plane by a conformal transformation⁽⁵⁰⁾. S matrix elements are then expressed as analytic functions on this plane without the threshold cuts. Let us consider the following two successive conformal transformations from s through k_1 to ω :

$$s = 4(k_1^2 + m_\pi^2) \quad (3.13)$$

$$k_1 = \frac{\Delta}{2} \left(\omega + \frac{1}{\omega} \right) \quad (3.14)$$

where

$$\Delta = (m_K^2 - m_\pi^2)^{1/2}, \quad (3.15)$$

in terms of ω and Δ k_2 will be

$$k_2 = \frac{\Delta}{2} \left(\omega - \frac{1}{\omega} \right). \quad (3.16)$$

By these transformations the four Riemann sheets are mapped onto the single " ω -plane". This can be easily seen by considering the inverse transformation:

$$\omega = \frac{1}{\Delta} (k_1 + k_2) \quad (3.17)$$

$$\frac{1}{\omega} = \frac{1}{\Delta} (k_1 - k_2). \quad (3.18)$$

Equations (3.17), (3.18) show that if a point S on sheet I of S - surface is mapped to a point ω on the ω -plane, then the point s on sheet II, (III, IV) is mapped to the point $-\omega^{-1}$, $(-\omega, \omega^{-1})$, (See Fig. 3.2).

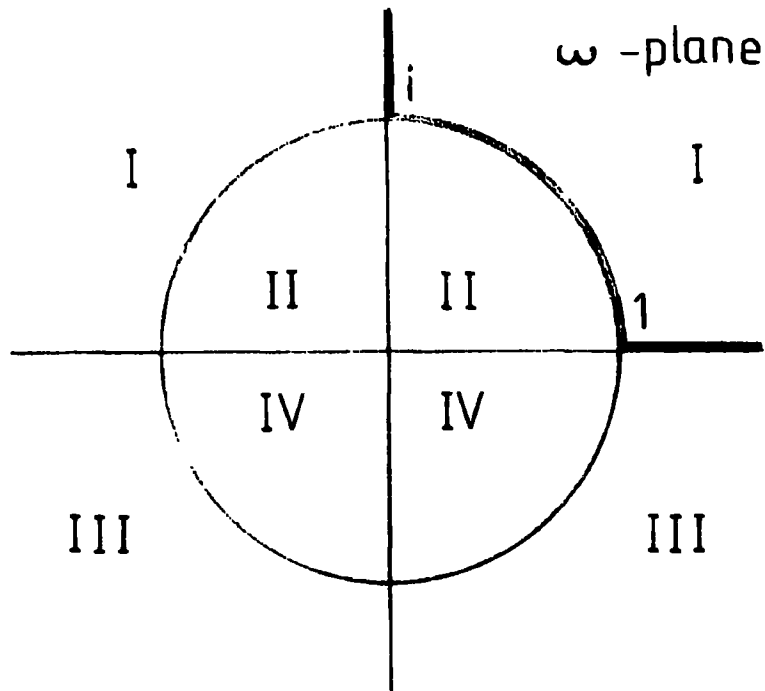


Figure 3.2: Images of the four Riemann sheets on the ω -plane. The bold line is the physical region. The points $i, 1$ on the ω -plane correspond to the first and second threshold points on the s -surface.

On the ω -plane, the S-matrix can be expressed in terms of its poles and zeroes, as well as its unphysical singularities. For such a general expression of the S-matrix, it is difficult to know explicitly what kind of conditions unitarity imposes. However, for practical purposes, it is often quite useful to have an approximate form of the S-matrix which includes only a few relevant poles⁽⁵⁰⁾.

If the S^* is a resonance, we should expect to describe it by the usual two-channel Breit-Wigner form. The S^* is located very near to the $K\bar{K}$ threshold, so we must take carefully into account the opening of the new channel by making the correct analytic continuation across the threshold. This can be achieved by taking

$$\begin{aligned}
 k_2 &= (s - 4m_K^2)^{1/2} / 2 && \text{above threshold} \\
 k_2 &= 0 && \text{at threshold} \\
 k_2 &= +i |k_2| = +i (4m_K^2 - s)^{1/2} / 2 && \text{below threshold (3.19)}
 \end{aligned}$$

The two-channel Breit-Wigner form corresponds to choosing

$$d(s) = m^2 - s - i(\gamma_1 k_1 + \gamma_2 k_2) \quad (3.20)$$

where m is the mass of the resonance, and $\gamma_{1,2}$ are the couplings to the $\pi\pi$ and $K\bar{K}$ channel respectively. The Breit-Wigner amplitudes, constructed from eq. (3.20), have two poles, one on sheet III and the other on either sheet II or IV. We can prove this easily by working on the ω -plane; the reality condition of the amplitude requires that any pole off the real axis is accompanied by its complex conjugate one. This means, a pole ω_r in the complex ω -plane is accompanied by a pole at $-\omega_r^*$. If we write (50,52,53)

$$d(s) = d(\omega) = \omega^{-2} (\omega - \omega_r) (\omega + \omega_r^*) (\omega - \omega_s) (\omega + \omega_s^*) \quad (3.22)$$

with the restrictions imposed by asymptotic behaviour of the S-matrix and unitarity

$$\rho \equiv |\omega_s| = |\omega_r|^{-1} > 1 \quad (3.22)$$

and,

$$A < 0, \quad |B| < |A| \quad (3.23)$$

where

$$A = \sin(\arg(\omega_s))$$

$$B = \sin(\arg(\omega_r)).$$

We can see that $d(\omega)$ in (3.21) is equal to $d(s)/\Delta^2$ of eq. (3.20). ($\Delta^2 = m_K^2 - m_\pi^2$). The m and $\gamma_{1,2}$ of eq. (3.20) are given by

$$\begin{aligned}
 m^2 &= 4 m_k^2 + \Delta^2 [(\rho - \rho^{-1})^2 + 4AB] \\
 \gamma_1 &= 2 \Delta (\rho - \rho^{-1}) (A - B) \\
 \gamma_2 &= 2 \Delta (\rho + \rho^{-1}) (A + B).
 \end{aligned}
 \tag{3.24}$$

The conditions (3.22) and (3.23) show that the pole ω_s should be on sheet III, while ω_r is either on sheet II or IV, (See Figure 3.2).^{†)} When a resonance occurs well above both thresholds, only the sheet III pole is manifest in the amplitudes. However when a resonance happens to be near a threshold, both of the poles play crucial role.

It is possible to describe the S^* effect in terms of "the $K\bar{K}$ scattering length", as an alternative parametrization. To recall the definition of the scattering length, let us assume there is only one channel open. The $L = 0$ amplitude is of the form

$$A = \frac{S - 1}{2i} = \frac{e^{2i\delta} - 1}{2i} = \frac{1}{\cot \delta - i}. \tag{3.25}$$

We can expand the " $\cot \delta$ " in the "zero effective range approximation" as⁽⁵⁴⁾,

$$k \cot \delta = \frac{1}{a} + \dots \tag{3.26}$$

where a is the scattering length. Similarly in the two channel case we can write

$$A_{22} = \frac{\eta e^{2i\delta_2} - 1}{2i} = \frac{e^{2i\Delta_2} - 1}{2i} = \frac{1}{\cot \Delta_2 - i} \tag{3.27}$$

†)

One can see from eq. (3.21) that the amplitude has four poles not two, but poles ω and $-\omega^*$ are described by the same parameters, therefore in eq. (3.21) there are only two independent poles. Here we are talking about these two independent poles.

where

$$\Delta_2 = \delta_2 - \frac{i}{2} \ln \eta .$$

In the zero effective range approximation:

$$k_2 \cot \Delta_2 = \frac{1}{\alpha} + \dots \quad (3.28)$$

where α is the complex scattering length of the second channel. If we write A_{22} in terms of α , we have

$$A_{22} = \frac{\alpha k_2}{1 - i\alpha k_2} .$$

We shall see that the amplitude will have a pole at

$$k_2 = -i / \alpha \quad (3.29)$$

on the sheet II. If $|\alpha|$ is large, the pole is near the second threshold, ($k_2 \approx 0$). This could happen in the $S^{\bar{K}}$ case; a large $K\bar{K}$ scattering length would give a sheet II pole very near the threshold and this pole can show itself as the $S^{\bar{K}}$ effect. Note that here we are dealing only with a single pole, (and its complex conjugate one), there is no nearby sheet III poles.

As we discussed in the previous section, the $S^{\bar{K}}$ is located on a large background which could be interpreted as a resonance, in the $\pi\pi$ channel. Therefore we have to parametrize the $S_{\pi\pi}^{I=0}$ amplitude by two overlapping structures. There are several ways to achieve this but none of them can serve perfectly. The most convenient way is to use eqs (3.10)-(3.12), employing a $d(s)$ function which can describe the overlapping structures. A suitable $d(s)$ function can be determined phenomenologically or from a dynamical model. For the dynamical determination, it is convenient to use the multi-channel \underline{N} over \underline{D} formalism, in which $d(s)$ can be

taken to be $\det \underline{D}$. We can write the S wave \underline{T} matrix of eq. (3.1) in the form:

$$\underline{T} = \underline{N} \underline{D}^{-1} \quad (3.30)$$

where \underline{N} has the left-hand cuts, arising from the crossed channels, and \underline{D} has the right-hand threshold cuts. In many channel cases, the normalisation of \underline{T} is such that:

$$\text{Im} \underline{T} = \underline{T}^* \underline{S} \underline{T} \quad , \quad (3.31)$$

with

$$S_{ij} = \theta(s - s_i) k_i \delta_{ij} \quad (3.32)$$

where s_i are the threshold points and k_i are the corresponding momenta. Using eqs. (3.29), (3.30)

$$\text{Im} \underline{D} = - \underline{S} \underline{N} \quad . \quad (3.33)$$

One of the most important questions of elementary particle theory is whether the low-energy mesons are predominantly $(q\bar{q})$ composites as in the naive quark model or whether some, or all are predominantly (meson-meson) states, as in the old "bootstrap" type models. If the mesons are $(q\bar{q})$ states, then in a many-channel model they would have to be inserted as CDD poles, since the quarks are permanently confined; they will never enter into an S-matrix description. However it may be possible to take a contrary view here: In the work on baryon resonances by Gustafson et al⁽⁵⁵⁾, who explicitly calculate the left hand cuts, it is claimed that the low-energy states are (meson-baryon) composites and that no CDD poles are required. This appears to rule out the

possibility that those baryons are (qqq) states as in the simple quark model. A similar argument is also possible for mesons; resonances could be predominantly (meson-meson) states and in the quark scheme we have to treat them as (qqq \bar{q}) states. Even within a particular realisation of the quark model this problem is not solved. For instance in the MIT bag model of mesons, in addition to the (q \bar{q}) states, there are (qq $\bar{q}\bar{q}$) states with similar masses^(6,7). Therefore it will be useful to consider different possible structures of the resonances and see to what extent the data can distinguish between them. This should help illuminate the nature of low-energy resonances.

Here we consider three different dynamical models for the S^* and the background (the ξ meson) to parametrize the $\pi\pi \rightarrow \pi\pi$, $\pi\pi \rightarrow K\bar{K}$ S wave in the $K\bar{K}$ threshold region. We also discuss two phenomenological parametrizations, one of which gives physical mass and couplings of S^* and ξ , and the other which explores the two-channel zero-effective-range approximation.

I) Exchange Model

In this model we assume that the amplitudes are dominated by forces in the $\pi\pi$ and $K\bar{K}$ channels, together with a coupling between them. We parametrize the diagonal elements of \underline{D} by linear functions of s and the off-diagonal elements by constants. We add appropriate threshold terms, multiplied by arbitrary constants. Thus

$$\underline{D} = \begin{pmatrix} S_\xi - s - i\gamma_1 k_1 & A - iB k_1 \\ C - iD k_2 & S_\eta - s - i\gamma_2 k_2 \end{pmatrix} \quad (3.35)$$

which corresponds to an \underline{N} given by

$$\underline{N} = \begin{pmatrix} \gamma_1 & B \\ 0 & \gamma_2 \end{pmatrix} .$$

We calculate $\underline{T} = \underline{N} \underline{D}^{-1}$ and impose the condition $T_{12} = T_{21}$. This yields

$$B = D , \quad C = [\gamma_1 A - B(S_E - S_R)] / \gamma_2 . \quad (3.36)$$

Thus, for $\det \underline{D}$ we have the 6-parameter form

$$d(s) \equiv \det \underline{D} = (S_E - s - i\gamma_1 k_1)(S_R - s - i\gamma_2 k_2) - \frac{1}{\gamma_2} (A - iB k_1) [\gamma_1 A - B(S_E - S_R) - i\gamma_2 B k_2] . \quad (3.37)$$

In the limit in which the $\pi\pi \rightarrow K\bar{K}$ coupling is ignored this model permits a resonance in $\pi\pi$ and one in $K\bar{K}$. The former, which we identify with the ξ , gives the background to the $S^{\bar{K}}$ state in the $K\bar{K}$ channel.

II) Mixed Model

Here we permit an ξ background in the $\pi\pi$ state as before, but we do not include any forces in the $\pi\pi \rightarrow K\bar{K}$ or $K\bar{K} \rightarrow K\bar{K}$ amplitudes. Instead we include a $q\bar{q}$ channel in which there is a bound state. Thus

$$\underline{D} = \begin{pmatrix} S_E - s - i\gamma_1 k_1 & 0 & A - iB k_1 \\ 0 & 1 & C - iD k_2 \\ E & F & S_3 - s \end{pmatrix} . \quad (3.38)$$

We have ignored the threshold terms in the $q\bar{q}$ channel since we assume that these are sufficiently distant not to affect the results. When we impose $T_{12} = T_{21}$ we find

$$B = 0, \quad D = -\gamma_1 A F / E. \quad (3.39)$$

We can therefore write

$$d(s) = \det \underline{Q} = (S_\varepsilon - s - i\gamma_1 k_1)(S_R - s - i\gamma_2 k_2) - AE \quad (3.40)$$

which has five effective parameters (S_ε , $S_R \equiv S_3 - CF$, γ_1 , $\gamma_2 \equiv \gamma_1 AF^2/E$, AE).

We see that this model is identical to model I except that it has the additional restriction that B of model I is zero.

III) Quark Model

Here we ignore all forces in the meson channels and we treat the $\pi\pi \rightarrow q\bar{q}$ coupling to lowest significant order. It is convenient to include two $q\bar{q}$ channels (e.g. \underline{a}_1 and $\underline{8}$ of SU(3)) and parametrize each as a linear function of s.

Thus we put

$$\underline{Q} = \begin{pmatrix} 1 & 0 & A + iBk_1 & C + iDk_1 \\ 0 & 1 & E + iFk_2 & G + iHk_2 \\ I & J & S_3 - s & Y \\ K & L & X & S_4 - s \end{pmatrix}. \quad (3.41)$$

Provided we do not go beyond second order off-diagonal terms, we obtain

$$d(s) = \det \underline{Q} = (s^2 - as + b + ik_1(c + ds) + ik_2(e + fs)) \quad (3.42)$$

where a, b, c, d, e, f are six real constants. Although they both have six parameters, (3.37) and (3.42) are different. In particular (3.42) does not allow any term of the form $(ik_1)(ik_2)$.

IV) Breit-Wigner and Background

This model has been used by several authors to determine the S^* parameters^(11,46,52,53). The idea is to modify the Breit-Wigner $d(s)$ function in eq. (3.20) to allow a background effect. This can be achieved by choosing the $d(s)$ function to have the factorized form:

$$d(s) = d^R(s)d^B(s). \quad (3.43)$$

In this form we can separate out S^* and the background. $d^R(s)$ is given by (3.20). $d^B(s)$ can be parametrized in several ways. Here we choose to parametrize $d^B(s)$ in terms of an elastic $\pi\pi$ resonance (the ξ meson).

$$d^B(s) = \frac{m_\xi^2}{m_\xi^2 - s - i\gamma_\xi k}. \quad (3.44)$$

V) Constant Inverse K Matrix

Let us consider the one-channel zero effective range approximation (see eq. (3.26)). If we write $M = 1/\alpha$ in eq. (3.26), then the amplitude in eq. (3.25) would be

$$A^{-1} = M/k - i.$$

If we generalize this to the two-channel problem

$$\underline{A}^{-1} = \underline{M} \underline{k}^{-1} - i \underline{1},$$

thus we would get the usual \underline{M} matrix parametrization of the amplitudes,

$$\underline{A} = \underline{k}^{1/2} (\underline{M} - i \underline{k})^{-1} \underline{k}^{1/2}. \quad (3.45)$$

In the zero-effective-range approximation, all the elements of $\underline{M} = \underline{k}^{-1}$ matrix are taken to be real constants. The $K\bar{K}$ scattering length defined in eq. (3.28) is given in terms

of M_{ij} by

$$\alpha = \frac{M_{11} - i k_1'}{\det \underline{M} - i k_1' M_{22}} \quad (3.46)$$

where $k_1' = k_1 (s=4m_K^2)$. In this formalism the $d(s)$ function would be

$$d(s) = \det(\underline{M} - i \underline{k}) = (M_{11} - i k_1)(M_{22} - i k_2) - M_{12}^2 \quad (3.47)$$

This 3-parameter description can provide a sheet II pole and the large background phase. For instance, the $\pi\bar{\pi} \rightarrow \pi\bar{\pi}$ S matrix element can be written

$$S_{11} = \left(\frac{k_R^* - i k_2}{k_R - i k_2} \right) \left(\frac{M_{11} + i k_2}{M_{11} - i k_1} \right) \quad (3.48)$$

where

$$k_R = \frac{1}{\alpha} = M_{22} - \frac{M_{12}^2}{M_{11} - i k_1} \quad (3.49)$$

In equation (3.48), the first term can give the sheet II pole, while the second term supplies the large $\pi\pi$ background phase provided $|M_{11}| \ll k_1$.

3.3 $\pi\pi \rightarrow \pi\pi (K\bar{K})$ Coupled Channel Analysis in the S^* Region

In order to study the properties of the S^* we have performed a coupled channel analysis by fitting $\pi\bar{\pi}$ and $K\bar{K}$ production amplitudes direct to $\pi^-\rho \rightarrow \pi^+\pi^-\eta$ (16) and $\pi^-\rho \rightarrow K^+K^-\eta$ (47, 56) data. We have used t -channel $\pi^+\pi^-$ moments for $\pi^-\rho \rightarrow \pi^+\pi^-\eta$ (with $-t < 0.15$ GeV²) in 20 MeV bins through the mass range $0.8 < M_{\pi\pi} < 1.2$ GeV (see Figure 3.3). We have ignored the amplitudes produced by A_1 exchange, which have been shown to

be negligible in the small t -region by an analysis of $\pi^- p \rightarrow \pi^+ \pi^- n$ polarization data⁽⁵⁷⁾. For $\pi^- p \rightarrow \kappa^+ \kappa^- n$ we have used the t -channel moments obtained at 6 GeV/c by the Argonne EMS group⁽⁴⁷⁾.

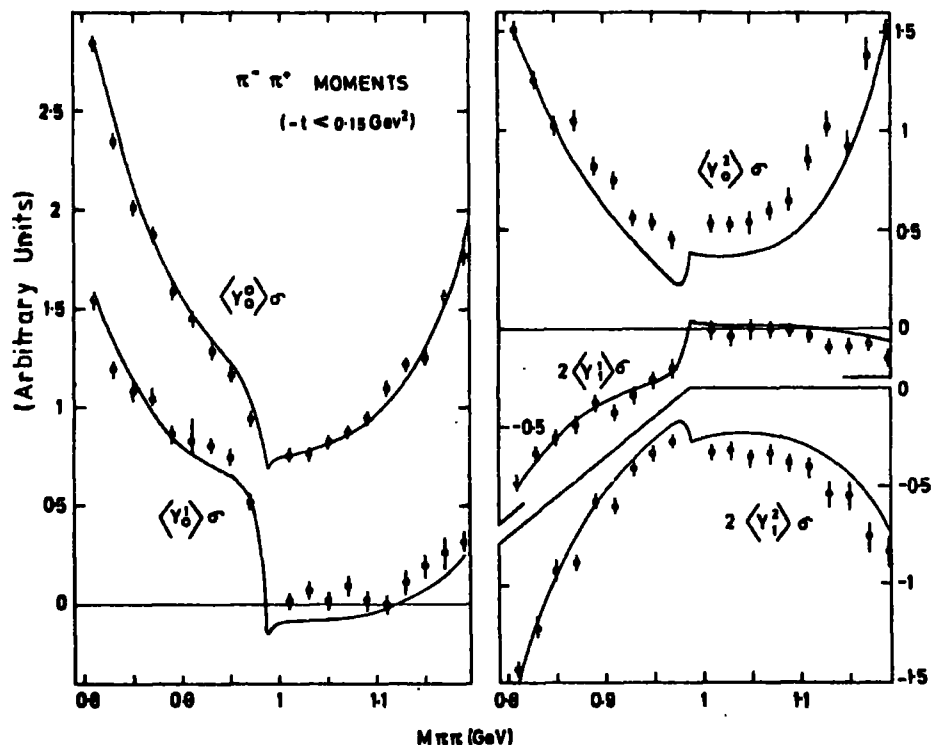


Figure 3.3: The mass spectra of the unnormalised $\pi\pi$ moments in the region $0.8 < M_{\pi\pi} < 1.2$ GeV. Here $\sigma = N$ of eq. (2.14). The data are that of the CERN-Münich 17.2 GeV/c $\pi^- p \rightarrow \pi^- \pi^+ n$ experiment (16), integrated over the t range $t_{min} < -t < 0.15$ GeV². The curves are the fit using model I.

($-t < 0.08$ GeV²) and at 18.4 GeV/c by the CERN-Münich collaboration⁽⁵⁶⁾ ($-t < 0.2$ GeV²). The exchange mechanisms are more complicated in this reaction (compare Tables 2.2 and 2.3) and to study the $M_{\kappa\bar{\kappa}}$ dependence it is desirable to consider data extrapolated to the π -exchange pole. Such a cross-section extrapolation has been done by the

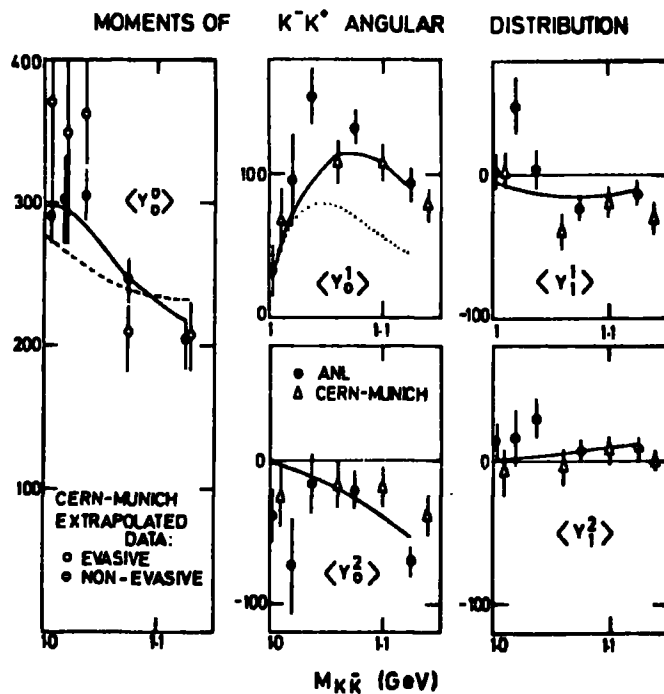


Figure 3.4: The t -channel moments of the K^-K^+ angular distribution in the process $\pi^-p \rightarrow K^-K^+n$. Here $\langle Y_m^l \rangle \equiv \mathcal{N} \langle Y_m^l \rangle$ in arbitrary units. The data for $\langle Y_0^0 \rangle$ were obtained by the CERN-Munich group by extrapolating the cross section to the π -exchange pole (56). All the other moments shown are normalized to these (non-evasive) extrapolated values. The curves correspond to the fit of model I (the dotted curve for $\langle Y_1^0 \rangle$ is obtained if the β tail phase is input). The dashed curve for $\langle Y_0^0 \rangle$ is the fit using the constant M matrix, model V.

CERN-Munich group⁽⁵⁶⁾, and so we normalized all the observed moments to these values. The moments obtained in this way are shown in figure 3.4.

We have analysed the data using the "Ochs-Wagner" method^(32, 33). That is we have written the $\pi\bar{\pi}$ and $K\bar{K}$ production amplitudes in terms of π exchange via Chew-Low formulae in the form:

$$L_0 \equiv H_{++0}^{L(+)} = C_N \frac{M}{\sqrt{k_1}} \cdot A^L$$

$$L_- \equiv H_{++1}^{L-(-)} = \sqrt{L(L+1)} L_0 / C(M)$$

$$|L_+| \equiv |H_{++1}^{L+(-)}| = |L_-| \quad (3.50)$$

Here we neglect the A_2 exchange. The observation of $\langle Y_{M>1}^3 \rangle = 0$ leads us to assume $|L_+| = |L_-|$. We use $L = S, P, D, F$ for $L = 0, 1, 2, 3$ production amplitudes of the $\pi\pi(K\bar{K})$ system, C_N is the overall normalization factor, M is the effective $\pi\pi(K\bar{K})$ mass, and $C(M)$ is a real function of M , (see Section 2.3 and eq. (2.41)). The isospin decomposition of the amplitudes of $\pi^+\pi^- \rightarrow \pi^+\pi^-$ is

$$A^L = \frac{2}{3} A_L^0 + \frac{1}{3} A_L^2 \quad \text{for } L \text{ even}$$

$$A^L = A_L^1 \quad \text{for } L \text{ odd,} \quad (3.51)$$

and that for $\pi^+\pi^- \rightarrow K^+K^-$ is

$$A^L = \frac{1}{\sqrt{3}} A_L^0 \quad \text{for } L \text{ even}$$

$$A^L = \frac{1}{\sqrt{2}} A_L^1 \quad \text{for } L \text{ odd,} \quad (3.52)$$

where A_L^I are given by equation (3.9). We have fixed C_N for the $\pi\pi$ system by requiring $|A_1^1(\pi\pi)| = 1$ at the ρ peak, and for $K\bar{K}$ fixing the ρ meson $\pi\pi/K\bar{K}$ couplings at their $SU(3)$ value and fitting the $\langle Y_0^4 \rangle$ moment for $\pi^-\rho \rightarrow K^+K^-n$. We parametrized $C(M)$ as a quadratic function of M in each channel. We give the list of density matrix elements in terms of the $L_{0\pm}$ amplitudes in Appendix VI.

The observable $\pi\bar{n}$ and $K\bar{K}$ moments can be expressed in terms of $L(\pi\pi \rightarrow \pi\bar{n})$ and $L(\pi\bar{n} \rightarrow K\bar{K})$ using the relations

given in Appendices I and VI. For each reaction we have fitted the observed unnormalised moments $N \langle Y_M^J \rangle$ with $J \leq 2$, $M \leq 1$, in terms of S, P and D production amplitudes. A small contribution to $\pi\pi$ production from the g resonance tail was also included. We fixed the A_1^1 and A_2^0 amplitudes using ρ and ω resonant forms with the relative $\pi\pi / K\bar{K}$ couplings fixed at their SU(3) values. We fixed the A_0^2 amplitude in terms of the elastic phase

$$\delta_0^2 = 8.9 - 31.3 M_{\pi\pi}$$

and set

$$A_2^2 \equiv 0.$$

We have investigated the $I = 0$ S wave parametrizations discussed in Section 3.2 by fitting to the data keeping the other partial waves fixed. The curves on Figs. 3.3 and 3.4 correspond to the best fit obtained using the model I parametrization, eq. (3.37). The parameters obtained are

$$\begin{aligned} S_R &= 0.94 \pm 0.08 & \gamma_2 &= 0.94 \pm 0.03 \\ S_E &= 1.4 \pm 0.9 & \gamma_1 &= 9 \pm 10 \\ A &= -0.22 \pm 0.42 & B &= 0.06 \pm 0.55 \end{aligned} \quad (3.53)$$

in units of GeV. There are systematic discrepancies in the description of some of the $\pi\pi$ moments which may be due to using fixed Breit-Wigner forms to describe the tails of the ρ and ω resonances. Similar systematic misfits in this region were also found⁽³²⁾ in the CERN-München phase-shift analysis based on resonance parametrizations. In the fit we allowed the P wave phase $\delta_1^1(\pi\pi \rightarrow K\bar{K})$ to be free. We found that it is in agreement with that predicted by the tail of the ρ resonance just above the $K\bar{K}$ threshold,

but by $M_{K\bar{K}} = 1.1$ GeV that it needed to be some 30° larger. If $\delta_1^1(\pi\pi \rightarrow \kappa\bar{\kappa})$ is assumed to be given by the ρ tail, and the other parameters left unchanged, then the dotted curve is obtained for $N\langle Y_0^1 \rangle$ for $K\bar{K}$ production, (see Fig. 3.4).

The values of four of the six parameters of model I, eq. (3.53), are poorly determined and suggest that the $I = 0$ S wave is over-parametrized. S_ρ is badly determined because γ_1 is large and the parameters are strongly correlated. As expected from the values of B in eq. (3.53), model II, which has this $B = 0$, gives essentially the same fit. Moreover, the model IV, equation (3.43), with four effective parameters $S_R = m_{S^*}^2$, $\gamma_1 = g_{\pi\pi}^2$, $\gamma_2 = g_{\kappa\bar{\kappa}}^2$ and δ_B^{\dagger} also gives an essentially identical fit, with

$$\begin{aligned} M_{S^*} &= 0.978 \pm 0.05 & g_{\pi\pi}^2 &= 0.199 \pm 0.014 \\ \delta_B(1\text{ GeV}) &= 86.5^\circ & g_{\kappa\bar{\kappa}}^2 &= 0.792 \pm 0.099 \end{aligned} \quad (3.54)$$

in units of GeV. The conventional $\pi\pi$ partial width is

$$\Gamma_{\pi\pi}^{S^*} = (95 \pm 7) \text{ MeV}. \quad (3.55)$$

We have found that model III, equation (3.42), was ruled out by the data since it is unable to reproduce the necessary background in the $\pi\pi$ channel. Also the constant $M = K^{-1}$ matrix parametrization was unable to give a satisfactory fit to the data. The best fit, using equation (3.47), had

$$M_{11} = 0.095, \quad M_{22} = -0.045, \quad M_{12} = 0.163 \quad (3.56)$$

†)

In practice δ_B was parametrized in terms of a broad elastic $\pi\pi$ resonance. The best values were $m_\rho = 1.1$, $g_{\pi\pi}^2 = 3.7$ with large, strongly correlated errors.

in units of GeV. It gave the behaviour of $N\langle Y_0^0 \rangle$ for $K\bar{K}$ production shown by the dashed line in Fig. 3.4. However in this parametrization we were able to fit $K\bar{K}$ $N\langle Y_0^1 \rangle$ keeping $\delta_1^1(\pi\bar{\pi} \rightarrow K\bar{K})$ as given by the \mathcal{P} tail.

In this case there is only a nearby sheet II pole, and the absence of a nearby sheet III pole does not allow $N\langle Y_0^0 \rangle$ to decrease rapidly enough with increasing $M_{K\bar{K}}$. (52)

The $I = 0$ S wave amplitudes obtained in the fits are shown in the Argand plots of Figure 3.5. There is no ambiguity in the sign of the S wave $A_{12}^{I=0}$ since the interference with the resonance tail contributions is compatible with the $K\bar{K}$ production data provided $g_{K\bar{K}}^{S^*} / g_{\pi\pi}^{S^*}$ is positive (46). In Table 3.1 we show the S^* pole positions corresponding to the various parametrizations. We notice that the sheet II pole position is very stable to changes of the parametrization. In order to check this stability, we have also fitted the data, parametrizing the $I = 0$ S wave directly in terms of its poles (plus background) on ω -plane (53). We again found the same sheet II pole position.

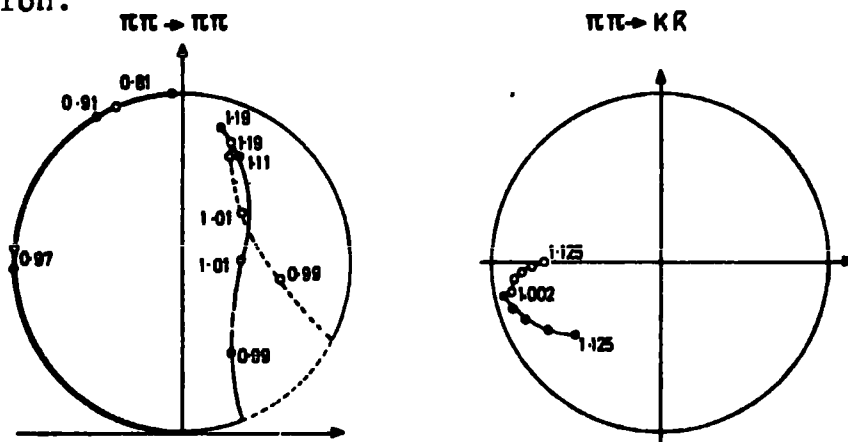


Figure 3.5: The Argand plots of the $L = 0$ A_{11} and A_{12} respectively. The continuous curves, with the mass marked in GeV, are the S wave amplitudes obtained in the fit using Model I. The dashed curve (open points) correspond to Model V. The unmarked points for $\pi\pi \rightarrow K\bar{K}$ correspond to $M_{K\bar{K}} = 1.02, 1.0375, 1.075$ GeV respectively.

In Table 3.1 we also give the ratio of the S^* couplings to the two channels, defined as $|T_{22} / T_{11}|$ at the sheet II pole position and $K\bar{K}$ scattering length for model V, as defined in eq. (3.46).

Model	Sheet II	Sheet III	$(g_{\pi\pi}^{S^*} / g_{K\bar{K}}^{S^*})^2$
I) Exchange	0.997 - i 0.017 $\pm 0.002 \pm 0.002$	0.837 - i 0.148 $\pm 0.013 \pm 0.008$	4.0
II) Mixed	0.996 - i 0.017 $\pm 0.002 \pm 0.001$	0.835 - i 0.146 $\pm 0.008 \pm 0.005$	3.9
IV) Bre. Wig.	0.996 - i 0.016 $\pm 0.003 \pm 0.002$	0.876 - i 0.077 $\pm 0.010 \pm 0.008$	4.0
V) M Mat.	0.988 - i 0.012 $\pm 0.003 \pm 0.002$	$\alpha = -9.2 + i 10.1$	

Table 3.1: The S^* pole positions and couplings, the $K\bar{K}$ scattering length in units of GeV.

The S^* is also evident in the $\pi\pi$ spectrum observed in the reaction $K^- p \rightarrow \pi^- \pi^+ (\Lambda, \Sigma^0)$ ⁽⁵⁸⁾. The data with the ρ tail subtracted ⁽⁵⁸⁾ are shown in Fig. 3.6 together with our predictions for the shape of the spectrum.

We have proposed forms of parametrization of the coupled channel ($\pi\pi, K\bar{K}$) $I = 0$ S wave which allow for the presence of overlapping S^* and ξ resonances and permit an investigation of the nature of these mesons. We found that model III (the quark model) is not able to fit the data. This shows, it is not possible to explain these mesons as only $(q\bar{q})$ states and forces in the meson-meson

($qq\bar{q}\bar{q}$) sector are also important. We also saw that models I and II are overparametrized. Indeed, in the relevant range of $M_{\pi\pi}$ it is possible to describe the $I = 0, S$ wave with only four parameters ($m_{S^*}, g_{\pi\pi}^{S^*}, g_{K\bar{K}}^{S^*}, \delta_B$). Although the results support model II (mixed model), within the range of the analysis, the data does not contain enough information to study the quark structure of S^* and ξ in detail. Even the determination of the ξ parameters is not possible. Similar analyses over a wider range of $M_{\pi\pi}$ may be informative, but small changes of the higher partial waves effect the $I = 0 S$ wave structure drastically. Therefore it is better to study the $I = 0 S$ wave further where it is dominant, i.e. in $\pi\pi \rightarrow K\bar{K}$ channel.

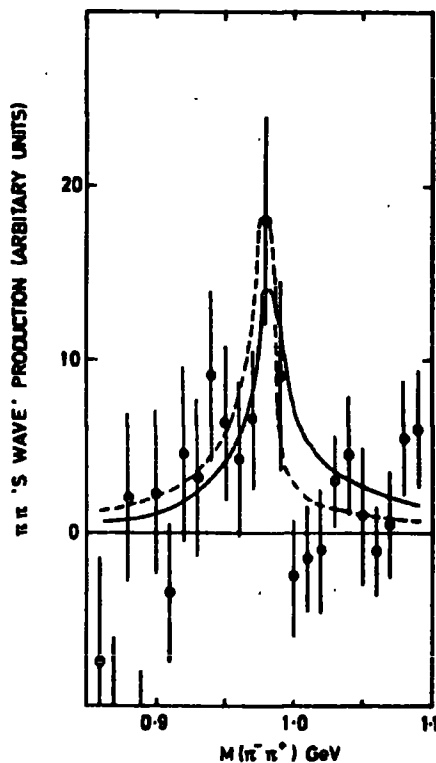


Figure 3.6: The $\pi^-\pi^+$ mass distribution observed in $K^-\rho \rightarrow \pi^-\pi^+(\Lambda, \Sigma^0)$ in the S^* region with the background and ρ resonance events subtracted (58). The continuous curve corresponds to the prediction for Model I and the dashed curve to that for model V.

We found that the sheet II S^* pole is determined by the data accurately, independent of the form of the parametrization. The data favour the two-pole (Breit-Wigner) description of the S^* . However this is not compatible with prediction of ρ tail $\delta_1^1(\pi\pi \rightarrow \kappa\bar{\kappa})$ phase. It is interesting to note that the single sheet II pole description (constant M matrix) is compatible with the ρ tail $\delta_1^1(\pi\pi \rightarrow \kappa\bar{\kappa})$ phase. But with a single sheet II pole we cannot observe the normal resonance behaviour of $I = 0$, $S(\pi\pi \rightarrow \kappa\bar{\kappa})$, (see in Fig. 3.5 open circles of $\pi\pi \rightarrow \kappa\bar{\kappa}$).

CHAPTER IV

Analysis of the $\pi^- p \rightarrow (K^- K_s^0) p$ Reaction

4.1 Introduction

The high statistics data for the reaction $\pi^- p \rightarrow K^- K^0 p$ allow a study of the meson spectrum that is more selective than that for $K^+ K^-$, $K^0 \bar{K}^0$ production. The $K^- K^0$ channel has isospin 1 and is thus accessible to even spin states of odd G-parity (such as the $\delta(0^{++})$, $A_2(0^{++})$) and to odd spin states of even G-parity (such as the $g(3^{--})$), (see equation (2.3)). The data that are available on $K^- K_s^0$ production, therefore complement the information available from the $K^+ K^-$, $K_s^0 K_s^0$, $\pi^+ \pi^-$, $\pi^0 \pi^0$ production data.

The even and odd G-parity $K^- K^0$ states are produced by different exchange mechanisms. The allowed natural and unnatural parity exchanges (denoted by NPE and UPE) are shown in Table 2.4. From studies of the SU(3)-related reactions $KN \rightarrow (K\pi)N$ we expect isoscalar NPE (pomeron, f , and ω exchange) and isovector UPE (π exchange) to be dominant^(59, 60, 61). The possibility of pomeron exchange means that at high energies even L $K^- K^0$ states should be more copiously produced than those with odd L.

The $K^- K^0$ production data is very important as far as the 0^{++} mesons are concerned. The properties of the recently observed S wave enhancement at around $M_{KR} \approx 1.3$ GeV is not certain^(9, 10). Although it has peak in the

small t region, its t -dependence is different from π -exchange. In addition to this, the interference between isoscalar and isovector ($K\bar{K}$)S waves has a distinctive t -dependence in this region⁽¹⁹⁾. An amplitude analysis of K^-K^0 production data can answer the question of whether the $M_{K\bar{K}} \approx 1.3$ GeV S wave enhancement has an $I = 1$ component and if it has, how big this component is.

To extract the $\pi^-p \rightarrow K^-K^+p$ amplitudes from the experimental moments we use the combination of helicity amplitudes with definite asymptotic exchange naturality (i.e. eq. (2.23)). Introducing the spectroscopic notation, we write

$$|L_{0; \pm}|^2 = |H_{+-0; 1}^{L \pm}(t)|^2 + |H_{++0; 1}^{L \pm}(t)|^2 \quad (4.1)$$

The interference terms can be rewritten in the form

$$\text{Re}(L'L^*) = |L'| |L| (\xi \cos \phi)_{L'L} \quad (4.2)$$

where ξ is the degree of nucleon spin coherence ($0 \leq \xi \leq 1$) and ϕ is the relative phase between amplitudes L' and L .

4.2 Amplitude Analysis in the A_2 Mass Region

The t structure of the observed K^-K^0 t -channel moments in the A_2 mass region, $1.2 < M_{K\bar{K}} < 1.4$ GeV, is shown in Fig. 4.1. The five largest moments $N\langle Y_{0,0}^{4,2,0} \rangle$, $N\langle Y_{2,2}^{4,2} \rangle$ show the dominance of the NPE amplitude $H_{++1}^{2+(4)} \equiv D_+$, and indicate that all other amplitudes will be much less reliably determined. The non-zero $N\langle Y_{3,3}^4 \rangle$ moment is attributable to interference of D_+ with the helicity-two NPE amplitude of D_{2+} . The structure of $N\langle Y_{0,2}^3 \rangle$ can be accounted for by P_+D_+ interference and show no evidence for

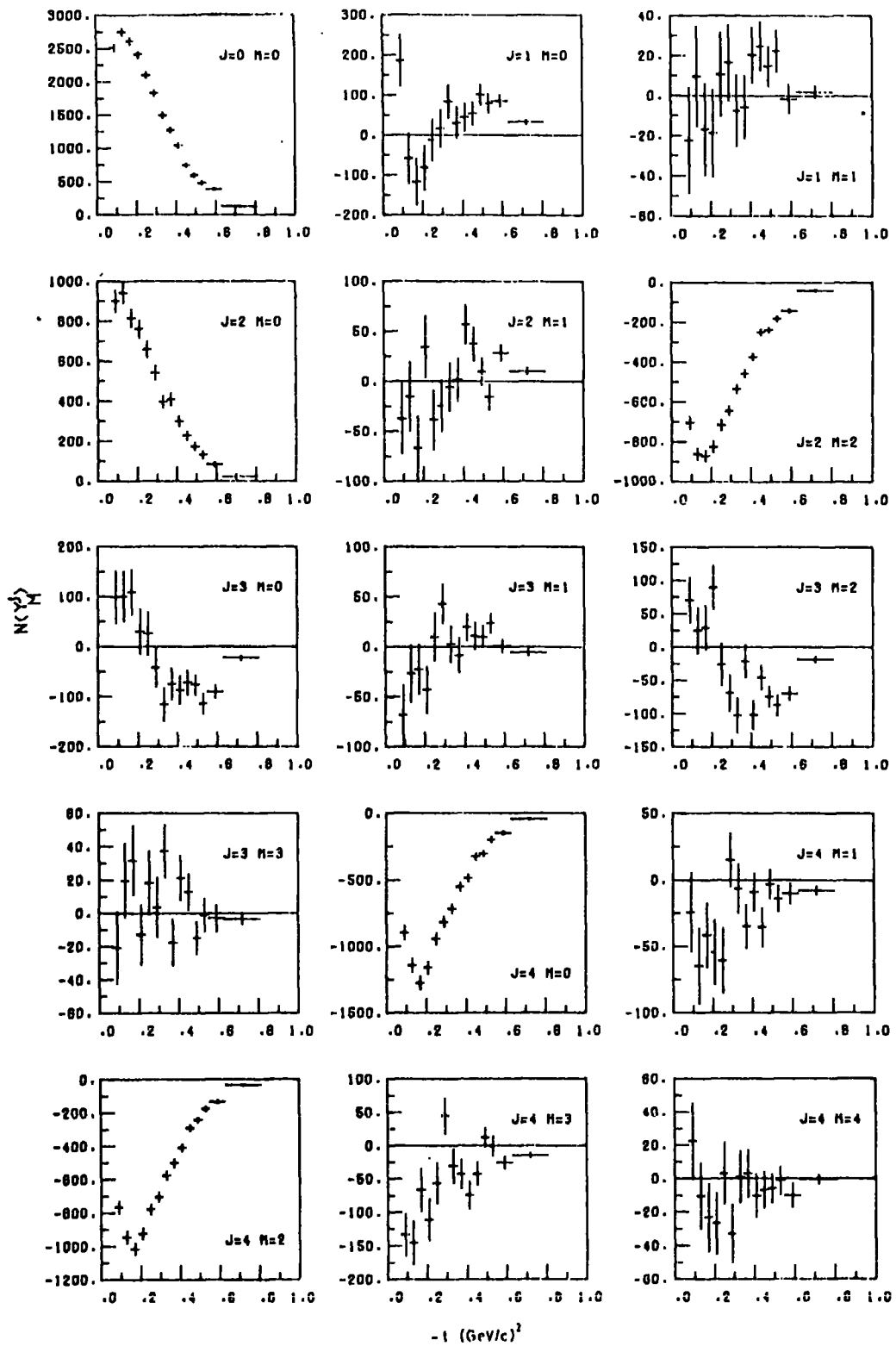


Figure 4.1: Corrected spherical harmonic moments of the angular distribution of the K^- , in the t_0 channel helicity rest frame of the produced K^-K^0 system, as a function of t in the A_2 mass region, $1.2 < M_{K^-K^0} < 1.4 \text{ GeV}$. The data are for $\bar{p}p \rightarrow K^-K^0p$ at $10 \text{ GeV}/c$.

a $P_0 D_0$ interference effect. The UPE amplitudes are much harder to isolate. The moments $N\langle Y_1^4 \rangle$ and $N\langle Y_1^3 \rangle$, taken together with $N\langle Y_3^4 \rangle$, imply small $D_0 D_-$ interference, but a larger $S_0 D_-$ contribution. There is no evidence of either a P_0 or P_- effect, except possibly $S_0 P_0$ interference in the first t-bin of $N\langle Y_0^1 \rangle$.

As a result of these observations we performed an amplitude analysis of the $J \leq 4, M \leq 4, N\langle Y_M^J \rangle$ moments in the A_2 mass region in terms of the magnitudes and coherences of the NPE amplitudes D_+, D_{2+}, P_+ and of the UPE amplitudes D_0, D_-, S_0 . Neglect of P_0, P_- means the moments $N\langle Y_1^{3,1} \rangle$ are not included in the analysis, and as $N\langle Y_3^3 \rangle$ is also compatible with zero we do not determine the $P_+ D_{2+}$ coherence. Moreover the data cannot determine reliably the individual coherences in the weak UPE sector. We therefore assume nucleon spin coherence and, motivated by π - B exchange degeneracy, $(\omega \rightarrow \phi)_{D_0 D_-} = -1$.

The relations between amplitudes and moments have been given in Appendices I and VI. We list the contributions of D_{2+} below:

$$\begin{aligned} N\langle Y_3^3 \rangle &= -1.134 \operatorname{Re}(P_+ D_{2+}^*) \\ N\langle Y_4^4 \rangle &= -0.597 |D_{2+}|^2 \\ N\langle Y_3^4 \rangle &= -0.845 \operatorname{Re}(D_+ D_{2+}^*). \end{aligned} \quad (4.3)$$

Some other moments also have contributions involving D_{2+} :

$$\begin{aligned}
 N \langle Y_0^0 \rangle &: |D_{2+}|^2 \\
 N \langle Y_1^1 \rangle &: 1.095 \operatorname{Re}(P_+ D_{2+}^*) \\
 N \langle Y_2^0 \rangle &: -0.639 |D_{2+}|^2 \\
 N \langle Y_2^1 \rangle &: 0.783 \operatorname{Re}(D_+ D_{2+}^*) \\
 N \langle Y_3^0 \rangle &: -0.293 \operatorname{Re}(P_+ D_{2+}^*) \\
 N \langle Y_3^1 \rangle &: 0.143 |D_{2+}|^2 \\
 N \langle Y_3^2 \rangle &: -0.319 \operatorname{Re}(D_+ D_{2+}^*) . \quad (4.4)
 \end{aligned}$$

The results are shown in Fig. 4.2. We see the expected dominance of the NPE amplitude, D_+ , in $\pi^- p \rightarrow A_2^- p$. The clear $N \langle Y_3^1 \rangle$ signal is described by a D_{2+} contribution of approximately 10% the magnitude of D_+ . The suppression of the UPE D wave amplitudes (associated with B, Z exchange) is to be compared with their relatively stronger π exchange structure in $K^+ p \rightarrow K^*(1420)^+ p$, (see Fig. 4 of Ref. (59)).

We may compare the values of $|D_0|$ of Fig. 4.2 with those obtained from charge-exchange A_2^0 production. Data are available for $\pi^+ n \rightarrow A_2^0 p$ at 4 GeV/c⁽⁶²⁾, and for $\pi^- p \rightarrow A_2^0 n$ at 12 and 15 GeV/c⁽⁶³⁾. We interpolated the measured t-channel partial cross-sections $\int_{0_0}^D d\sigma/dt$ using the form $\rho_{\text{Lab}}^{2-2\alpha}$ with $\alpha(t) = -0.2 + 0.8t$. To convert to $|D_0|^2$ we included a 4.7% $A_2 \rightarrow K\bar{K}$ branching ratio⁽³⁷⁾, we multiplied by $\frac{1}{2}$ due to isospin, and corrected to a $1.2 < M_{K\bar{K}} < 1.4$ mass interval. The values obtained for $|D_0|$ at $p_L = 10$ GeV/c are indicated by the dashed line on Fig. 4.2. The agreement between $|D_0|$ obtained from charge-exchange and non-charge-exchange reactions means that there is no evidence for isoscalar UPE in $\pi^- p \rightarrow A_2^- p$.

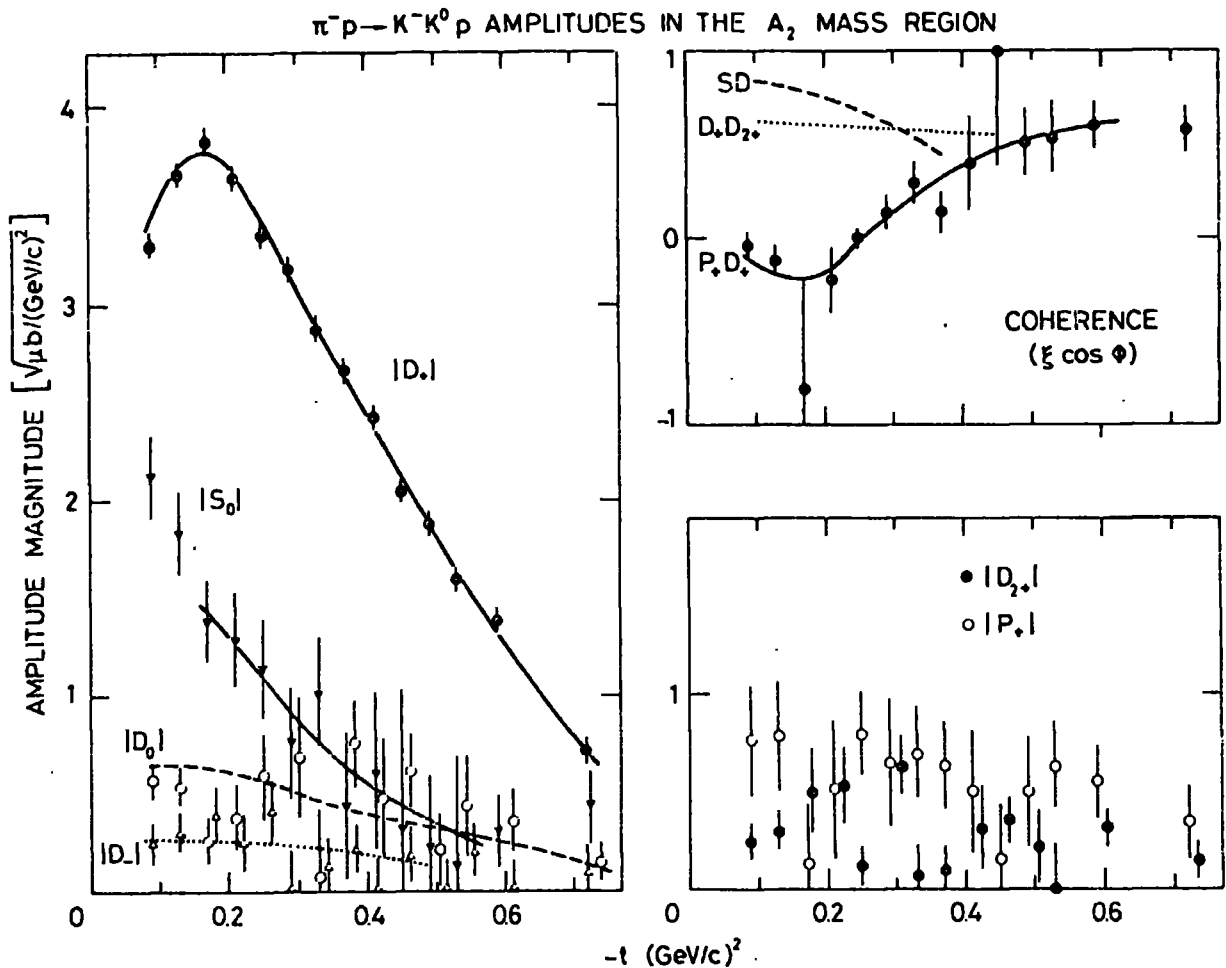


Figure 4.2: The 10 GeV/c $\pi^- p \rightarrow K^- K^0 p$ amplitudes in the A_2 mass region. The curve of $|D_0|$ shows the prediction obtained CEX A_2^0 production (62, 63). The coherences $S D_+$ and $-S D_-$ are assumed equal, and are denoted SD. The SD and $D_+ D_{2+}$ coherences are not well determined and the curves only indicate the trend of the results.

An interesting feature of this analysis is the importance of S wave K^-K^0 production in the A_2 mass region (see Fig. 4.2). In general, it is difficult to extract lower partial waves, and to study the reliability of this determination of S_0 we repeated the analysis with P_0 included, together with $P_- \equiv -0.5 P_0$, but with S_0 omitted. The description of the moments was again reasonable, though not quite as good as that with S_0 included and P_0 omitted. Essentially the only change in the amplitude components shown in Fig. 4.2 is that $|S_0| \rightarrow |P_0|$ and, of course, no SD interference. There are indicators that the solution with large S_0 is the physical one. First, by comparing to ω exchange for $K_p \rightarrow K^*(890)p$, and by comparing the P wave background in the g region (see the next section), there are indications that $|P_0| \lesssim |P_4|$. Second by comparing K^+K^- (19) and $K_s^0K_s^0$ (9) production data (in particular the equality of the $N\langle Y^2 \rangle$ moments) it has been noted that the P wave π -exchange amplitude is small in our mass range. Quantitatively we find this P_0 cannot account for the required UPE contribution needed in K^-K^0 production. For these reasons we favour the K^-K^0 amplitude solution with the relatively large S_0 and a small P_0 contribution. Even if the two most forward points shown for $|S_0|$ are over-estimated, due to the omission of a possible P_0 contribution which peaks at small t (π -exchange) and due to large acceptance corrections, the t -structure still implies a strong non-flip component (Z -exchange) in S_0 at small t . This suggests that the bump observed in the S wave at $M_{KR} \approx 1.3$ GeV in K^+K^- and $K_s^0K_s^0$ has a rather large $I = 1$ component.

A_2 production by NPE in the process $\pi^- p \longrightarrow A_2^- p$ proceeds via pomeron and f exchange. A comparison with $K^*(1420)$ diffractive production can give valuable information on \mathbb{P} and f exchange. We may write the D_+ amplitude

$$D_+(A_2) = \mathbb{P} + f. \quad (4.5)$$

This contribution to the differential cross-section for A_2 production, $|D_+(A_2)|^2$, is shown in Fig. 4.3. It is obtained from $D_+(K^-K^0)$ of Fig. 4.2 after correction for (i) the unseen A_2 decay modes (using an $A_2 \longrightarrow K\bar{K}$ branching ratio of 4.7%), and (ii) for the finite mass interval (1.2-1.4 GeV) using an A_2 Breit-Wigner form.

This can be compared with $K^*(1420)$ production isolated from the related $K^\pm p \longrightarrow K^0 \pi^\pm p$ reactions. High statistics data for these latter processes have been taken at the same beam energy. These data were analysed⁽⁵⁹⁾ to determine the $K^0 \pi^\pm$ production amplitudes in the mass region $1.34 < M_{K\pi} < 1.5$ GeV and $K^*(1420)$ production was also found to proceed dominantly via the NPE amplitudes $D_+(K^* \pi^\pm)$. The differential cross-sections for $K^*(1420)$ production, or more precisely $|D_+|^2$, are also plotted in Fig. 4.3, after correction for the unseen^{†)} $K^*(1420)$ decay modes and for the finite mass bin. The crossover at $-t = 0.3$ GeV² has been interpreted in terms of the pomeron, f and ω exchange contributions,⁽⁶⁰⁾

$$D_+(K^{*\pm}) = \gamma \mathbb{P} + \beta (f \mp \omega) \quad (4.6)$$

where the coefficients γ and β are introduced as we define \mathbb{P} and f by eq. (4.5). Before confronting the data, it

†) We include a factor 3/2 to allow for $K^* \longrightarrow K^\pm \pi^0$, and use a $K^* \longrightarrow K\pi$ branching ratio of 56.1%.

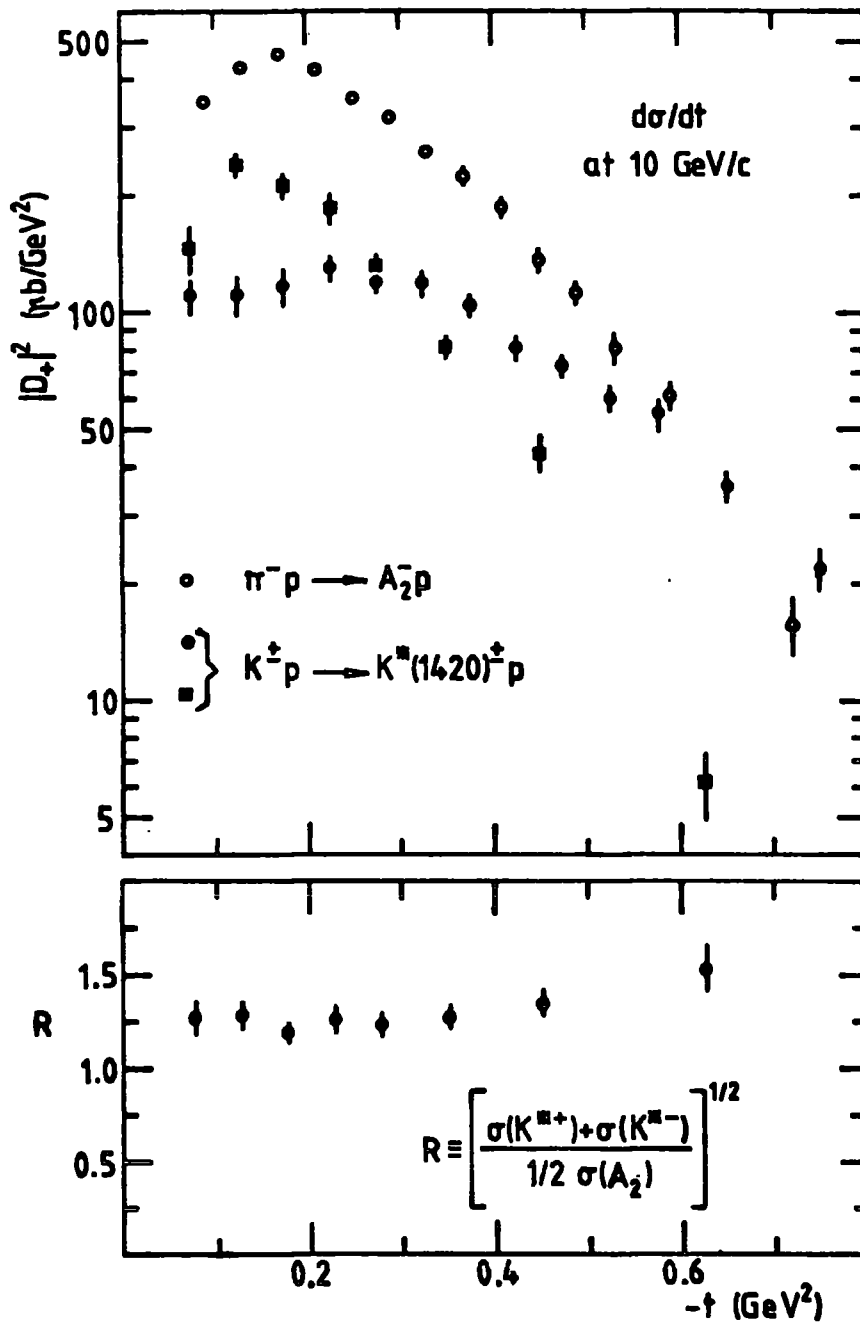


Figure 4.3: The NPE cross-sections, $|D_{+}|^2$ for $\pi^- p \rightarrow A_2^- p$ and $K^\pm p \rightarrow K^*(1420)^\pm p$ at 10 GeV/c. The cross sections are corrected for the unseen decay modes and for the tails of the Breit-Wigner distributions outside the fitted mass intervals. This latter correction is a factor 1.50 and 1.52 for the A_2 and $K^*(1920)$ mass intervals respectively. The ratio R is discussed in section 4.2.

is informative to anticipate values of the coefficients γ and β . From SU(3)-invariance and magic f, f' mixing we expect $\beta = 1/2$. To estimate the relative coupling of the pomeron, γ , we may use the f, f' -dominated pomeron hypothesis⁽⁶⁴⁾. According to this scheme^(65,66)

$$\gamma = \frac{1}{2} (1 + r) \quad \text{with} \quad r(t) = \frac{\alpha_P - \alpha_f}{\alpha_P - \alpha_{f'}} \quad (4.7)$$

where $\alpha_i(t)$ are the usual trajectory functions. In the symmetry limit $r = 1$, and the pomeron is an SU(3)-singlet. The departure of r from 1 represents the effect of SU(3) mass breaking.

To facilitate the comparison of A_2 and $K^{*}(1420)$ production we plot in Fig. 4.3, the ratio

$$R \equiv \left[\frac{\sigma(K^{*+}) + \sigma(K^{*-})}{\sigma(A_2)/2} \right]^{1/2} \quad (4.8)$$

versus t , where we used the differential cross-sections $\sigma \equiv d\sigma/dt \equiv |D_+|^2$, shown in the upper part of the figure. We have used the sum of K^{*+} and K^{*-} cross-sections to remove the interference contributions between the even (\mathbb{P}, f) and odd (ω) G-parity exchanges. If we assume $|\omega|^2$ is small compared to $|\mathbb{P} + f|^2$, then R is an indicator of the relative strength of the pomeron and f contributions. If the processes are dominated by pomeron exchange then we expect that $R \approx 1 + r$, whereas if f exchange is dominant we expect $R \approx 1$. From Fig. 4.3 we see that $R = 1.25$, with a small error, for $-t < 0.4 \text{ GeV}^2$. Suppose, for example, at $-t = 0.2 \text{ GeV}^2$ that $r(t) \approx 0.5$ and that the relative pomeron- f phase is 60° . Then this value of R implies that the $\mathbb{P} : f$ contribution is 1:1 in $\pi^- p \rightarrow A_2^- p$, and is 1.5:1 in $K p \rightarrow K^*(1420) p$ at 10 GeV/c.

4.3 Amplitude Analysis in the g Meson Region

The t structure of the moments of the K^-K^0 angular distribution in the g mass region, $1.55 < M_{KK} < 1.85$ GeV, is shown in Fig. 4.4. The data do not allow a full amplitude determination. We use the t -channel moments $N\langle Y_M^J \rangle$ with $J \leq 8$, $M = 0, 2$ to determine the magnitudes and coherences of the NPE amplitudes L_+ , and of the UPE amplitudes L_0 , with $L \leq 4$. We are led to this simplification by the results in the A_2 mass region. From the A_2 analysis we expect that L_+L_{2+}' interference terms will contribute to the $M = 1$ moments at least as strongly as L_0L_{-}' interference terms. The data are unable to determine both L_- and L_{2+} . However these small amplitudes only contribute quadratically to the $M = 0, 2$ moments and so it should be reliable to use these moments to determine the more dominant L_0 and L_+ amplitudes.

The $N\langle Y_{0,2}^6 \rangle$ moments show that g resonance production proceeds mainly by UPE (F_0), and to a much lesser extent by NPE (F_+). The dominance of the $N\langle Y_2^4 \rangle$ and $N\langle Y_2^2 \rangle$ moments, as compared to the other $M = 2$ moments, indicates a very strong D_+ component in the g region. Moreover the $J = 8$ moments suggest that $L = 4$ (K^-K^0) production by NPE exchange (G_+) must be included in this mass interval. The presence of sizeable D_+ and G_+ amplitudes make the determination of $|F_+|$ very difficult. The difficulty is apparent from the expression for the $J = 6, M = 2$ moment

$$N\langle Y_2^6 \rangle = -0.431 |F_+|^2 - 0.258 |G_+|^2 - 0.844 \operatorname{Re}(D_+ G_+^*).$$

The "background" amplitudes, D_+ and G_+ , are associated with pomeron exchange and are therefore enhanced relative to the ω -exchange resonant amplitude F_+ .

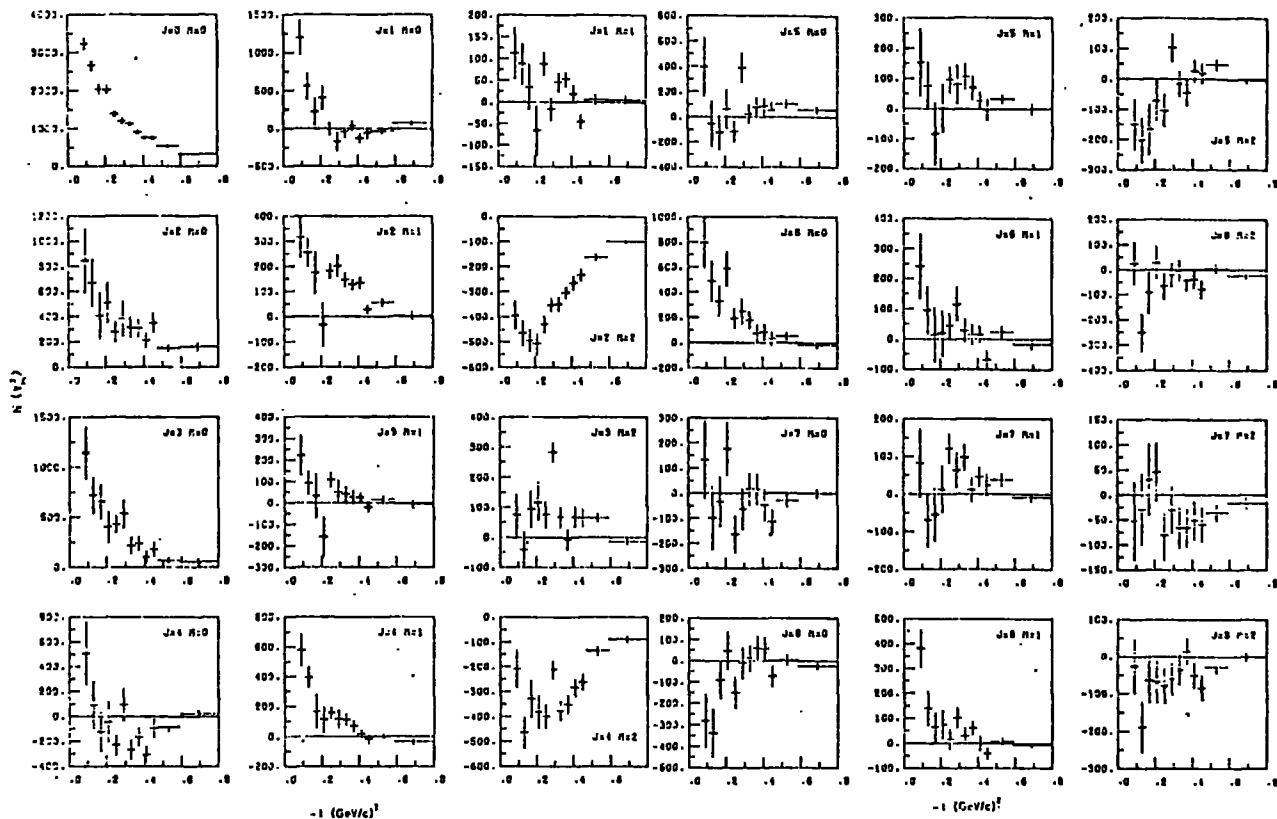


Figure 4.4: As for Fig. 4.1, but in the ρ meson mass region, $1.55 < M_{K\bar{K}} < 1.85$ GeV.

There is no evidence for the $L = 4$ UPE amplitude G_0 , either from Fig. 4.4 or from the moments as a function of the produced K^-K^0 mass (see Fig. 4.7). If we compare $|D_+|$ and $|D_-|$ in Fig. 4.2 for A_2 production, since $L = 2$ and $L = 4$ amplitudes are produced by the same exchange mechanism, we expect a very small G_0 in comparison to G_+ . We therefore set $G_0 = 0$, and include only $J \geq 7$ moments with $M = 2$ in the analysis.

In each t -bin we use the $J \leq 8$, $M = 0, 2$ moments to determine the magnitudes and relative phases of the amplitudes within the NPE sector (P_+ , D_+ , F_+ , G_+) and within the UPE sector (S_0 , P_0 , D_0 , F_0). For each t -bin all the solutions are enumerated using the Barrelet zeros technique⁽⁶⁷⁾. The detailed explanation of our method is given in Appendix VII. In each t interval we selected the physical solution by imposing the continuity of the imaginary parts of zeros as a function of t and by requiring amplitude magnitudes consistent with the presence of the A_2 and g resonances. The ambiguity is essentially only in the lower partial waves; in particular for the $S, P_{0,+}$ and D_0 amplitudes. We note also, that the analysis assumes, within each sector, that the amplitudes have a common coherence factor, ξ . Within the UPE sector there is no reason why this should be correct and so only the dominant UPE coherence may be meaningful. F_0 is the dominant UPE amplitude and the other UPE quantities are much less reliably determined. To sum up, we note that the analysis should be reliable and unambiguous for D_+ , F_+ , G_+ and F_0 .

The results for the g production amplitudes and the D and G waves, together with their respective coherences, are shown in Fig. 4.5. The lower partial waves are, in general, not so well determined and depend on the Barrelet solution that is selected. For our solution the magnitudes of $S_0, P_0; P_+$ are approximately 1.0, 0.6, 0.7 $\sqrt{\mu b} / \text{GeV}$ respectively at $-t = 0.15 \text{ GeV}^2$; and 0.3, 0.1, 0.2 $\sqrt{\mu b} / \text{GeV}$ at $-t = 0.5 \text{ GeV}^2$. The coherence of $S_0 F_0$ is positive for all t , that of $P_0 F_0$ is ~ -0.4 for $-t < 0.3$

$\pi^- p \rightarrow K^- K^0 p$ AMPLITUDES IN THE g REGION

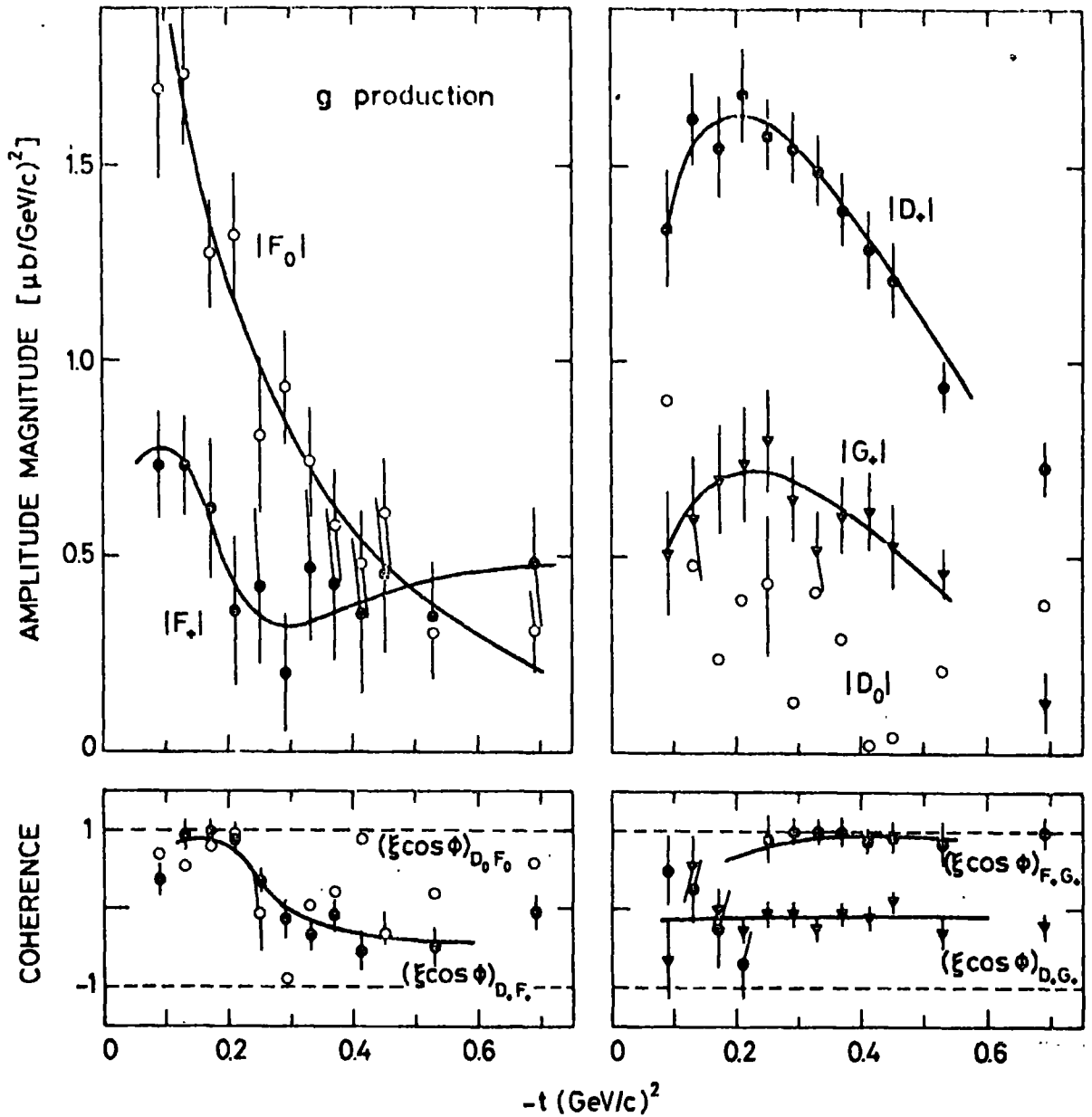


Figure 4.5: The 10 GeV/c $\pi^- p \rightarrow K^- K^0 p$ amplitudes in the g mass region, $1.55 < M_{K^0 K^-} < 1.85$ GeV, obtained from the data of Fig. 4.4. The extreme fluctuations seen in the $3 \leq J \leq 5$ moments at $-t = 0.29$ GeV² were removed before analysis. Only representative errors are shown for $|D_0|$ and the D, F_0 coherence.

GeV² and that of P₊D₊ is negative for all t.

The difference of odd-L and even-L (K⁻K⁰) production mechanisms is strikingly evident in Fig. 4.5 (see Section 2.4.III and Table 2.4). For UPE, the g production amplitude F₀ (π-exchange) dominates the background D₀ amplitude (B, Z exchange). On the other hand for NPE, g production proceeds via F₊ (ω exchange) which is smaller, and of different t structure, than the even-L D₊, G₊ amplitudes (P, f exchange). The expected single-helicity-flip character of the NPE amplitudes is clearly apparent for D₊ and G₊.

The structure of |F₊| for g production may be compared with the ω-exchange contribution isolated from the ρ production reactions

$$\frac{d\sigma_{\omega}(\rho)}{dt} \equiv \frac{1}{2} \left(\rho_{11}^{11} + \rho_{1-1}^{11} \right) \left[\frac{d\sigma}{dt} (\pi^+ p \rightarrow \rho^+ p) + \frac{d\sigma}{dt} (\pi^- p \rightarrow \rho^- p) - \frac{d\sigma}{dt} (\pi^- p \rightarrow \rho^0 n) \right]. \quad (4.9)$$

Following Hoyer et al⁽⁶⁸⁾ we apply finite-mass-sum-rules and two-component duality to relate the ω-exchange contributions to these resonance production reactions at a given energy

$$\frac{d\sigma_{\omega}(\rho)/dt}{d\sigma_{\omega}(\rho)/dt} \approx \left(\frac{m_{\rho}^2}{m_g^2} \right)^{-2} \alpha_{\omega}(t). \quad (4.10)$$

From our results for |F₊| (see Fig. 4.5) we can estimate g production by ω-exchange at 10 GeV/c, provided we are given the g → K \bar{K} branching ratio,

$$\frac{d\sigma_{\omega}(g)}{dt} = |F_+|^2 / [\text{B.R.}(g \rightarrow K\bar{K})]. \quad (4.11)$$

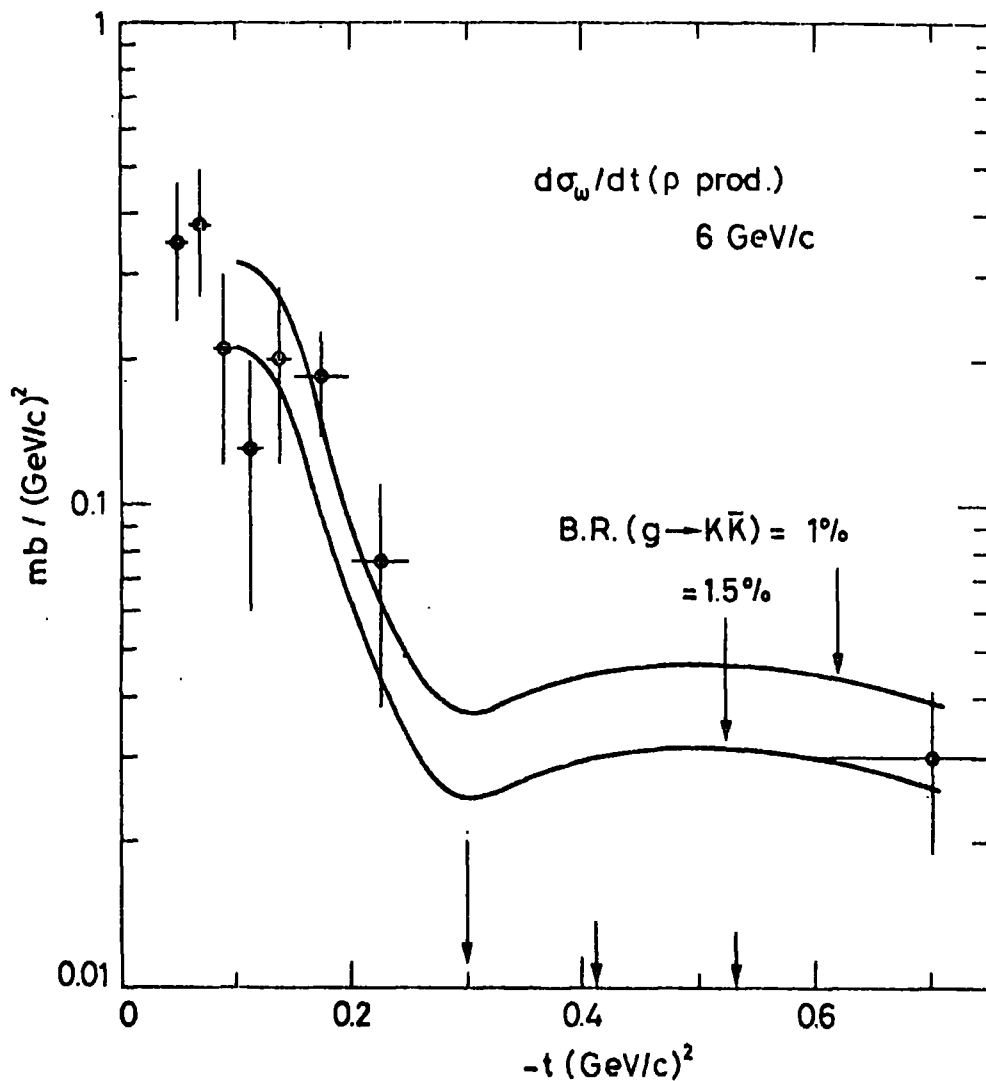


Figure 4.6: Data for ρ production by ω -exchange at 6 GeV/c, taken from ref. (69). The curves are the finite-mass-sum rule predictions, obtained from the g production amplitude F_+ of Fig. 4.5, for two different values of the $g \rightarrow K\bar{K}$ branching ratio.

Taking $\alpha_\omega(t) = 0.4 + 0.9t$ in eq. (4.10), we then calculate $d\sigma_\omega(\rho)/dt$. In figure 4.6 we compare our prediction with 6 GeV/c ρ production data⁽⁶⁹⁾, after allowing for the different beam momenta using the usual $p_L^{2-2\alpha_\omega}$ dependence. The curves, shown for two different $g \rightarrow K\bar{K}$ branching ratios, result from the curve through $|F_+|$ on Fig. 4.5. The comparison, which is most relevant for $0.1 < -t < 0.2 \text{ GeV}^2$, favours a branching ratio

$$\frac{\Gamma(g \rightarrow K\bar{K})}{\Gamma(g \rightarrow \text{all})} \cong 0.015 . \quad (4.12)$$

The 16 GeV/c data for isospin-zero-NPE ρ production⁽⁷⁰⁾ has larger errors but a similar comparison yields compatible results.

The structure of $|F_0|$ of Fig. 4.5 is indicative of π exchange, and the values may be extrapolated to the π pole ($t = m_\pi^2$) to give a more direct determination of the $g \rightarrow K\bar{K}$ branching ratio than that we obtained from $|F_+|$. To do this we use the Chew-Low form (see eq. (2.38))

$$\frac{d\sigma}{dt} = \frac{1}{p_L^2 m_n^2} \frac{G^2}{4\pi} \left[\frac{-t e^{b(t-m_\pi^2)}}{(t-m_\pi^2)^2} \right] (2L+1) \frac{M_{K\bar{K}}^2}{k_{\pi\pi}} |A_L|^2 dM \quad (4.13)$$

with $L = 3$, where $k_{\pi\pi} = (M_{K\bar{K}}^2/4 - m_\pi^2)$, and

$$A_L = \frac{m_R \sqrt{\gamma_{\pi\pi} \gamma_{K\bar{K}}}}{m_R^2 - M_{K\bar{K}}^2 - i m_R \gamma}$$

We integrate over the experimental mass bin 1.55 - 1.85

GeV. The total width of the g resonance is $\Gamma = \Gamma_{\pi\pi} + \Gamma_{K\bar{K}} + \Gamma_{\text{rest}}$

, where

$$\gamma_i(M_{K\bar{K}}) = \Gamma_i \left(\frac{k_i}{k_i^R} \right)^2 \frac{D(k_i^R; R)}{D(k_i; R)}$$

with a barrier factor $D(x) = 225 + 45x^2 + 6x^4 + x^6$ and interaction radius $R = 3.5 \text{ GeV}^{-1}$. We take the mass and width of the g resonance to be $m_R = 1.69 \text{ GeV}$, $\Gamma_i^{\text{tot}} = 0.18 \text{ GeV}$; and the momentum of the other decay channels, in addition to the $\pi\pi$ and $K\bar{K}$ channels, to be represented by $k_0 \equiv k_{K\bar{K}}$. We fit $|F_0|^2$ to eq. (4.13) with $(\Gamma_{\pi\pi}, \Gamma_{K\bar{K}})$ and the slope, b , as free parameters. We omit the point at $-t = 0.09 \text{ GeV}^2$ due to the large acceptance corrections in the near forward direction. The fit is shown by the curve through $|F_0|$ on Fig. 4.5 and corresponds to

$$\sqrt{\Gamma_{\pi\pi} \Gamma_{K\bar{K}}} / \Gamma = 0.056 \pm 0.017$$

$$b = 4.5 \pm 1.1 \text{ GeV}^{-2}.$$

If we take the particle table value of the $g \rightarrow \pi\pi$ branching ratio, $\Gamma_{\pi\pi} / \Gamma = 0.24$, then we find the $g \rightarrow K\bar{K}$ branching ratio is

$$\Gamma_{K\bar{K}} / \Gamma = 0.013 \pm 0.004.$$

This determination is in agreement with the independent estimation $\Gamma_{K\bar{K}} / \Gamma \simeq 0.015$, which we obtained from the NPE amplitude, F_+ .

The above numbers yield a ratio of $K\bar{K}$ and $\pi\pi$ decay modes of the g resonance of

$$\Gamma_{K\bar{K}} / \Gamma_{\pi\pi} = 0.056 \pm 0.017.$$

This is to be compared with the SU(3) prediction value

$$\frac{\Gamma_{K\bar{K}}}{\Gamma_{\pi\pi}} = \frac{1}{2} \left[\frac{k_{K\bar{K}}^R}{k_{\pi\pi}^R} \right]^2 = 0.13.$$

Note that SU(3) comparisons are better satisfied without including barrier factors⁽⁷¹⁾. To agree with the SU(3) prediction, we would have had to input $\Gamma_{\pi\pi} / \Gamma = 0.16$ which would have led to $\Gamma_{K\bar{K}} / \Gamma = 0.02$.

4.4 Amplitudes As a Function of $M_{K\bar{K}}$

Here we analyse the same data as a function of the effective mass of the produced (K^-K^0) system. We use the moments $N \langle Y_M^J \rangle$, of the K^- angular distribution in the t -channel, in 50 MeV intervals over the mass range $1 \leq M_{K\bar{K}} < 2 \text{ GeV}$, integrated over the t interval $0.07 < -t < 1.0 \text{ GeV}^2$,

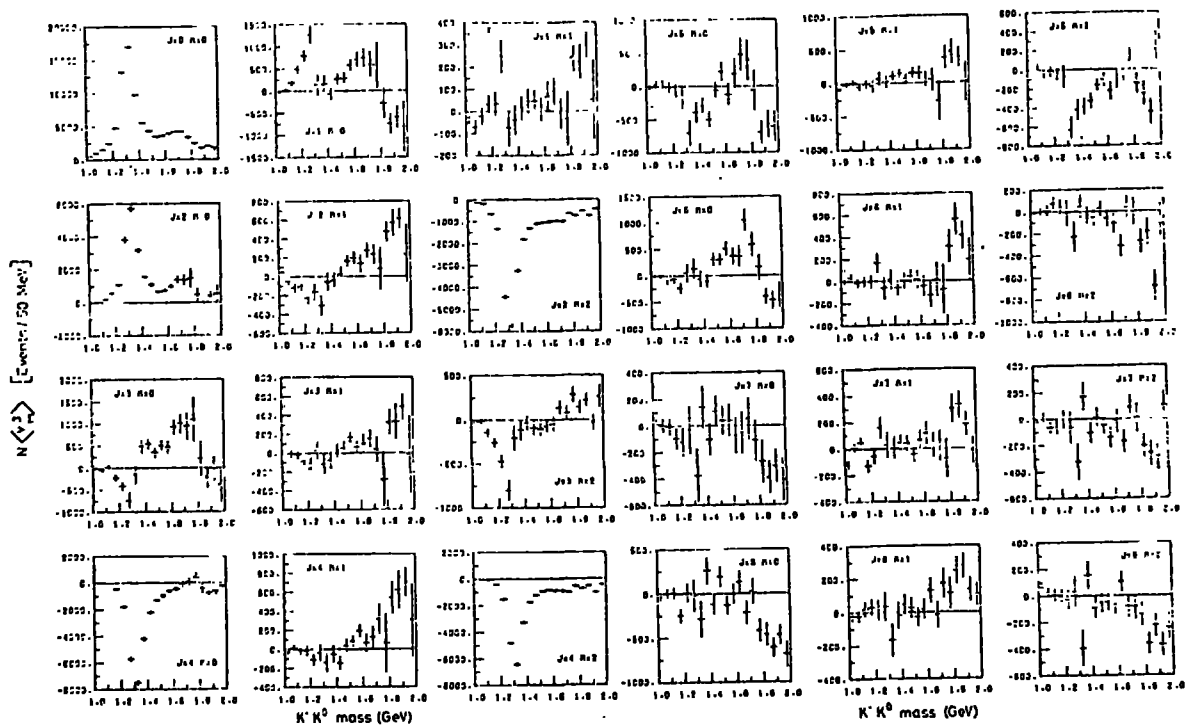


Figure 4.7: The mass spectra of the t -channel acceptance corrected moments for 10 GeV/c $\pi^- p \rightarrow \kappa^- \kappa^0 p$ data, after allowance for the observed $\kappa^0 \rightarrow \kappa^{\pm} \rightarrow \pi^+ \pi^-$ decay. The data are integrated over the t interval $0.07 < -t < 1 \text{ GeV}^2$. The sensitivity of the data is 7671 corrected events per cb .

(see Fig. 4.7). To analyse the data we use the same method to determine the amplitudes as the one we used in the g resonance region. That is, we use the $M = 0, 2$ moments with $J \leq 8$ to determine the magnitudes and relative phases of the amplitudes in the NPE sector (P_+, D_+, F_+, G_+) and in the UPE sector (S_0, P_0, D_0, F_0, G_0) as a function of $M_{K\bar{K}}$ in the range $1 < M_{K\bar{K}} < 2 \text{ GeV}$. The relations among the amplitudes and moments are given in eqs. (4.1), (4.2) and Appendices I and VI. For example, for each mass bin above $M_{K\bar{K}} = 1.8 \text{ GeV}$,

where the amplitudes up to $L = 4$ are required, we use 16 moments to determine 9 amplitude magnitudes and 7 relative phases. In principle, this assumes that, within each sector, the amplitudes have a common coherence factor ξ . There is no certainty that this is correct. However, in practice, at a given mass, often only one interference term is important within each sector, and then the data give a reliable determination of the corresponding spin-phase coherence $\xi \omega \phi$. For example, in the A_2 mass region the data determine $\xi \omega \phi$ for $S_0 D_0$ and $P_+ D_+$ interference.

Even then the amplitude determination is not unique. The data determine only $(\omega \phi)_{L L'}$, and not the relative phases $\phi_{L L'}$, and so there remain discrete ambiguities. At each mass bin we obtain all possible solutions by using the method explained in Appendix VII. We find that the amplitude G_0 , describing $L = 4$ $K^- K^0$ production by UPE, is compatible with zero. This can be anticipated by inspection of the $N \langle Y_{0,2}^8 \rangle$ moments. In the results presented below we have therefore set $G_0 \equiv 0$. For $M_{K\bar{K}}$ below 1.7 GeV we fix G_+ to be given by the tail of a spin four resonance and fit only moments with $J \leq 7$. For $M_{K\bar{K}}$ below 1.5 GeV we fix the $L = 3$ amplitudes, F_0 and F_+ , to be given by the tail of the g resonance and fit only moments with $J \leq 5$. The resonance forms are normalised to fit the amplitude determinations in the higher mass bins. We tabulate all the allowed solutions in each mass bin. In the majority of mass bins these solutions give an

†) The value represents the spin-phase coherence averaged over the t interval of the data, $0.07 < -t < 1 \text{ GeV}^2$.

essentially exact description of the data. In all but the mass bin about 1.325 GeV (see the data fluctuations in Fig. 4.7) and those above 1.85 GeV the fits have an acceptable χ^2 . In Figs. 4.8 and 4.9 we present the solution that is selected at each mass bin by requiring:

- i) the dominance of S_0 just above the K^-K^0 threshold (the higher partial waves should be suppressed by the factor of $(k_{K\bar{K}})^L$ in this region),
- ii) The continuity of $\text{Im}\mathcal{Z}$; (UPE sector) and $\text{Im}\mathcal{Z}'_1$ (NPE sector) as a function of the K^-K^0 effective mass,
- iii) amplitude behaviour consistent with the presence of the A_2 and g resonances.

Leading resonant waves are essentially unchanged in magnitude by Barrelet transformations and the third criterion is mainly helpful off resonance. The first two criteria eliminate an alternative solution with P_0 similar in magnitude and structure to that shown for S_0 below 1.4 GeV (see Fig. 4.9) and with S_0 smaller and structureless.

Above $M_{K\bar{K}} = 1.6$ GeV we see the emergence of $L = 4$ K^-K^0 production. Unfortunately the data do not allow reliable partial-wave analysis above 2 GeV so as to establish a resonance shape for G_+ . However, support for resonance identification comes from the behaviour of the D_+G_+ interference contribution. This is the dominant interference term in this mass range and, moreover, both $L = 2$ and $L = 4$ K^-K^0 states have the same production mechanisms. The behaviour of $(\omega \rightarrow \phi)_{D_+G_+}$ should therefore reproduce $\omega \rightarrow (\delta_2 - \delta_4)$, where δ_L are the $I = 1$ $K\bar{K}$

decay phases. Assuming δ_2 is given by the tail of the A_2 , we see that the behaviour of $\int \cos \phi$, as a function of $M_{K\bar{K}}$, gives further confirmation of the spin 4 resonance of mass $M \sim 1.9$ GeV reported by the Geneva group⁽⁷²⁾.

4.5 Conclusions

Here we summarize the main results of our study of K^-K^0 production data in A_2 and g resonance mass regions and as a function of $M_{K\bar{K}}$ in the range $1 < M_{K\bar{K}} < 2$ GeV by the reaction $\pi^- p \rightarrow K^- K^0 p$ at 10 GeV/c:

1. We find A_2 production proceeds dominantly by NPE. The t-channel D_+ amplitude is dominant, but a non-zero $N\langle Y_3^4 \rangle$ signal leads to a D_{2+} contribution which is, on average 10% of $|D_+|$. The curves shown through the $|D_+|$ and $|D_0|$ amplitudes in Fig. 4.8 and 4.9 correspond to A_2 Breit-Wigner fit with

$$\begin{aligned} m_{A_2} &= 1.318 \pm 0.001 \text{ GeV}, \\ \Gamma_{A_2} &= 0.113 \pm 0.004 \text{ GeV} \end{aligned} \quad (4.14)$$

with interaction radius $R = 3.5 \text{ GeV}^{-1}$.

2. The UPE amplitude D_0 is consistent in magnitude and t structure with that found in CEX A_2^0 production, and lends support to the assumption that UPE is dominantly isovector in $\pi^- p \rightarrow A_2^- p$.
3. S wave K^-K^0 production is important in the A_2 region, the t structure implying a strong non-flip component at small t (Z exchange). Both the t and $M_{K\bar{K}}$ structure of S_0 amplitude suggest the existence of an $I = 1, J^{PC} = 0^{++}$ resonance under the A_2 . We call it $\delta'(1300)$.

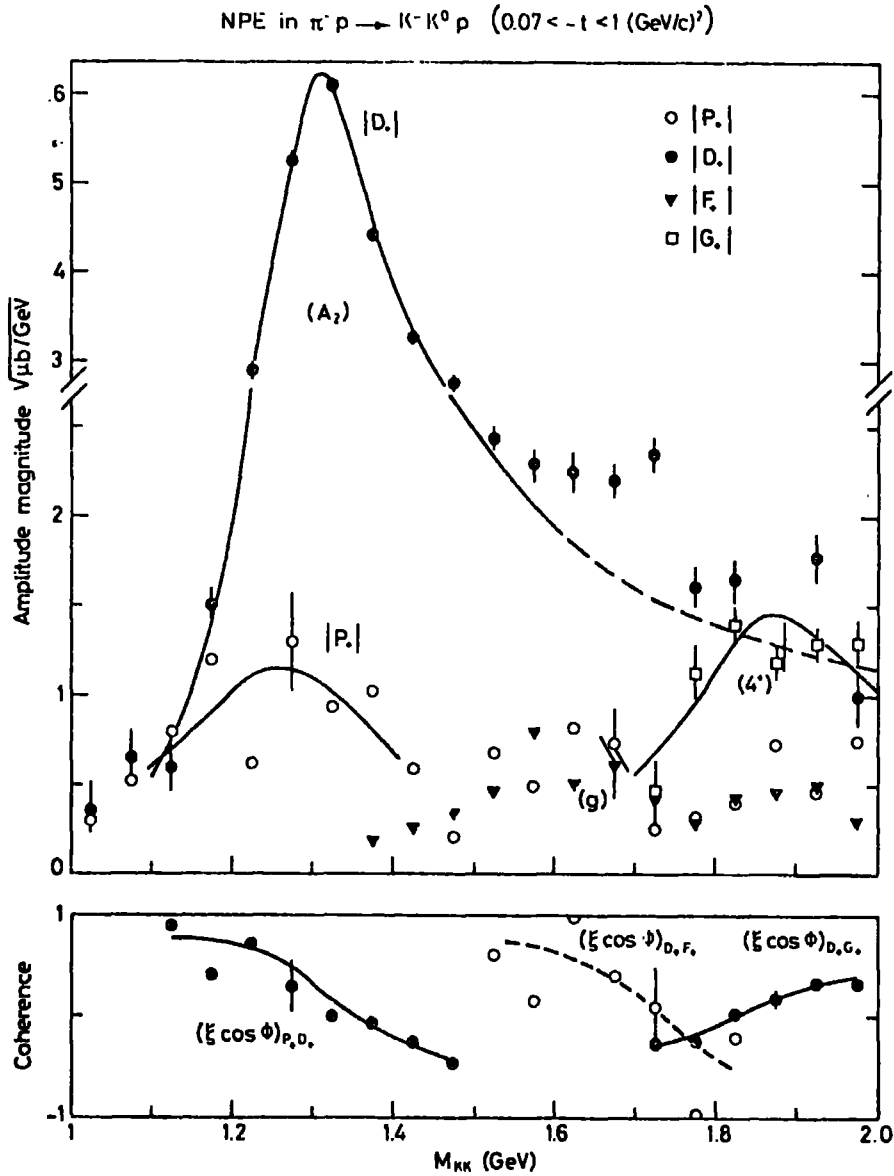


Figure 4.8: The t -channel amplitudes describing $K^- K^0$ production by NPE obtained by analysing the moments of Fig. 4.7. Representative errors are shown. The curves through the $L \geq 2$ amplitudes correspond to the Breit-Wigner fits of eq. (4.14) and (4.15). Only the coherences between significant amplitudes are shown.

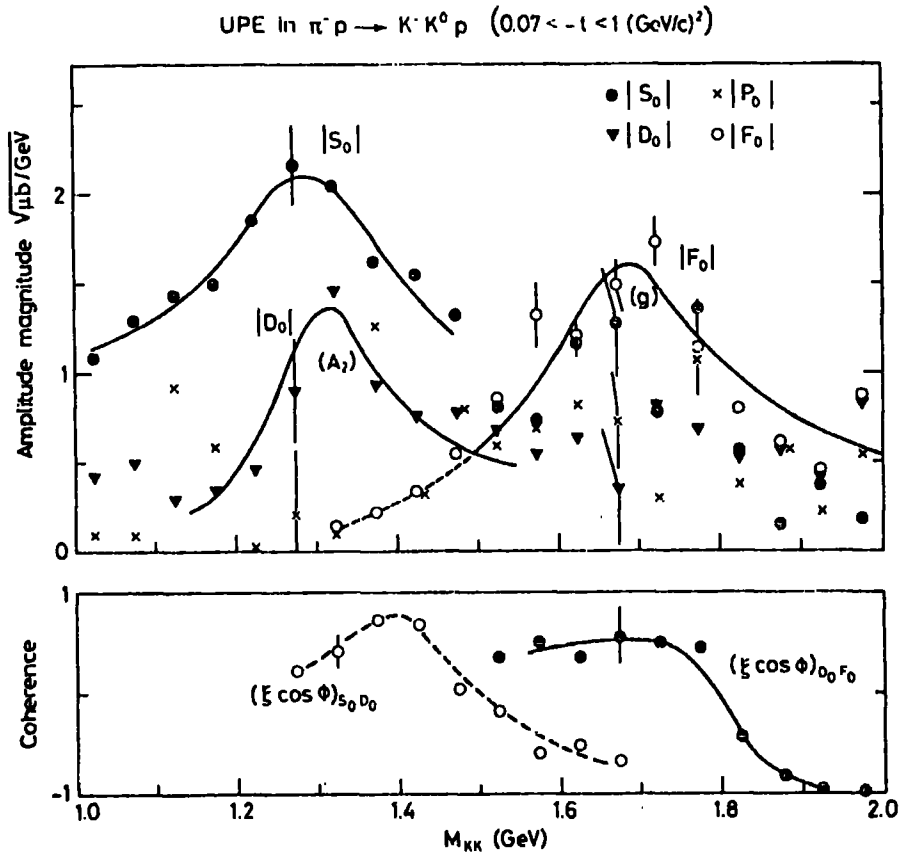


Figure 4.9: The same as Fig. 4.8, but for UPE $K^- K^0$ production

4. There is relatively little P wave $K^- K^0$ production, although the $P_+ D_+$ coherence is well determined.
5. A_2 and $K^*(1920)^\pm$ production are related using the $\{, \}^1$ dominated scheme for the pomeron. We estimate the pomeron relative to $\{$ exchange and find, for example, at $-t \sim 0.2$ GeV² a ratio 1:1 in $\pi^- p \rightarrow A_2^- p$ at 10 GeV/c.
6. We find g production proceeds dominantly by UPE (π exchange). We extrapolate to the π exchange pole and find

$$\sqrt{\Gamma_{\pi\pi} \Gamma_{K\bar{K}}} / \Gamma = 0.056 \pm 0.017.$$

Taking $\Gamma_{\pi\pi} / \Gamma = 0.24$ this gives

$$\frac{\Gamma_{K\bar{K}}}{\Gamma} = 0.013 \pm 0.004.$$

The curve shown through $|F_0|$ in Fig. 4.9 corresponds to g resonance Breit-Wigner fit with

$$\begin{aligned} m_g &= 1.698 \pm 0.012 \text{ GeV} \\ \Gamma_g &= 0.199 \pm 0.040 \text{ GeV} \end{aligned} \quad (4.15)$$

with $R = 3.5 \text{ GeV}^{-1}$.

7. g production by NPE (ω exchange) is masked by the production of $L = 2$ and $L = 4$ K^-K^0 systems which can proceed by pomeron and f exchange. Finite-mass-sum-rules and duality allow a comparison of the NPE amplitude, F_+ , with f production data. This hypothesis leads to an estimate of the $g \rightarrow K\bar{K}$ branching ratio of $\Gamma_{K\bar{K}} / \Gamma \simeq 0.015$.
8. Above 1.6 GeV we see the emergence of $L = 4$ K^-K^0 production. The t structure of G_+ shows that $L = 4$ K^-K^0 system is produced by NPE (\mathbb{P} , f exchanges). The data do not allow a determination of the mass and width of this resonance, but the behaviour of the D_+G_+ interference term is evidence for G_+ resonant structure.

CHAPTER V

Analysis of $\pi^- p \rightarrow (K^+ K^-) n$, $\pi^+ n \rightarrow (K^+ K^-) p$
Reactions

5.1 Introduction

The $(K^+ K^-)$ system has a rich resonance spectrum, because its quantum numbers allow it to couple many natural parity meson resonances with $I = 0, 1$, $P = C = (-)^L$, $G = (-)^{I+L}$, (see Sec. 2.1, eqs. (2.1)-(2.5)). Therefore the data of the reactions

$$\pi^- p \rightarrow (K^+ K^-) n \quad (5.1)$$

$$\pi^+ n \rightarrow (K^+ K^-) p \quad (5.2)$$

allow a study of resonances with $L^{PC} = 0^{++} I = 0 S^*$, ξ ; $I = 1 \delta, \delta'$; $L^{PC} = 1^{--} I = 0 \phi$; $I = 1 \rho$; $L^{PC} = 2^{++} I = 0 \delta, \delta'$; $I = 1 A_2$; $L^{PC} = 3^{--} I = 1 g$, etc. In particular the sum and the difference of the moments of reactions (5.1) and (5.2) give valuable information on the interference of amplitudes with the same L^{PC} , but different I . Recall that if we denote $A(\pi^- p)$ as the amplitude of the process (5.1), $A(\pi^+ n)$ as that for (5.2), and $A(I = 0)$, $A(I = 1)$ as amplitudes for producing a $(K\bar{K})$ system of isospin $I = 0, 1$ respectively, we find

$$\begin{aligned} A(\pi^- p) &= A(I = 0) + A(I = 1) \\ A(\pi^+ n) &= A(I = 0) - A(I = 1), \end{aligned} \quad (2.58)$$

(see Sec. 2.4.II, eq. (2.58)), where

$$\begin{aligned}
 A(I=0) &= S^\pi, S^{A_1}; P^B, P^Z; D^\pi, D^{A_1}; \dots \text{ for } L = 0, 1, 2 \dots \\
 A(I=1) &= S^B, S^Z; P^\pi, P^{A_1}, D^B, D^Z; F^\pi, F^{A_1} \dots \\
 &\text{for } L = 0, 1, 2, 3 \dots
 \end{aligned}$$

here the superscripts denote the appropriate Regge exchanges for producing a (K \bar{K}) system by unnatural parity exchange, (we neglect the NPE exchanges). We define using the relations (2.58):

$$\begin{aligned}
 \Sigma \langle Y_M^J \rangle &\equiv (N \langle Y_M^J \rangle)^{\pi p} + (N \langle Y_M^J \rangle)^{\pi^+ n} \sim \text{Re} (A'(I=0) A^*(I=0)) + \\
 &\qquad \qquad \qquad \text{Re} (A'(I=1) A^*(I=1)) \\
 \Delta \langle Y_M^J \rangle &\equiv (N \langle Y_M^J \rangle)^{\pi p} - (N \langle Y_M^J \rangle)^{\pi^+ n} \sim \text{Re} (A'(I=1) A^*(I=0)) + \\
 &\qquad \qquad \qquad \text{Re} (A'(I=0) A^*(I=1)) \quad (5.3)
 \end{aligned}$$

where a known sum over $\text{Re}(A' A^*)$ terms is implied. Thus it is possible to study $S^* - S$; $f, f' - A_2$; $S^*, \varepsilon - S'$; ... interference effects. However the determination of the amplitudes is ambiguous. The data cannot fix the ratio of $A(I=0)/A(I=1)$. To illustrate this, let us suppose only $S(I=0)$ and $S(I=1)$ amplitudes are different from zero: then the data can be written as

$$\begin{aligned}
 \Sigma \langle Y_0^0 \rangle &= 2 |S(I=0)|^2 + 2 |S(I=1)|^2 \\
 \Delta \langle Y_0^0 \rangle &= 4 \text{Re} (S(I=0) S^*(I=1)). \quad (5.4)
 \end{aligned}$$

For a given value of $\Sigma \langle Y_0^0 \rangle$ and $\Delta \langle Y_0^0 \rangle$, there are three unknowns to be determined: $|S(I=0)|$, $|S(I=1)|$ and $\phi_{S_0 S_1}$. Therefore there are infinite number of solutions of equations (5.4), according to different values of $S(I=0)/S(I=1)$. It is easy to show that with the presence of higher partial waves this ambiguity remains for all values of L . Therefore in order to have a meaningful determination of the amplitudes we have to input some information into the analysis. This input can be a dynamical model, or some already known amplitudes, or both.

The exchange mechanisms of the reactions (5.1) and (5.2) have been discussed in Sec. 2.4.II (see Table 2.3). We expect the dominance of the π -exchange amplitudes in the small t region. This allows us to perform a $\pi\pi \rightarrow K\bar{K}$ phase shift analysis. But in the small t region, some other amplitudes also give sizeable contributions (see $|S_0|$ and $|O_0|$ in Fig. 4.2). In particular the $I = 1$ S wave, arising from B and Z exchanges, has a large magnitude in the small t region. Therefore we have to include such contributions, besides the OPE, in order to perform a reliable extrapolation to the pion exchange pole.

The data only determine the relative phases of the amplitudes. A natural way to fix the overall phase of the OPE amplitudes is to assume that the phase of the $L = 2$, $I = 0$ amplitude is given by ρ, ρ' decay phases. Therefore we need to know the detailed structure of the $D(I = 0)$ amplitude, i.e. the details of $\rho-\rho'$ interference.

In this chapter we first analyse the observed $\sum \langle Y_3^4 \rangle$ and $\Delta \langle Y_3^4 \rangle$ moments to determine the structure of the $D(I = 0)$ amplitude. Then we study $S^\pi - \rho$ interference, taking into account the K^+K^- and K^0, \bar{K}^0 mass difference. In the fourth section we perform a $\pi\pi \rightarrow K\bar{K}$ phase shift analysis, inputting the previously determined $I = 1$ S and D wave contributions, found studying the (K^-K^0) system. We use the ρ, ρ' decay phase to fix the overall phase. We discuss the resulting $S(I = 0)$ amplitude in conjunction with $S^{I=0}(\pi\pi \rightarrow \pi\pi)$ amplitude. In the last section we give our conclusions.

5.2 D Wave Studies

The sum and the difference of the observed $N \langle Y_0^4 \rangle$ of reactions (5.1) and (5.2) show many interesting structures indicating the existence of, and interference between, the f , f' and A_2 resonances⁽¹⁹⁾, (see also Fig. 5.1). The data are available in three t intervals as a function of $M_{K\bar{K}}$, suitable for a mass and t -dependent analysis. The f and f' are produced by π and A_1 exchange, while the A_2 is produced by B and Z exchange. If we denote the appropriate amplitudes by the symbols of these produced spin 2 mesons, then using relations (5.3) we see that

$$\begin{aligned} \Sigma \langle Y_0^4 \rangle &\sim |f|^2 + |f'|^2 + 2 \operatorname{Re}(f f'^*) + |A_2|^2 \\ \Delta \langle Y_0^4 \rangle &\sim \operatorname{Re}(f A_2^*) + \operatorname{Re}(f' A_2^*) . \end{aligned}$$

Now $\Sigma \langle Y_0^4 \rangle$ shows a peak in the f - A_2 mass region ($\sim |f|^2 + |A_2|^2$) and a drastic drop around $1.48 < M_{K\bar{K}} < 1.54$ GeV which could be attributed to f - f' interference ($\sim \operatorname{Re}(f f'^*)$), (73, 74). The difference of the moments, $\Delta \langle Y_0^4 \rangle$, shows no evident structure in the f , A_2 region, but there is a clear structure in the middle t -bin ($0.08 < -t < 0.2$ GeV²), in the region $1.35 < M_{K\bar{K}} < 1.5$ GeV which may be attributed to f' - A_2 interference⁽⁷⁴⁾. There are similar, but not so evident structures in the other t bins with large error bars.

We fitted t -channel $\Sigma \langle Y_0^4 \rangle$, $\Sigma \langle Y_1^4 \rangle$, $\Sigma \langle Y_2^4 \rangle$ and $\Delta \langle Y_3^4 \rangle$ moments as functions of both $M_{K\bar{K}}$ and t simultaneously in order to determine the $L = 2$ ($K\bar{K}$) production amplitudes. The relations between amplitudes and exchanges have been given in Sec. 2.4.II. We write the D wave amplitudes, using relations (2.55) and the Table 2.3 as:

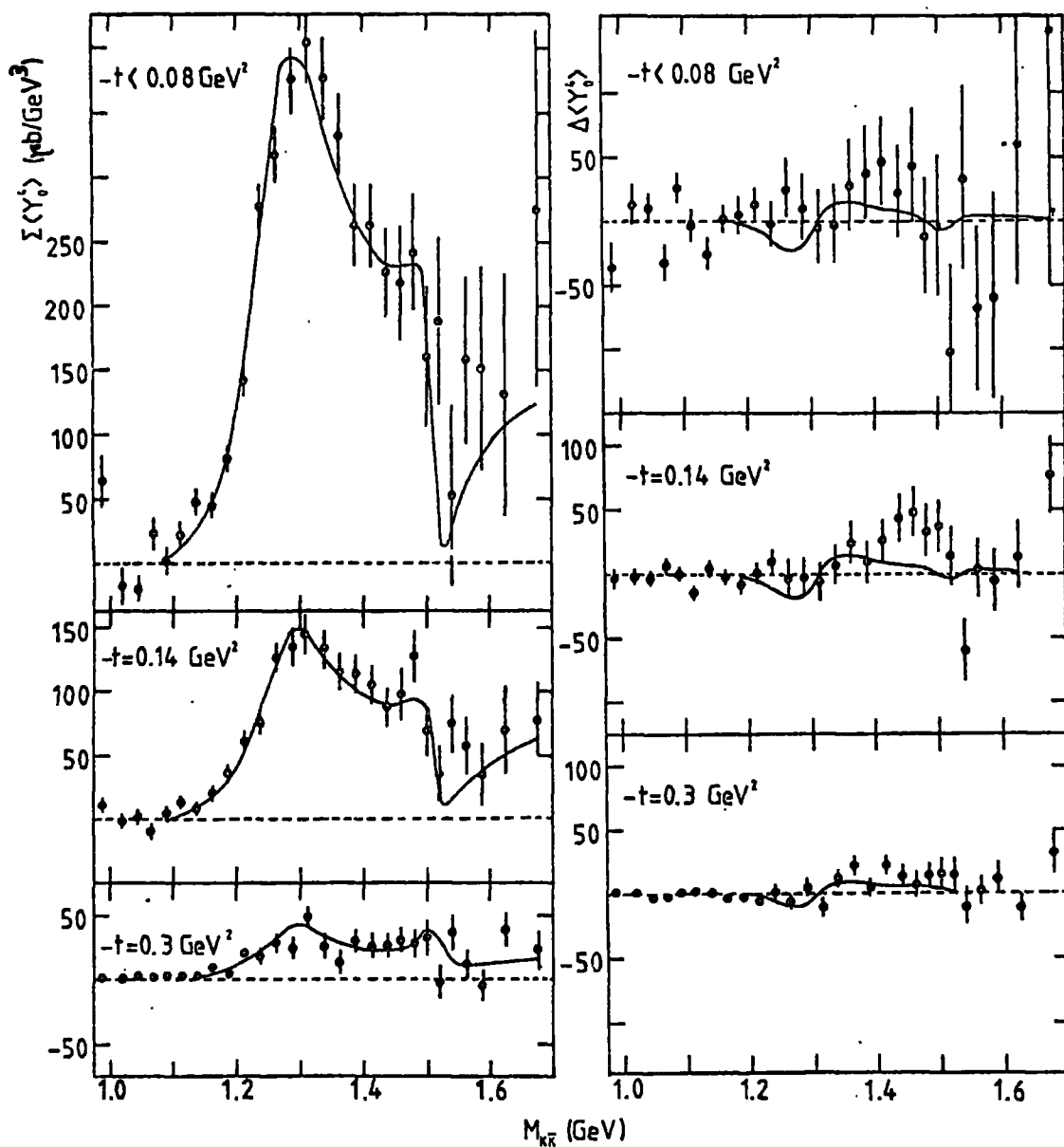


Figure 5.1: The sum and difference of $N\langle Y_0^4 \rangle$ of reactions (5.1) and (5.2) at 6 GeV/c(19). The curves are the result of the parametrization described in the text. To take into account the t_{min} effect, we used the averaged $|t|$ value for each mass bin, in the first t -bin ($-t < 0.08 \text{ GeV}^2$).

$$\begin{aligned}
 D_0^\pi &= H_{++0}^{2(+)} (I=0, f, f') \\
 D_-^\pi &= H_{++1}^{2(-)} (I=0, f, f') \\
 D_+^{A_2} &= H_{++1}^{2(+)} (I=0, f, f') \\
 D_0^B &= H_{++0}^{2(+)} (I=1, A_2) \\
 D_0^{A_1} &= H_{+-0}^{2(+)} (I=0, f') \\
 D_0^Z &= H_{+-0}^{2(+)} (I=1, A_2) .
 \end{aligned} \tag{5.5}$$

That is we assume: (i) that f, f' are produced by π and A_2 exchange, A_2 by B and Z exchange and that f' can also be produced by A_1 exchange; (ii) the A_1, B, Z exchange amplitudes with $\lambda_R = \pm 1$ are zero, (we use λ_R to denote the t-channel helicity of the produced resonance); (iii) amplitudes with $\lambda_R = \pm 2$ are zero; (iv) the f exchange amplitudes are zero.

We write the D_0 amplitudes in a factorized form⁽³⁴⁾:

$$D_0 = A_{\text{pro}}(t) A_{\text{dec}}(M_{\mathbf{k}\bar{\mathbf{k}}}) \tag{5.6}$$

where $A_{\text{pro}}(t)$ is the "production" amplitude and contains all the t-dependence of the amplitude. In other words it contains all the information on the exchanged object and we ignore the possible $M_{\mathbf{k}\bar{\mathbf{k}}}$ -dependence of this amplitude. For pion exchange we use

$$A_{\text{pro}}^\pi(t) \propto \frac{\sqrt{-t}}{t - m_\pi^2} e^{b_\pi(t - m_\pi^2)}, \tag{5.7}$$

and for the other Regge exchanges, R, we took a simple Regge form:

$$A_{\text{pro}}^R(t) = g_R (-t)^{\alpha_R} (1 + \zeta_R e^{-i\pi\alpha_R}) \Gamma(\alpha_R - \alpha_R) (\rho_L)^{\alpha_R - 1} \tag{5.8}$$

where g_R is the coupling constant, $n_R = \frac{1}{2}$ for B exchange, 0 for A_1 Z exchanges, ζ_R is the signature, $a_R = 0$ for B, for A_1 and Z exchanges, and α_R is the Regge trajectory.

The amplitude $A_{\text{dec}}^{(M_{\mathbf{K}\bar{\mathbf{K}}})}$ describes the decay of the produced resonance into the $(\mathbf{K}\bar{\mathbf{K}})$ channel. We assume that it has no t -dependence. For π exchange it has the form

$$A_{\text{dec}}^{\pi}(M_{\mathbf{K}\bar{\mathbf{K}}}) = C_{\pi} \frac{\sqrt{5}}{\sqrt{3}} \frac{M_{\mathbf{K}\bar{\mathbf{K}}}}{\sqrt{k_{\pi\pi}}} A_{L=2}^{I=0}(\pi\pi \rightarrow \mathbf{K}\bar{\mathbf{K}}), \quad (5.9a)$$

and for the other Regge exchanges it is

$$A_{\text{dec}}(M_{\mathbf{K}\bar{\mathbf{K}}}) = \frac{\gamma_{\mathbf{K}\bar{\mathbf{K}}}}{m_R^2 - M_{\mathbf{K}\bar{\mathbf{K}}}^2 - i \sum \gamma^2} \quad (5.9b)$$

where $C_{\pi} \approx \sqrt{2} (G^2/4\pi)^{1/2} / \rho_{\text{lab}} m_n$ and

$$\gamma_i^2 = m_R \Gamma_i^R \left(\frac{k_i}{k_i^R} \right)^5 \frac{D(k_i^R; R)}{D(k_i; R)},$$

m_R is the mass of the produced resonance, Γ_i^R is the partial decay width of resonance R into the channel i, k_i the channel momenta, k_i^R is the channel momenta at $M_{\mathbf{K}\bar{\mathbf{K}}} = m_R$, $R = 3.5 \text{ GeV}^{-1}$ is the interaction radius and

$$D(x) = 9 + 3x^2 + x^4$$

for $L = 2$.

D_0^{π} amplitude is to be parametrized in terms of overlapping $\{, \}^i$ resonances. In particular we have to be able to include the appropriate signs of the $\{ \rightarrow \pi\pi, \mathbf{K}\bar{\mathbf{K}}$ and the $\{^i \rightarrow \pi\pi, \mathbf{K}\bar{\mathbf{K}}$ couplings. Now, we can write some of the $2^{++} \rightarrow 0^{-+} 0^{-+}$ decay couplings in terms of A^1 , the singlet coupling, A^8 , the octet coupling and θ , the 2^{++} octet-singlet mixing angle⁽⁷¹⁾. We find:

$$R(\rho \rightarrow \pi\pi) = \frac{1}{\sqrt{2}} \left(\frac{\sqrt{6}}{4} \cos \theta A^1 + \frac{\sqrt{15}}{5} \sin \theta A^8 \right)$$

$$R(\rho \rightarrow K\bar{K}) = \left(-\frac{1}{2} \cos \theta A^1 + \frac{\sqrt{10}}{10} \sin \theta A^8 \right)$$

$$R(\rho' \rightarrow \pi\pi) = \frac{1}{\sqrt{2}} \left(\frac{\sqrt{6}}{4} \sin \theta A^1 - \frac{\sqrt{15}}{5} \cos \theta A^8 \right)$$

$$R(\rho' \rightarrow K\bar{K}) = \left(-\frac{1}{2} \sin \theta A^1 - \frac{\sqrt{10}}{10} \cos \theta A^8 \right)$$

$$R(\rho' \rightarrow \eta_8 \eta_8) = \frac{1}{\sqrt{2}} \left(-\frac{\sqrt{2}}{4} \sin \theta A^1 - \frac{\sqrt{5}}{5} \cos \theta A^8 \right)$$

$$R(K^*(1420) \rightarrow K\pi) = \frac{3\sqrt{5}}{10} A^8 \quad (5.10)$$

We have compared these relations with the experimentally known widths using the definition

$$\Gamma = \frac{1}{m_R} |R|^2 k_R^{2L+1} \quad (5.11)$$

where m_R is the mass of the resonance k_R is the appropriate channel momentum at the resonant mass m_R . This fit gives

$$\theta = 30.5 \pm 3.0, \quad A^8 = 44.5 \pm 2.4, \quad A^1 = 87.3 \pm 1.9. \quad (5.12)$$

The results of the fit are shown in Table 5.1 (the experiment values are taken from reference (37)):



Decay	Exp. Width (MeV)	SU(3) Prediction (MeV)
$f \rightarrow \pi\pi$	145.8 ± 1.8	145.6
$f \rightarrow K\bar{K}$	6.8 ± 1.3	7.5
$f' \rightarrow \pi\pi$	-	0.5
$f' \rightarrow K\bar{K}$	40.0 ± 10.0	48.3
$f' \rightarrow \eta_8\eta_8$	-	13.7
$K^* \rightarrow K\pi$	60.6 ± 9.0	55.5

Table 5.1: Some of the $2^{++} \rightarrow 0^{-+}0^{-+}$ experimental decay widths compared with the SU(3) predictions.

In particular the values of θ , A^8 and A^2 , which are given in (5.12), yield the f, f' coupling signs

$$\begin{aligned} R(f \rightarrow \pi\pi) : (+) , \quad R(f \rightarrow K\bar{K}) : (-) \\ R(f' \rightarrow \pi\pi) : (-) , \quad R(f' \rightarrow K\bar{K}) : (-) \end{aligned} \quad (5.13)$$

and

$$\Gamma_{\eta_8\eta_8}^{f'} = 0.283 \Gamma_{K\bar{K}}^{f'}$$

The formalism, which is to describe the overlapping f, f' resonances, should be able to incorporate and check these sign differences. We shall use the mass matrix formalism, (see for instance ref. (75) and references therein). We shall modify the formalism of ref. (75) slightly to produce the usual Breit-Wigner form for single resonance case. For two channels (labelled by i, j) and two resonances (labelled by μ, ν) we write the partial wave \mathcal{T} matrix elements as

$$T_{ij} = G_{i\mu}^T P_{\mu\nu} G_{\nu j} , \quad (5.14)$$

where \underline{G} is the coupling matrix

$$G_{i\mu} = g_{i\mu} k_i^L$$

and \underline{P} is the propagator matrix. \underline{P} is related to the \underline{M}^2 matrix as follows:

$$(\underline{P}^{-1})_{\mu\nu} = (\underline{M}^2)_{\mu\nu} - s \delta_{\mu\nu}$$

where $S = M_{\bar{k}\bar{k}}^2$. The unitarity condition for T_{ij} (c.f. eq. (3.31)) requires the \underline{M}^2 matrix elements to satisfy, (assuming the time reversal invariance):

$$-\text{Im}(\underline{M}^2)_{\mu\nu} = \sum_i g_{\mu i} g_{\nu i} k_i^{2L+1}. \quad (5.15)$$

Unitarity can only fix the imaginary part of the \underline{M}^2 matrix; therefore we have the freedom to choose the real part of the mass-squared matrix. Moreover, the mass-squared matrix is not hermitian in general, so unitarity cannot be diagonalized simultaneously with the mass-squared matrix⁽⁷⁵⁾. We choose the real part of the mass matrix as

$$\text{Re}(\underline{M}^2) = \begin{pmatrix} M_{\bar{k}}^2 & \Delta M^2 \\ \Delta M^2 & M_{\bar{l}}^2 \end{pmatrix}.$$

In terms of the function $d(s)$, which we introduced in Chapter III (see eqs. (3.10)-(3.12)), this gives

$$d(s) \equiv \det(\underline{P}^{-1}) = (M_{\bar{k}}^2 - s - i(\gamma_{\bar{k}1}^2 + \gamma_{\bar{k}2}^2)) \times (M_{\bar{l}}^2 - s - i(\gamma_{\bar{l}1}^2 + \gamma_{\bar{l}2}^2)) - (\Delta M^2 - i(\gamma_{\bar{k}1}\gamma_{\bar{l}1} + \gamma_{\bar{k}2}\gamma_{\bar{l}2}))^2 \quad (5.16)$$

where

$$\gamma_{\bar{k}i}^2 = g_{\bar{k}i}^2 k_i^{2L+1}. \quad (5.17)$$

The $d(s)$ in eq. (5.16) incorporates the sign difference

of the couplings because the term

$$(\Delta M^2 - i(\gamma_{\rho_1} \gamma_{\rho_1} + \gamma_{\rho_2} \gamma_{\rho_2}))^2$$

contains terms like

$$\gamma_{\rho_i} \gamma_{\rho_i} \sim (\Gamma_{\rho_i} \Gamma_{\rho_i})^{1/2} \sim R_{\rho_i} R_{\rho_i} .$$

Note that the form of $d(s)$ in eq. (5.16) does not give us directly physical masses and widths of two resonances, since it is not in factorized form of the two Breit-Wigner $d(s)$ function. However if the

$$(\Delta M^2 - i(\gamma_{\rho_1} \gamma_{\rho_1} + \gamma_{\rho_2} \gamma_{\rho_2}))^2$$

term turns out to be negligibly small, to a good approximation, $d(s)$ in eq. (5.16) can yield the physical parameters of two resonances. This formalism is closely related to the $\underline{K} = \underline{M}^{-1}$ matrix formalism. If we set $\Delta M^2 = 0$, the formalism would correspond to adding two real poles in the \underline{K} matrix:

$$\underline{T} = (\underline{K}^{-1} - i \underline{K}^L)^{-1}$$

$$K_{ij} = \frac{g_{\rho_i} g_{\rho_j}}{M_{\rho}^2 - s} + \frac{g_{\rho_i} g_{\rho_j}}{M_{\rho}^2 - s} .$$

To fix the t -dependence of the amplitudes we take the Regge trajectories as⁽³⁵⁾:

$$\begin{aligned} \alpha_{\pi}(t) &= -0.016 + 0.825 t \\ \alpha_B(t) &= -0.246 + 0.825 t \\ \alpha_Z(t) &= -0.350 + 0.825 t \\ \alpha_{A_1}(t) &= 0.825 t . \end{aligned} \tag{5.18}$$

The t -dependence of OPE amplitudes is given by eq. (5.7)

with b_{π} as a free parameter. We include a factor of

$| (1 + e^{-i\pi \alpha_{\pi}}) | / (1 + e^{i\pi \alpha_{\pi}})$ in the B exchange

amplitude in order to relate its phase to the OPE amplitude by π - B exchange-degeneracy. We fix D_0^B and D_0^Z amplitudes by taking

$$\begin{aligned} m_{A_2} &= 1.31 \text{ GeV} \\ \Gamma_{A_2}^{K\bar{K}} &= 0.005 \text{ GeV} \\ \Gamma_{A_2}^{+\text{ot}} &= 0.102 \text{ GeV} \end{aligned}$$

and fitting to the values of $|D_0|$ found for (K^0K^-) system, (see Fig. 4.2). We extrapolate from $p_L = 10 \text{ GeV}/c$ of the (K^0K^-) data to $p_L = 6 \text{ GeV}/c$ of the (K^+K^-) data by including a factor $(p_L)^{\alpha-1}$ in amplitudes (see eq. (5.8)). We take the f' mass and its $\pi\pi$ and $K\bar{K}$ widths as free parameters and fix the $f' \rightarrow \eta\eta$ width to its SU(3) predicted value, (c.f. eq. (5.13)). We fix the f meson parameters as

$$\begin{aligned} m_f &= 1.275 \text{ GeV} \\ \Gamma_f^{\pi\pi} &= 0.146 \text{ GeV} \\ \Gamma_f^{K\bar{K}} &= 0.007 \text{ GeV} \\ \Gamma_f^{\text{rest}} &= 0.027 \text{ GeV} . \end{aligned}$$

That is, we use the branching ratio $(f \rightarrow K\bar{K}) / (f \rightarrow \text{all}) = 3.8\%$ which was determined by the experimental group⁽¹⁹⁾.

To allow for decay channels other than $\pi\pi$ and $K\bar{K}$ for the f and f' resonances we use an extended version of $d(s)$ of eq. (5.16), assuming that the f' can couple only to $\pi\pi$, $K\bar{K}$ and $\eta\eta$ channels and that the other decay channels of the f can be associated with momentum $k_{K\bar{K}}$, by writing:

$$\begin{aligned} d(s) = & (m_f^2 - s - i(\gamma_{f\pi\pi}^2 + \gamma_{fK\bar{K}}^2 + \gamma_{f\text{rest}}^2)) (m_{f'}^2 - s - i(\gamma_{f'\pi\pi}^2 + \gamma_{f'K\bar{K}}^2 + \gamma_{f'\eta\eta}^2)) \\ & - (\Delta M^2 - i(-\gamma_{f\pi\pi}\gamma_{f'\pi\pi} + \gamma_{fK\bar{K}}\gamma_{f'K\bar{K}}))^2 \end{aligned} \quad (5.19)$$

where ΔM^2 is a free parameter. Note that we input the relative sign of the $f \rightarrow \pi\pi$, $f' \rightarrow \pi\pi$ in the second term of eq. (5.19). We relate the overall normalization of $D_0^{A_1}$ to D_0^Z assuming $A_1 - Z$ exchange-degeneracy, and allow a free parameter $r = g_{A_1}/g_Z$ to measure possible exchange-degeneracy breaking effects. The $M_{K\bar{K}}$ -dependence of $D_0^{A_1}$ is given by a simple f' Breit-Wigner form (c.f. eq. (5.9b)). We neglect the A_2 exchange amplitude and parametrize the D_-^π (and D_+) amplitude using the Ochs-Wagner method^(32,33); that is we write for first two t intervals

$$D_-^\pi = -c_1 D_0^\pi, \quad |D_+| = |D_-^\pi|,$$

where c_1 are ($i = 1,2$) free parameters for each t bin. In the third t -interval, observing that $\sum \langle Y_2^4 \rangle$ is not consistent with zero everywhere⁽¹⁹⁾, we take

$$D_-^\pi = -c_3 D_0^\pi, \quad |D_+| = c_4 |D_0^\pi|,$$

where c_3 and c_4 are free parameters. In the analysis we also include an $L = 3$, F_0^π , amplitude fixed by the g meson tail with a $g \rightarrow \pi\pi$ branching ratio 24%, a $g \rightarrow K\bar{K}$ branching ratio 1.3%, $m_g = 1.69$ GeV, $\Gamma_g^{\text{tot}} = 0.18$ GeV. The analysed moments can be expressed in terms of amplitudes of eq. (5.5) as follows:

$$\begin{aligned} \sum \langle Y_0^4 \rangle = & 2 \left[0.857 (|D_0^\pi|^2 + |D_0^B|^2 + |D_0^{A_1}|^2 + |D_0^Z|^2) + 0.546 |F_3^\pi|^2 \right. \\ & \left. - 0.571 (|D_+|^2 + |D_-^\pi|^2) \right] \end{aligned}$$

$$\sum \langle Y_1^4 \rangle = 2 \left[1.107 \operatorname{Re} (D_0^\pi D_-^{\pi*}) \right]$$

$$\sum \langle Y_2^4 \rangle = 2 \left[0.452 (|D_-^\pi|^2 - |D_+|^2) \right]$$

$$\Delta \langle Y_0^4 \rangle = 4 \left[0.857 \operatorname{Re} (D_0^\pi D_0^{B*} + D_0^{A_1} D_0^{Z*}) \right].$$

The results of this ($M_{K\bar{K}}, t$) dependent amplitude analysis are shown in Fig. 5.1. They correspond to the parameter values

$$\begin{aligned}
 m_{f'} &= 1.513 \pm 0.003 \text{ GeV} \\
 \Gamma_{f'}^{\pi\pi} &= 0.68 \pm 0.11 \text{ MeV} \\
 \Gamma_{f'}^{K\bar{K}} &= 33 \pm 7 \text{ MeV} \\
 \Delta M^2 &= 0.0072 \pm 0.0037 \text{ GeV}^2 \\
 b_{\pi} &= 2.2 \pm 0.3 \text{ GeV}^{-2} \\
 r = g_{A_1} / g_Z &= 0.256 \pm 0.042 \\
 C_1 &= 0.165 \pm 0.013 \\
 C_2 &= 0.293 \pm 0.015 \\
 C_3 &= 0.257 \pm 0.015 \\
 C_4 &= 0.722 \pm 0.042 .
 \end{aligned} \tag{5.20}$$

The resulting amplitudes are shown in Figs. 5.2 and 5.3.

We summarize the main results of this analysis below:

1) The data are compatible with the SU(3) predicted sign difference of $f \rightarrow \pi\pi$ and $f' \rightarrow \pi\pi$ couplings. We checked this by changing the $-\gamma_{f\pi\pi} \gamma_{f'\pi\pi}$ to $+\gamma_{f\pi\pi} \gamma_{f'\pi\pi}$ with the parameter values in (5.20). The $\sum \chi^2$ jumped to 432.1 from 191.5 for 230 data points, and the $\pi\pi \rightarrow K\bar{K} \quad A_{L=2}^{I=0}$ wave changed to the dotted curve in Fig. 5.3. We refitted the data keeping the sign positive. The best fit gave $\sum \chi^2 = 218.5$ with $m_{f'} \approx 1.6 \text{ GeV}$ and $\Gamma_{f'}^{\pi\pi} = 0 \text{ GeV}$. This means that the data definitely determine the $R(f \rightarrow \pi\pi) / R(f' \rightarrow \pi\pi)$ ratio to be negative.

(ii) The second term in eq. (5.19) is small. Because ΔM^2 is small, and because $\gamma_{f\pi\pi} \gamma_{f'\pi\pi}$ and $\gamma_{fK\bar{K}} \gamma_{f'K\bar{K}}$ have similar magnitude but opposite sign, and so cancel each

other, Thus we can interpret the resulting f' parameters, to a good approximation, as the physical ones:

$$m_{f'} = 1513 \pm 3 \text{ MeV}$$

$$\Gamma_{f'}^{\text{tot}} = 43 \pm 9 \text{ MeV}$$

$$(\mathcal{B}(f' \rightarrow \pi\pi)/\mathcal{B}(f' \rightarrow a_0 b)) = 1.6 \pm 0.6\% .$$

The mass and total width of the f' are in agreement with PDG values⁽³⁷⁾. The values that the experimental group determined⁽¹⁹⁾, ($m_{f'} = 1.506 \pm 5 \text{ GeV}$, $\Gamma_{f'}^{\text{tot}} = 66 \pm 10 \text{ MeV}$) are different from our results. However their simple parametrization of the $\pi\pi \rightarrow K\bar{K}$, $J=0$ D wave does not include unitarity constraints, the effect of which could change their values considerably. In our model unitarity is built in by the use of the $d(s)$ function. The $f' \rightarrow \pi\pi$ branching ratio exceeds the upper limit of 0.9% obtained by Beusch et al⁽⁷³⁾. This ratio is very sensitive to the interference effect and the unitarity constraints. The authors of ref. (73) do not consider the unitarity, this means their results could be in error. The quality of our fit to $\sum \langle Y_0^4 \rangle$, together with unitarity, is evidence that our analysis is meaningful.

iii) We find a $f'-A_2$ interference shape within the error bars, but we are unable to produce the structure in $\Delta \langle Y_0^4 \rangle$ in the region $1.35 < M_{KK} < 1.5 \text{ GeV}$. by $f'-A_2$ interference. To maximize the $f'-A_2$ interference term we add an extra phase to the $D_0^{A_1}$ amplitude and we produce the curves shown in Fig. 5.1 for $\Delta \langle Y_0^4 \rangle$ in that mass region with

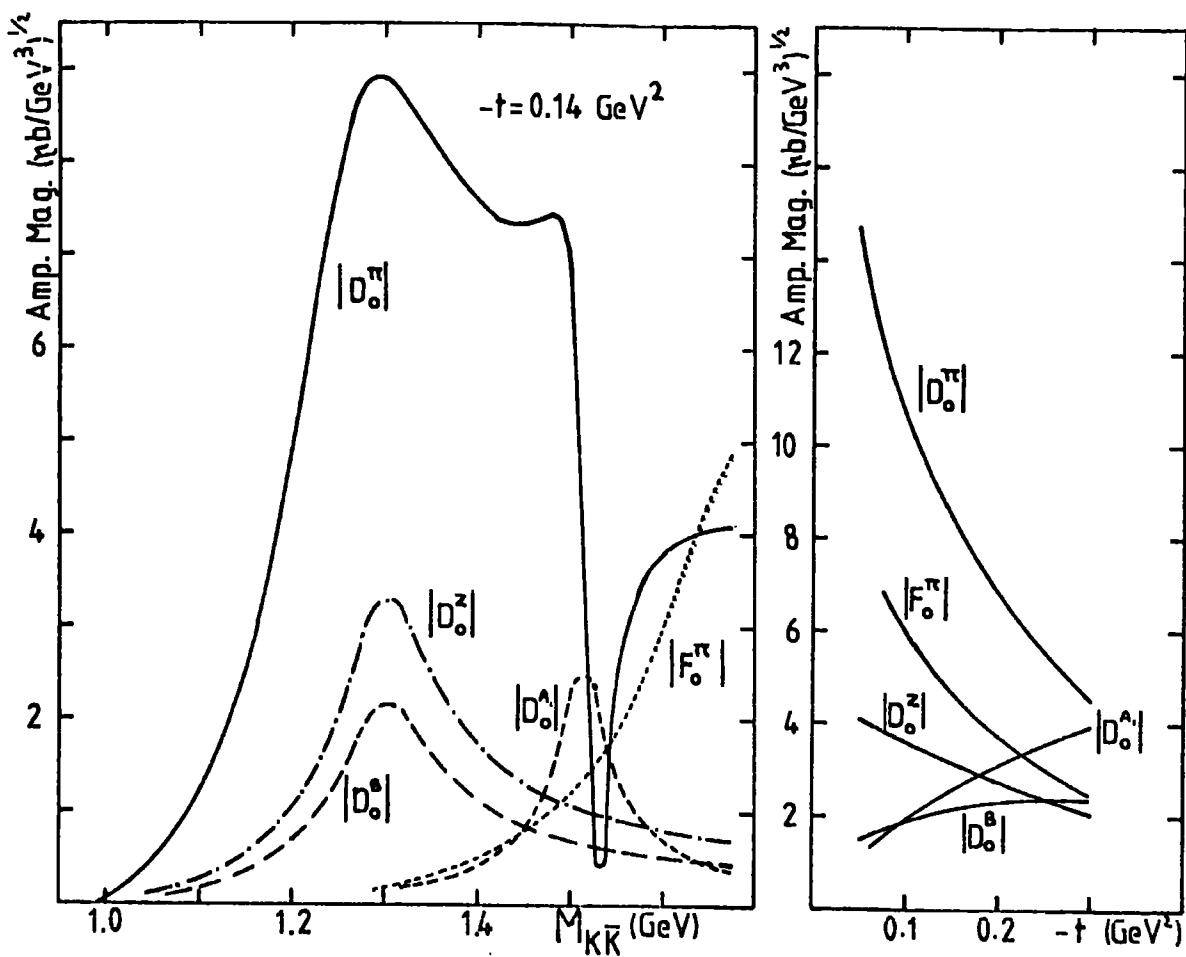


Figure 5.2: The mass and t -dependence of the $L = 2,3$ amplitudes of the produced (K^+K^-) system at $6 \text{ GeV}/c$. The t -dependent curves are drawn at the $M_{K\bar{K}}$ values that the amplitudes are largest. That is $M_{K\bar{K}} = 1.2875 \text{ GeV}$ for $|D_0^\pi|$; 1.3125 for $|D_0^z|$ and $|D_0^A|$; 1.52 GeV for $|F_0^\pi|$; and 1.675 GeV for $|F_0^\pi|$.

$\theta_{\text{ext}} = -127^\circ$. Recall that we have fixed $|D_0^z|$ from (K^-K^0) production and $|D_0^A|$ is well constrained by $\Sigma \langle Y_0^+ \rangle$. The $f_1 - A_2$ interference term, which is $2 \text{Re}(D_0^A D_0^{z*})$, can be at most $2 |D_0^A| |D_0^z|$, and so cannot produce such a large effect. The same problem occurs in the similar analysis, which was performed by the experimental group⁽¹⁹⁾. However we believe their conclusion is in error. Their values of $|f_1|^2$ and $|A_2|^2$ cannot produce the $f_1 - A_2$ interference structure that they show. This is probably because their

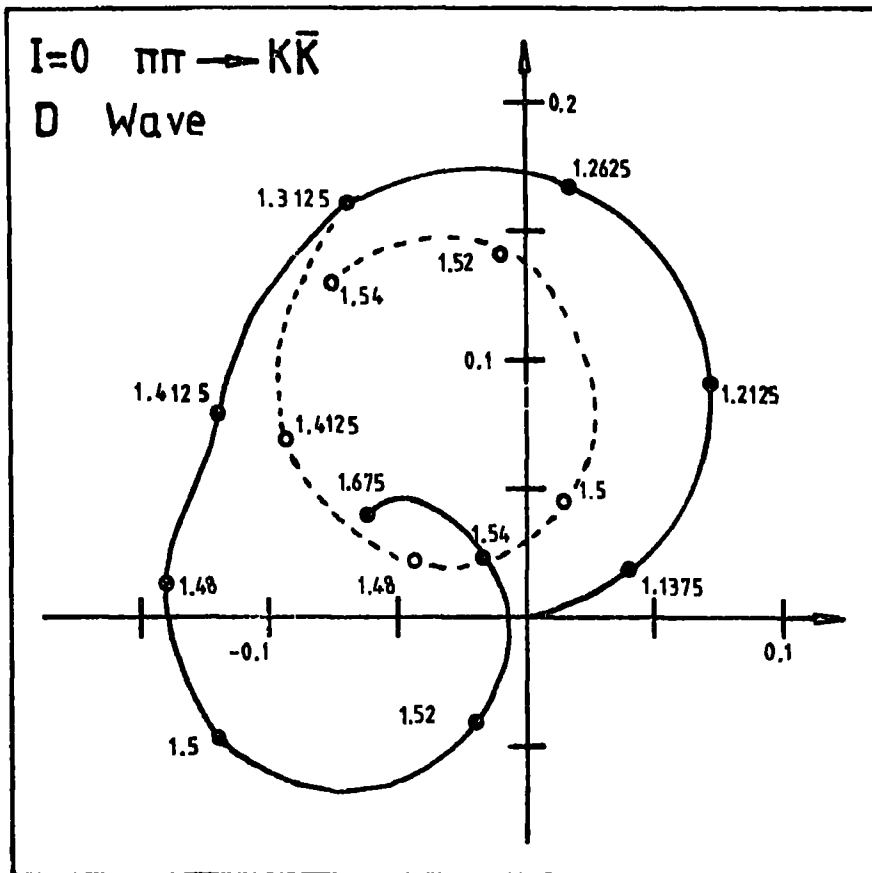


Figure 5.3: The $\pi\pi \rightarrow K\bar{K}$ $A_{L=2}^{I=0}$ D wave Argand amplitude. The marked points are the $M_{K\bar{K}}$ values in GeV. The dotted curve corresponds to the positive $R(j \rightarrow \pi\pi)$, $R(j' \rightarrow \pi\pi)$ relative sign. Note that the radius of the Argand circle is 0.5.

parametrization does not satisfy the required Schwarz-type inequalities, $|\beta'| |A_2| \geq \text{Re}(\beta' A_2^*)$.

iv) The parameter $r = g_{A_1} / g_Z$ is not equal to that which would be expected for strong $A_1 - Z$ exchange-degeneracy. However we expect such an EXD violation, as the A_1 and Z trajectories have $\Delta\alpha = -0.35$.

v) The presence of the β' changes the β Breit-Wigner form of the $L = 2, I = 0, \pi\pi \rightarrow K\bar{K}$ amplitude, (see Fig. 5.3). However the β and β' couplings are such that we see very little effect of the β' in $\pi\pi \rightarrow \pi\pi$, or of the β in the $K\bar{K} \rightarrow K\bar{K}$ channel.

vi) The slope $b_{\pi} = 2.2 \pm 0.3 \text{ GeV}^{-2}$ found in this analysis is consistent with $b = 4.5 \pm 1.1 \text{ GeV}^{-2}$ determined from fitting the t -dependence of $|F_0|^2$ for the (K^-K^0) system in g meson region, (see Sec. 4.3, Fig. 4.5). Note that we should compare $b/2 = 2.25 \pm 0.55 \text{ GeV}^{-2}$ with b_{π} . This is evidence that the OPE amplitudes have been isolated reliably in both analyses.

5.3 Threshold Region Analysis

The data of reactions (5.1) and (5.2) allow a study of $S^* - \delta$ interference. As we have discussed before, a unique determination of the amplitudes is not possible without feeding some extra information into the analysis. The δ resonance production in the reaction $\pi^- p \longrightarrow (K^- K_S^0) p$ is overshadowed by strong $\delta(1300)$ resonance production so it is not possible to determine the δ meson production amplitudes from the results of the previous chapter. There are no other data with sufficient statistics to fix the δ production amplitudes. Similarly there is no way of fixing the S^* production amplitudes accurately. Therefore we have to study the exchange mechanisms for S^* and δ production and to relate them using a simple dynamical model.

From relations (2.55) and Table 2.3 we see that the S^* is produced by $\bar{\pi}$ (and A_1) exchange and that the δ meson is produced via B and Z exchanges. The data are available for $-t < 0.4 \text{ GeV}^2$ and $M_{K\bar{K}} < 1.1 \text{ GeV}^{(19)}$. They show the dominance of the OPE wave amplitude (see Fig. 5.4). In this region of $M_{K\bar{K}}$, the amplitudes with $L > 0$ are small and $\Sigma \langle Y_0^0 \rangle$ and $\Delta \langle Y_0^0 \rangle$ are given mainly in terms of S wave amplitudes as in eqs. (5.4). $\Delta \langle Y_0^0 \rangle$ can thus be

expressed in terms of the exchange amplitudes as follows:

$$\Delta \langle Y^0 \rangle = 4 \operatorname{Re} (S^\pi S^{B^*} + S^{A_1} S^{Z^*}) . \quad (5.21)$$

As in $\pi N \rightarrow (\pi\pi) N$ studies, it is a good approximation to neglect A_1 exchange. The data show a large $\Delta \langle Y^0 \rangle$ in the threshold region⁽¹⁹⁾. This suggests, together with the assumption $S^{A_1} \equiv 0$, that we have to include the S^B amplitude in the analysis. The data do not indicate whether or not there is a sizeable S^Z . It is not safe to assume that $S^Z = 0$ in the threshold region, especially knowing that the $\delta'(1300)$ production has a large S^Z component. However the data cannot determine S^π , S^B and S^Z simultaneously. For this reason, we first try to fit the data neglecting S^Z . Then we try to remove any resulting systematic discrepancies by introducing S^Z .

We relate S^π and S^B by π -B exchange-degeneracy (EXD)⁽³⁴⁾. We allow EXD breaking by taking the π and B trajectories as in eqs. (5.18) and by allowing the coupling ratio, g_B/g_π to be a free parameter.

To study the (K^+K^-) system near its production threshold, we have to face the problem arising from K^+ , K^- and K^0 , \bar{K}^0 mass differences. We define the channel momenta for the (K^+K^-) and $(K^0\bar{K}^0)$ states as, respectively

$$\begin{aligned} k_c &= (M_{K\bar{K}}^2/4 - m_{K^+}^2)^{1/2} \\ k_o &= (M_{K\bar{K}}^2/4 - m_{K^0}^2)^{1/2} \end{aligned} \quad (5.22)$$

with $m_{K^+}^2 = 0.244 \text{ GeV}^2$ and $m_{K^0}^2 = 0.248 \text{ GeV}^2$. Strong interactions do not distinguish the (K^+K^-) system from the $(K^0\bar{K}^0)$ system, but instead distinguish $|K\bar{K}; I=0\rangle$ from

$|K\bar{K}; I=1\rangle$. These states can be expressed in terms of $|K^+K^- \rangle$ and $|K^0\bar{K}^0 \rangle$:

$$\begin{aligned} |K\bar{K}; I=0\rangle &= \frac{1}{\sqrt{2}} |K^0\bar{K}^0\rangle - \frac{1}{\sqrt{2}} |K^+K^- \rangle \\ |K\bar{K}; I=1\rangle &= \frac{1}{\sqrt{2}} |K^0\bar{K}^0\rangle + \frac{1}{\sqrt{2}} |K^+K^- \rangle . \end{aligned} \quad (5.23)$$

The scattering amplitudes with definite isospin do not have definite channel momentum. In Appendix VIII we derive the S^* contribution to the $\pi\pi \rightarrow K^+K^-$ amplitude, and the δ contribution to the $\pi\eta \rightarrow K^+K^-$ amplitude, taking explicit account of this kinematic difference, $k_0 \neq k_c$.

We have fitted t-channel observables $\Sigma \langle Y^J \rangle$, $\Delta \langle Y^J \rangle$ with $J \leq 2$ in four mass bins (centred on $M_{K\bar{K}} = 0.9987, 1.02, 1.045$ and 1.08 GeV) as functions of t and $M_{K\bar{K}}$ in the region $-t < 0.4$ GeV² (19) (see Fig. 5.4). The moments with $M = 1, 2$ are compatible with zero indicating that amplitudes with $\lambda_R \neq 0$ are negligible. We include the π and B exchange amplitudes with $L \leq 2$:

$$\begin{aligned} S^\pi &= C_\pi(t, M_{K\bar{K}}) \frac{\sqrt{2}}{\sqrt{3}} A(\pi\pi \rightarrow K^+K^-) e^{i\theta_{\pi\pi}} \\ S^B &= C_\pi(t, M_{K\bar{K}}) \frac{R_B}{R_\pi} \left(\frac{\sqrt{|k_\pi|} g_{S^+}^{\pi\pi}}{\sqrt{|k_\eta|} g_B^{\pi\eta}} \right) \frac{\sqrt{2}}{\sqrt{3}} A(\pi\eta \rightarrow K^+K^-) \\ P_0^\pi &= C_\pi(t, M_{K\bar{K}}) \frac{\sqrt{3}}{\sqrt{2}} A(\rho) \\ P_0^B &= g_B' C_B(t) A_{dec}(\phi) \\ D_0^\pi &= C_\pi(t, M_{K\bar{K}}) \frac{\sqrt{5}}{\sqrt{3}} A(\rho) \\ D_0^B &= g_B'' C_B(t) A_{dec}(A_2) , \end{aligned} \quad (5.24)$$

where

$$C_{\pi}(t, M_{K\bar{K}}) = C \frac{\sqrt{-t}}{t - m_{\pi}^2} e^{b_{\pi}(t - m_{\pi}^2)} \frac{M_{K\bar{K}}}{\sqrt{k_{\pi}}}$$

$$\frac{R_B}{R_{\pi}} = \frac{g_B (1 - e^{i\pi\alpha_B}) \Gamma(-\alpha_B)}{g_{\pi} (1 + e^{i\pi\alpha_{\pi}}) \Gamma(-\alpha_{\pi})} (p_L)^{-0.23}$$

$$C_B(t) = \sqrt{-t} (1 - e^{i\pi\alpha_B}) \Gamma(-\alpha_B) (p_L)^{\alpha_B - 1} \frac{|(1 + e^{-i\pi\alpha_B})|}{(1 + e^{i\pi\alpha_{\pi}})},$$

$A(\rho)$ and $A(\rho')$ are the usual ρ and ρ' meson Breit-Wigner forms. For the ϕ and A_2 we use $A_{dec}(\phi)$ and $A_{dec}(A_2)$ in the form of eq. (5.9). We fix D_0^{π} and D_0^{ρ} as in the previous section (without the ρ' in D_0^{π}) and P_0^{π} as the ρ tail by fitting $\Delta \langle Y^3 \rangle \sim \text{Re}(D_0^{\pi} P_0^{\rho*})$ (19). We use $m_{\phi} = 1.02$

GeV and $\Gamma_{\phi} = 4$ MeV. The overall normalization of the OPE amplitudes is fixed by assuming that $(\rho \rightarrow K K) /$

$(\rho \rightarrow \text{all}) = 3.8\%$. $A(\pi\pi \rightarrow K^+ K^-)$ in S^{π} is given by eq.

(A.VIII.11) and $A(\pi\eta \rightarrow K^+ K^-)$ in S^B is given by eq.

(A.VIII.12). θ_{BG} is the $\pi\pi \rightarrow \pi\pi$ background phase and

taken to be 80° . In order to relate S^B to S^{π} by π -B EXD

we have included the factors R_B/R_{π} and $\left(\frac{\sqrt{k_{\eta}} g_{S^{\pi}}^{\pi\eta}}{\sqrt{k_{\eta}} g_{S^B}^{\pi\eta}} \right)$ in S^B

and to allow EXD breaking we let g_B/g_{π} be a free parameter.

The other free parameters are the mass and $\pi\pi$, $K\bar{K}$

coupling of the S^* , the π -exchange slope parameter, b_{π} , the

parameter g_B' giving the normalization of P_0^B . To fix

$(g_{\delta}^{K\bar{K}})^2$ we use the SU(3) prediction

$$(g_{\delta}^{K\bar{K}})^2 = \frac{3}{2} (g_{\delta}^{\pi\eta})^2.$$

To determine the δ meson parameters accurately we simultaneously fitted the $\pi\eta$ mass spectrum for the reaction

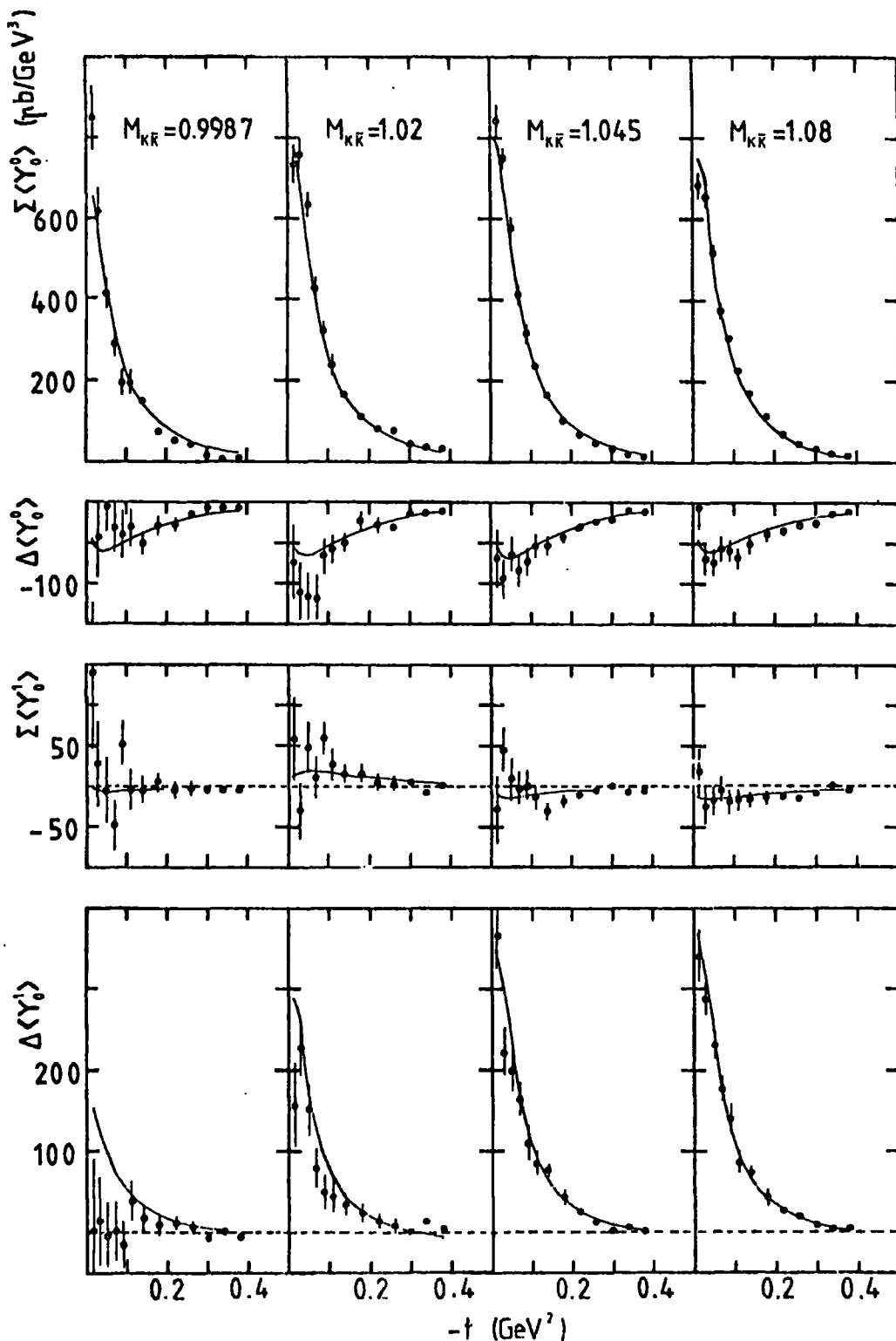


Figure 5.4a: The sum (Σ) and difference (Δ) of the t-channel moments of reactions (5.1) and (5.2) at 6 GeV/c (19). The $M_{K\bar{K}}$ values are given in units of GeV. Here we show $\Sigma \langle Y_0^0 \rangle$, $\Delta \langle Y_0^0 \rangle$, $\Sigma \langle Y_1^1 \rangle$, $\Delta \langle Y_1^1 \rangle$.

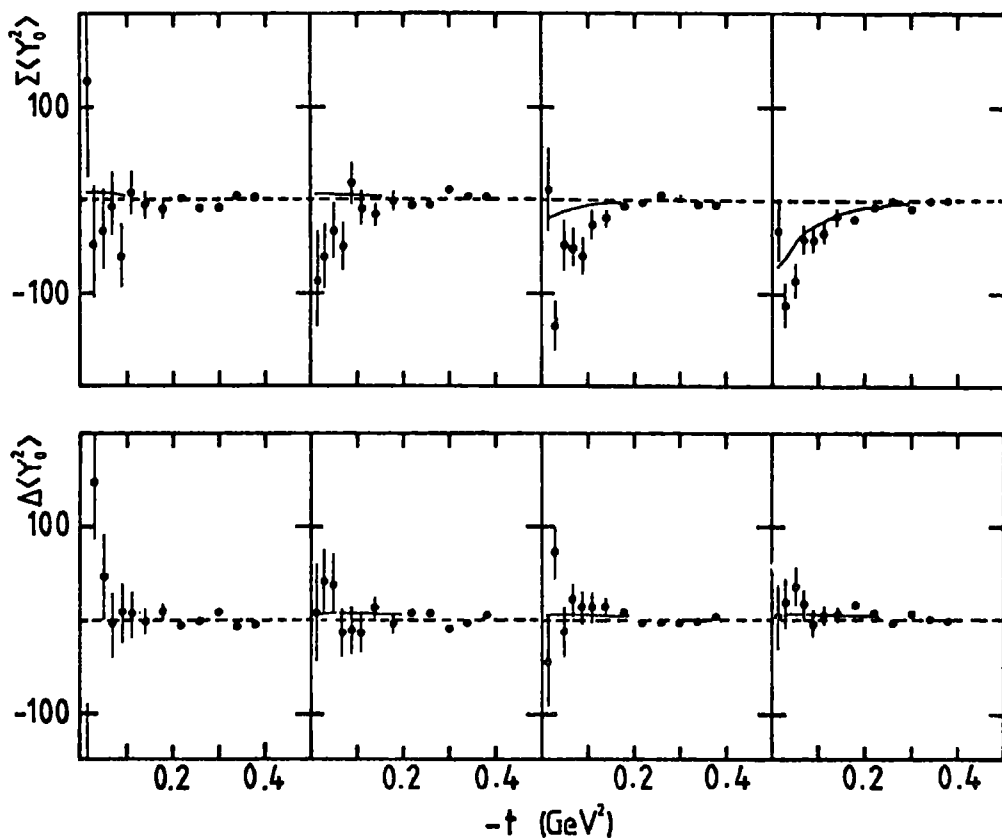


Figure 5.4b: As Fig. 5.4a but for $\Sigma \langle Y_0^2 \rangle$, $\Delta \langle Y_0^2 \rangle$.

$\kappa^- \rho \rightarrow \Sigma^+(1385) (\gamma \pi^-)$ at 4.2 GeV/c⁽⁷⁶⁾. We could not describe $\Delta \langle Y_0^2 \rangle$ in the last two mass bins without adding a linearly rising phase to ρ_0^π which is 23° at $M_{\kappa\bar{\kappa}} = 1.08$ GeV. The results of the best fit are shown in Figs. 5.4 and 5.5 which correspond to

$$\begin{aligned}
 m_{S^*} &= 1.01 \pm 0.03 \text{ GeV} \\
 (g_{S^*}^{\pi\pi})^2 &= 0.35 \pm 0.01 \text{ GeV} \\
 (g_{S^*}^{\kappa\bar{\kappa}})^2 &= 0.88 \pm 0.02 \text{ GeV} \\
 m_\delta &= 0.974 \pm 0.005 \text{ GeV} \quad (5.25) \\
 (g_\delta^{\pi\pi})^2 &= 0.251 \pm 0.018 \text{ GeV} \\
 b_\pi &= 3.3 \pm 0.5 \text{ GeV}^{-2} \\
 g_R/g_\pi &= 2.64 \pm 0.17 \\
 g_B &= -0.52 \pm 0.08 .
 \end{aligned}$$

The resulting amplitudes are shown in Figs. 5.6 and 5.7.

We summarize the main results of the analysis below:

i) We were able to fit the data without including the Z-exchange amplitude (S^Z). That is the δ meson is produced mainly via B exchange.

ii) The sign of the $S^{\pi} - S^B$ interference term (that is $\text{Re}(S^{\pi} S^{B*}) \sim \Delta \langle Y_0^0 \rangle$, predicted by π -B EXD, is compatible with the data. The R_B/R_{π} term (which contains the factor $(1 - e^{i\pi\alpha_B}) / (1 + e^{i\pi\alpha_{\pi}})$) gives a phase of -68° to S^B . S^{π} contains a background phase, θ_{BG} , of 80° . Thus apart from decay phases there is a 148° phase difference between S^B and S^{π} (see Fig. 5.7) which gives a large negative $S^{\pi} - S^B$ interference.

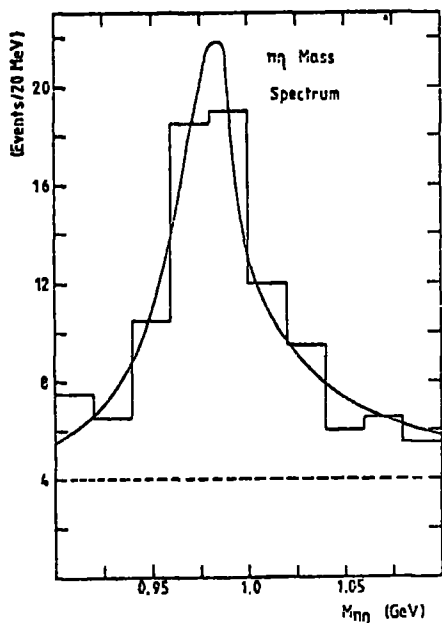


Fig. 5.5: The $(\pi\eta)$ mass spectrum observed in the reaction $K^-_p \rightarrow \Sigma^+(1385) (\eta \pi^-)$ at 4.2 GeV/c (76). The dashed line is the incoherent background to the δ resonance.

iii) P_0^B is negligible except at the ϕ resonance mass, $M_{KR} = 1.02$ GeV. Similarly D_0^B is very small in this mass region.

These two facts mean that we can determine the ratio,

$|S^{\pi}| / |S^B|$, accurately. We have

$$\Sigma \langle Y_0^0 \rangle \sim \text{Re}(S^B P_0^{B*}),$$

$$\Delta \langle Y_0^0 \rangle \sim \text{Re}(S^{\pi} P_0^{\pi*}),$$

$$\Sigma \langle Y_2^0 \rangle \sim \text{Re}(S^{\pi} D_0^{\pi*}) \text{ and}$$

$$\Delta \langle Y_2^0 \rangle \sim \text{Re}(S^B D_0^{B*}),$$

so $|S^B|$ is determined by

$$\Sigma \langle Y_0^0 \rangle, \Delta \langle Y_2^0 \rangle, \text{ and } |S^{\pi}| \text{ by } \Delta \langle Y_0^0 \rangle, \Sigma \langle Y_2^0 \rangle.$$

We find $g_B/g_{\pi} = 2.64$ to be

compared with unity expected from strong π -B EXD. Note that since $\alpha_{\pi} \neq \alpha_B$, we would expect some violation of EXD for the couplings.

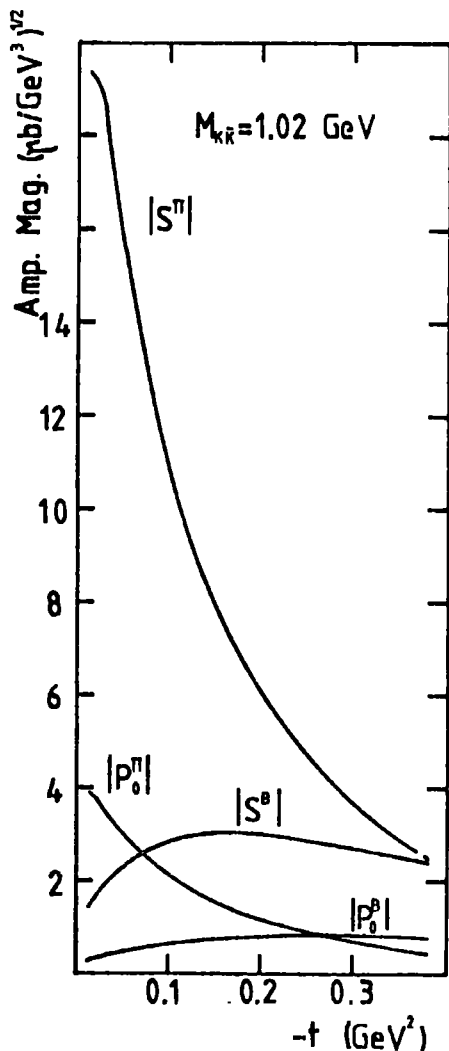


Figure 5.6: The t -dependence of the amplitudes obtained from the fit explained in the text and shown in Figs. (5.4) and (5.5).
 $10^4 |P_0^\pi|_{\max} = 0.34 (\text{pb}/\text{GeV}^2)^{1/2}$
 $10^4 |S^0|_{\max} = 0.03 (\text{pb}/\text{GeV}^2)^{1/2}$
 in this $M_{k\bar{k}}$ value.

iv) We determined the δ resonance parameters by fitting $(\pi\eta)$ mass spectrum, simultaneously with the (K^+K^-) production data, and requiring $(g_\delta^{K\bar{K}})^2 = 3/2 (g_\delta^{\pi\eta})^2$. The results

$$m_\delta = 974 \pm 5 \text{ MeV}$$

$$\Gamma_\delta^{\pi\eta} = 49.2 \pm 3.6 \text{ MeV}$$

are consistent with the PGD values⁽³⁷⁾

$$(m_\delta = 976 \pm 10 \text{ MeV}, \Gamma_\delta = 50 \pm 20 \text{ MeV})$$

. The S^* parameters are somewhat different from those determined in Chapter III. In this analysis we ignored all the information from the

$\pi\pi \rightarrow \pi\pi$, $I = 0$, S wave and used a very small region of $M_{k\bar{k}}$.

So it is not possible to determine reliable S^* parameters in such an analysis. However the resulting $L = 0$ $A(\pi\pi \rightarrow K\bar{K})$ amplitude is consistent with the results of Chapter III.

v) We found $b_\pi = 3.3 \pm 0.5 \text{ GeV}^{-2}$. This value is different from $b_\pi = 2.2 \pm 0.3 \text{ GeV}^{-2}$ determined in previous section. The same difference has been observed by the experimental group⁽¹⁹⁾. S^π and D_0^π are produced by the same exchange mechanisms (OPE) and a naive expectation would be that they have the same t -dependence. In our simple

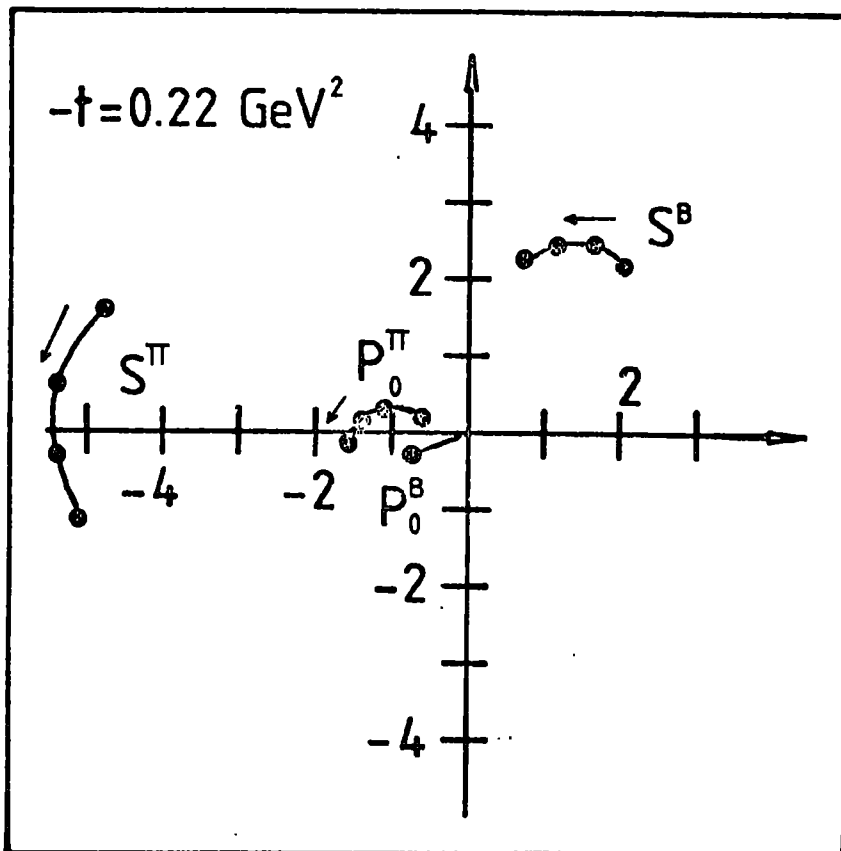


Figure 5.7: The amplitudes at $-t = 0.22$ GeV^2 , in units of $(\mu\text{b}/\text{GeV}^2)^{1/2}$. The arrows show the direction increasing $M_{K\bar{K}}$. The points correspond to the amplitude values at $M_{K\bar{K}} = 0.9987, 1.02, 1.045$ and 1.08 GeV respectively. P_0^B is only shown at the resonant mass, $M_{K\bar{K}}^0 = 1.02$ GeV , otherwise it is very small.

model we assume that b_π has no $M_{K\bar{K}}$ dependence. Perhaps a more detailed model could solve this problem.

v1) The data show evidence of ϕ production. The moment $\Sigma \langle Y_0^1 \rangle \sim \text{Re}(S^\pi P_0^{B*})$ is consistently positive at $M_{K\bar{K}} = 1.02$ GeV , which indicates the phase of production amplitude, P_0^B , is that of π -B EXD with a negative sign (see Fig. 5.7).

vii) We could not fit $\Delta \langle Y_0^1 \rangle \sim \text{Re}(S^\pi P_0^{\pi*})$ without adding some phase to P_0^π . We observed the same problem in Chapter III. The ignorance of the amplitudes P_0^Z, P_0^{A1} can

give such a discrepancy, but it is not possible to determine these amplitudes from the data for reactions (5.1) and (5.2).

viii) We have explicitly calculated the K^+ , K^- and K^0 , \bar{K}^0 mass difference effects (see Appendix VIII). Although this effect complicates the resonance forms, it does not effect the results appreciably. The mixing arises from a term proportional to

$$\frac{1}{4} (k_c - k_o)^2 = 0.00027 \text{ at } M_{\bar{K}K} = 1 \text{ GeV.}$$

The other modifications are of the form $g^2 k_{o,c}$ and $g^2 \frac{1}{2} (k_c + k_o)$. Their contributions are very small compared to $g^2 k_\pi$ and $g^2 k_\eta$.

5.4 $\pi\pi \rightarrow K\bar{K}$ Phase Shift Analysis

The $\pi\pi \rightarrow \pi\pi$ interaction has been studied intensively using data from OPE dominated reactions, such as $\pi^- p \rightarrow \pi^- \pi^+ n$. One may think a similar analysis of, for instance, $\pi^- p \rightarrow K^- K^+ n$ data can, in the same way, give reliable information about $\pi\pi \rightarrow K\bar{K}$ scattering. However the exchange mechanisms of the reaction $\pi^- p \rightarrow K^- K^+ n$ are more complicated than those for $\pi^- p \rightarrow \pi^- \pi^+ n$, (compare Tables 2.2 and 2.3). Therefore, the methods, used to determine the $\pi\pi \rightarrow \pi\pi$ amplitudes from $\pi^- p \rightarrow \pi^- \pi^+ n$ data, can give misleading results when applied to $\pi\pi \rightarrow K\bar{K}$ scattering. A good example of this danger is the confusion about the properties of the S wave peak observed in $(K^+ K^-)$ and $(K_S^0 K_S^0)$ final states, around $M_{\bar{K}K} = 1.3 \text{ GeV}^{(9,10)}$. Pawlicki et al.^(10, 19) have isolated $|S|^2$ from $\sum \langle Y_0^0 \rangle$ of reactions (5.1) and (5.2) in the forward scattering region ($-t < 0.08 \text{ GeV}^2$) and observed a strong peak around

$M_{K\bar{K}} = 1.3$ GeV. Having ignored the possible S^Z amplitude, which can play an important role in the small t region, they concluded that the $I = 0$ S wave (OPE S wave) should be ten times larger than $I = 1$ S wave in this t region. On the other hand Cason et al. concluded this peak is produced entirely by the $I = 1$ S wave, by inspecting the t -dependence of $|S|^2$ for the $(K_S^0 K_S^0)$ final state⁽⁹⁾. This confusion shows that it is misleading to draw conclusions from the data for reactions (5.1), (5.2) and $\pi^- p \rightarrow K_S^0 K_S^0 n$ without studying the exchange mechanisms carefully.

The results of Chapter IV and Sections 5.2 and 5.3 provide enough information to perform a reliable $\pi\bar{\pi} \rightarrow K\bar{K}$ phase shift analysis using the data for reactions (5.1) and (5.2) in the small t region ($-t < 0.08$ GeV²). Here we summarize our present knowledge about $(K\bar{K})$ production:

i) The OPE S wave is the dominant amplitude in the region $M_{K\bar{K}} < 1.1$ GeV. There is no sign of a sizeable Z exchange amplitude, S^Z , in this mass region. Moreover from Fig. 5.6 we see that $|S^{\pi}|/|S^B| \sim 10$ at $-t = 0.05$ GeV². There is an $I = 1, L = 0$ resonance with mass about 1.3 GeV in $(K\bar{K})$ system, which is produced by both B and, more dominantly at small t , Z exchange.

ii) The OPE P wave is compatible with the $\rho \rightarrow K\bar{K}$ tail. Indeed it is possible to fit $\Delta\langle Y_0^3 \rangle \sim \text{Re}(D_0^{\pi\bar{\pi}} P_0^{\pi\bar{\pi}*})$ in terms of ρ - ρ' interference⁽¹⁹⁾. $\Sigma\langle Y_0^3 \rangle$ is consistent with zero in the small t region, indicating that the $I = 0$ P wave is negligible.

iii) The OPE D wave has a strong ρ - ρ' interference effect. We use the $D(\pi\bar{\pi} \rightarrow K\bar{K})$ amplitude, determined in Sec. 5.2, to fix the overall phase of the $\pi\bar{\pi} \rightarrow K\bar{K}$

amplitudes. The K^+K^0 production analysis also gives the amount of A_2 resonance production by B and Z exchange.

iv) The OPE F wave is compatible with the g meson tail with branching ratios $B(\eta \rightarrow \pi\pi) = 24\%$, $B(\eta \rightarrow K\bar{K}) = 1.3\%$. There is no indication of sizeable $I = 0, L = 3$ amplitudes.

This information shows that we must subtract the known contributions of the S^B, S^Z, D_0^B, D_0^Z amplitudes from the K^+K^- production data before performing a $\pi\pi \rightarrow K\bar{K}$ phase shift analysis. In order to determine the S^B and S^Z amplitudes we fit $|S_0| \equiv (|S^B|^2 + |S^Z|^2)^{1/2}$ of the (K^+K^0) system as a function of $M_{K\bar{K}}$ and t . We write the amplitudes in the form:

$$\begin{aligned} S^B &= C_B \sqrt{-t} (1 - e^{i\pi\alpha_B}) \Gamma(-\alpha_B) (p_L)^{\alpha_B-1} D(\delta') \\ S^Z &= C_Z (1 + e^{i\pi\alpha_Z}) \Gamma(1-\alpha_Z) (p_L)^{\alpha_Z-1} D(\delta') \end{aligned} \quad (5.26)$$

where C_B and C_Z are free parameters, α_B and α_Z are given in eqs. (5.18) and

$$D(\delta') = \frac{\sqrt{\gamma}}{m_{\delta'}^2 - M_{K\bar{K}}^2 - i\gamma} \quad , \quad (5.27)$$

$$\begin{aligned} \gamma &= m_{\delta'} \Gamma_{\delta'} k/k_R \\ k &= \left(\frac{M_{K\bar{K}}^2}{4} - m_K^2 \right)^{1/2} \quad , \quad k_R = \left(\frac{m_{\delta'}^2}{4} - m_K^2 \right)^{1/2} \end{aligned}$$

with $m_{\delta'}$, and $\Gamma_{\delta'}$ as free parameters. Recall that the (K^+K^0) data is at $p_L = 10$ GeV/c and that the (K^+K^-) data is at 6 GeV/c. To fit to the $|S_0|$ obtained from the (K^+K^0) data as a function of t we integrate S^B and S^Z over the experimental mass interval $(1.2 < M_{K\bar{K}} < 1.4$ GeV), that is

$$|S_0| = \left[\int_{1.2}^{1.4} (|S^B|^2 + |S^Z|^2) dM_{K\bar{K}} \right]^{1/2} \quad (5.28)$$

We do not use the two most forward points or the points with $-t < 0.42 \text{ GeV}^2$. To fit the $|S_0|$ of $(K^0 K^-)$ as a function of $M_{K\bar{K}}$ we include a δ resonance tail contribution, parametrized as

$$B(s) = C e^{b(1 - M_{K\bar{K}})}$$

where C and b are free parameters. That is we use

$$|S_0| = [C_N |D(s)|^2 + |B(s)|^2]^{1/2} \quad (5.29)$$

where C_N is a free parameter. The results are shown in Fig. 5.8, and correspond to

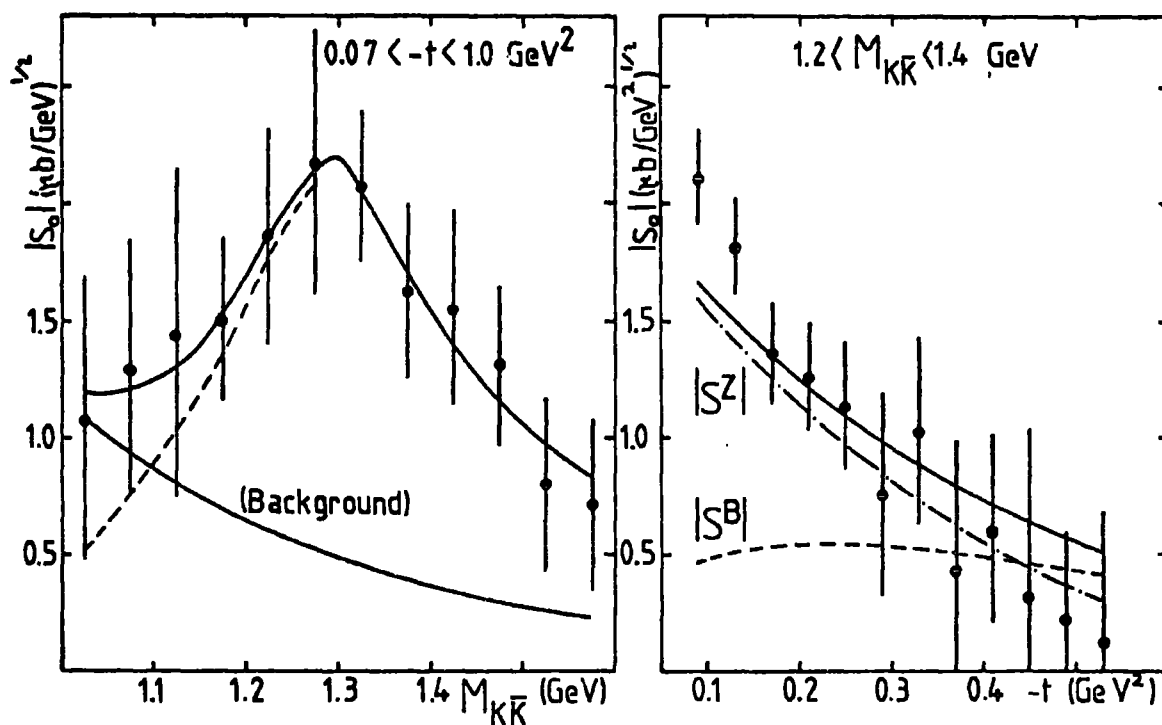


Figure 5.8: The mass and t -dependence of $|S_0|$ obtained from $(K^0 K^-)$ data. The curves correspond to the results explained in the text. In the mass-dependent figure, the background curve is the possible δ tail and the dashed curve is the δ' low energy tail.

$$\begin{aligned}
 C_B &= 16.2 \text{ (fixed)} \\
 C_Z &= 40.9 \pm 5.1 \\
 m_{\delta'} &= 1.302 \pm 0.023 \text{ GeV} \\
 \Gamma_{\delta'} &= 0.220 \pm 0.044 \text{ GeV} \\
 C &= 1.18 \pm 0.44 \\
 b &= 2.8 \pm 1.6 \\
 C_N &= 1.26 \pm 0.22 \quad . \quad (5.30)
 \end{aligned}$$

In the fit we fixed the magnitude of S^B by estimating the minimum size required by $\Delta \langle Y_0^0 \rangle \sim \text{Re}(S^{\bar{\pi}} S^{B*})$ for reactions (5.1) and (5.2), and by requiring that $|S_0|$ in eq. (5.28) should not exceed the error bars in the large t region.

As we already have enough information about the $L = 1, 2, 3$ (P, D, F) $\pi\pi \rightarrow K\bar{K}$ waves, the main purpose of this analysis is to determine the $\pi\pi \rightarrow K\bar{K}$ S wave amplitude. From the results of Chapter III and Section 5.3 we know that the S wave should start somewhere near 180° in the Argand circle (see Figs. 3.5 and 5.7). From the $M_{K\bar{K}}$ dependence of $\Sigma \langle Y_0^0 \rangle \sim |S^{\bar{\pi}}|^2$ just above the $K\bar{K}$ threshold, we can conclude that the S^* should be a normal Breit-Wigner resonance (associated with two poles), and not a large negative $K\bar{K}$ scattering length effect. As we have seen in Chapter III and Section 5.3, it is not possible to describe $\Delta \langle Y_0^1 \rangle$ by interfering S^* - ρ resonances. This misfit could be due to ignorance of P_0^B and P_0^Z which can interfere with S^B and S^Z . For this reason we do not fit $\Delta \langle Y_0^1 \rangle$ and $\Delta \langle Y_1^1 \rangle$ in the analysis. Instead we fix the $|P_0^{\pi}|$ by fitting $\Delta \langle Y_0^3 \rangle$ (with $-t < 0.08 \text{ GeV}^2$), taking the form of $P_0^{\bar{\pi}}$ as the ρ meson tail and $D_0^{\bar{\pi}}$ as the ρ meson.

We perform an energy-independent $\pi\pi \rightarrow K\bar{K}$ phase shift analysis using the observed $\Sigma\langle Y_0^0 \rangle$, $\Sigma\langle Y_0^2 \rangle$, $\Sigma\langle Y_1^1 \rangle$, $\Delta\langle Y_0^2 \rangle$, $\Delta\langle Y_1^1 \rangle$, $\Sigma\langle Y_2^0 \rangle$, $\Sigma\langle Y_2^2 \rangle$, with $-t < 0.08 \text{ GeV}^2$, of the reactions (5.1), (5.2). We first subtracted the

$$\begin{aligned} |S^{\bar{1}=1}|^2 &= |S^B|^2 + |S^Z|^2 \\ |D^{\bar{1}=1}|^2 &= |D_0^B|^2 + |D_0^Z|^2 \\ \text{Re}(S^{\bar{1}=1} D^{\bar{1}=1*}) &= \text{Re}(S^Z D^{Z*}) \end{aligned} \quad (5.31)$$

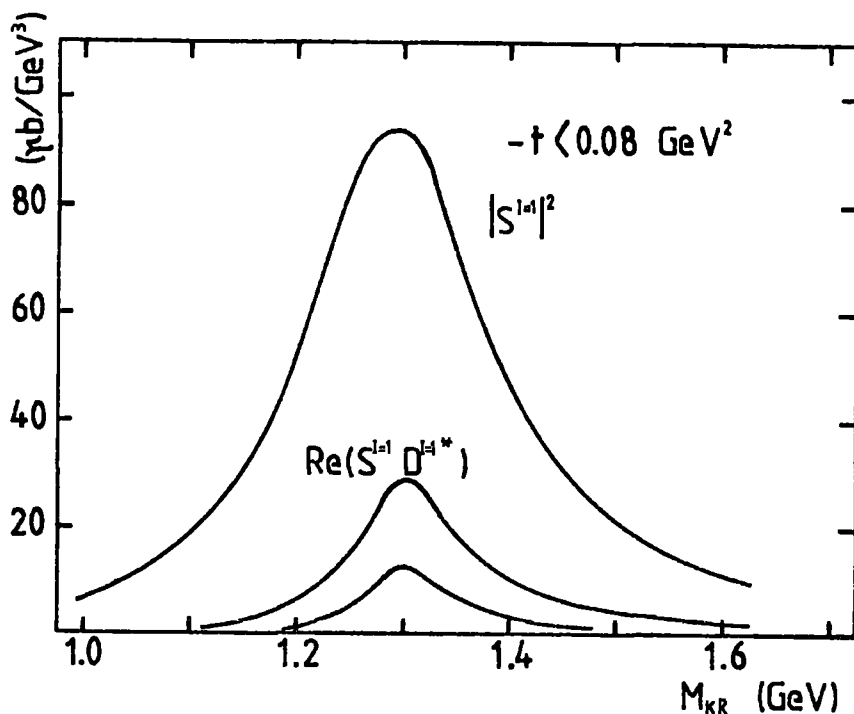


Figure 5.9: $|S^{\bar{1}=1}|^2$, $|D^{\bar{1}=1}|^2$ and $\text{Re}(S^{\bar{1}=1} D^{\bar{1}=1*})$ which are subtracted from the 6 GeV/c (K^+K^-) production data prior to the $\pi\pi \rightarrow K\bar{K}$ phase shift analysis. The lowest curve is for $|D^{\bar{1}=1}|^2$.

contributions, shown in Fig. 5.9, from the data. To do this we used the same D_0^B and D_0^Z as in Section 5.2 (see Fig. 5.2). We also used the S^Z and S^B given by (5.26) with the parameters

listed in (5.30) and $p_L = 6 \text{ GeV}/c$. The $S^Z - D_0^Z$ interference term was calculated assuming the phase between these amplitudes is given by $\theta_{S^Z} - \theta_{A_2}$ decay phases. We parametrize the other non-zero amplitudes as:

$$S^{\bar{\pi}} = C_{\bar{\pi}}(t, M_{K\bar{K}}) \frac{1}{\sqrt{3}} A_0^0(\bar{\pi}\bar{\pi} \rightarrow K\bar{K})$$

$$P_0^{\bar{\pi}} = C_{\bar{\pi}}(t, M_{K\bar{K}}) \frac{\sqrt{3}}{\sqrt{2}} A_1^1(\bar{\pi}\bar{\pi} \rightarrow K\bar{K})$$

$$P_- = c_p P_0^{\bar{\pi}}, \quad |P_+| = |P_-|$$

$$D_0^{\bar{\pi}} = C_{\bar{\pi}}(t, M_{K\bar{K}}) \frac{\sqrt{5}}{\sqrt{3}} A_2^0(\bar{\pi}\bar{\pi} \rightarrow K\bar{K})$$

$$D_- = c_D D_0^{\bar{\pi}}, \quad |D_+| = |D_-|$$

$$F_0^{\bar{\pi}} = C_{\bar{\pi}}(t, M_{K\bar{K}}) \frac{\sqrt{7}}{\sqrt{2}} A_3^1(\bar{\pi}\bar{\pi} \rightarrow K\bar{K}) \quad (5.32)$$

where $A_L^I(\bar{\pi}\bar{\pi} \rightarrow K\bar{K})$ are the $\bar{\pi}\bar{\pi} \rightarrow K\bar{K}$ Argand amplitudes as given by the A_{12} element in eq. (3.9), $C_{\bar{\pi}}(t, M_{K\bar{K}})$ is given by eq. (5.24) with $b_{\bar{\pi}} = 2.2 \text{ GeV}^{-2}$. We take t_{\min} into account by evaluating all the t -dependent factors at the average $|t|$ values of each mass bin. This average value increases with increasing $M_{K\bar{K}}$ due to the t_{\min} effect. We fix $|A_1^1|$ as explained above, and $|A_3^1|$ as in section 5.2 (see Fig. 5.10), and the overall normalization as in Section 5.3. The free parameters are $|A_0^0|$, $|A_2^0|$, θ_{S^Z} , θ_{P^Z} , c_p and c_D for each mass bin. We obtain a perfect description of the data in each mass bin. The resulting $|A_0^0|$ and $|A_2^0|$ are shown in Fig. 5.10. Note that since we have fixed $|A_1^1|$, there is no ambiguity in the determination of $|A_0^0|$. The resulting c_p and c_D , which specify the absorptive effects, are shown in Fig. 5.11. There are

two possible solutions for the phases of the A_0^0 and A_1^1 amplitudes, which correspond to the substitutions $\theta_{S_0} \leftrightarrow -\theta_{S_0}$ and $\theta_{P_0} \leftrightarrow -\theta_{P_0}$. We fix the overall phase by assuming the phase of A_2^0 is given by $\rho - \rho'$ decay phases (see Fig. 5.3). We plot in Fig. 5.12 the phases of A_0^0 , A_1^1 of the solution for which the resulting A_1^1 phase is

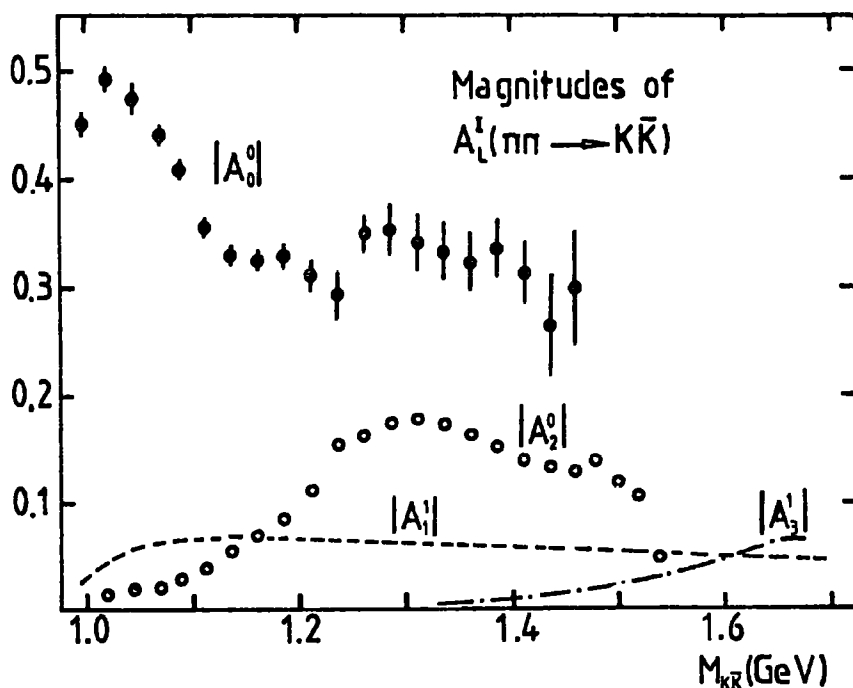


Figure 5.10: Magnitudes of $A_L^i (\pi\pi \rightarrow \kappa\bar{\kappa})$ amplitudes. The errors on the $|A_1^1|$ are very small and are not shown. $|A_1^1|$ is the ρ tail prediction as explained in the text. $|A_2^0|$ is the g meson tail with $B(g \rightarrow \kappa\bar{\kappa}) = 1.3\%$ and $B(g \rightarrow \pi\pi) = 24\%$.

compatible with ρ tail phase at the lower $M_{\kappa\bar{\kappa}}$ values. The phases of the A_0^0 , A_1^1 amplitudes of the other possible solution move rapidly anticlockwise in the Argand circle, and the A_1^1 phase is very different from the expected ρ tail phase. Since A_2^0 is very small in the region $M_{\kappa\bar{\kappa}} < 1.2$ GeV it is not possible to determine the θ_{S_0} and θ_{P_0} reliably. Indeed we can only determine these phases with very large errors ($\pm 60^\circ$ on average).

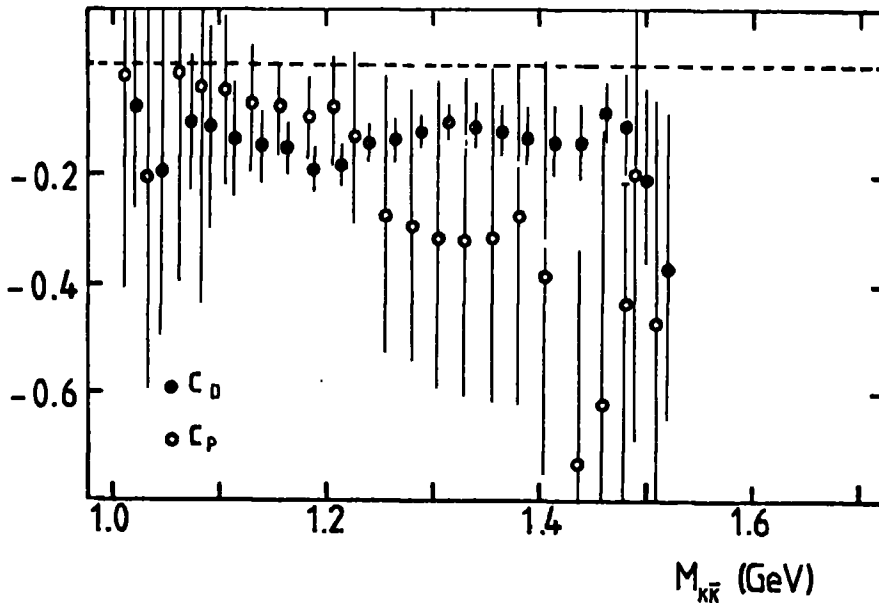


Figure 5.11: The c_P and c_D in eqs. (5.32).

Our two solutions are similar to Cohen's solutions III.a and III.b⁽⁷⁷⁾. We favour the solution with the slow variation of the A_0^0 and A_1^1 phases (similar to Cohen's III.b). We disregarded the other solution for two reasons:

i) Although the A_1^1 phase is consistent with the ρ tail near the threshold, it rapidly moves away from the ρ -tail phase, for instance $\delta_1^1 = 245^\circ$ at $M_{K\bar{K}} = 1.1125$ GeV.

ii) The phase variation in the $I = 0$ S wave of the elastic ($\pi\bar{\pi} \rightarrow \pi\bar{\pi}$) channel is unable to match the fast phase resulting for A_0^0 ($\pi\bar{\pi} \rightarrow K\bar{K}$). In the favoured solution, the A_1^1 phase is consistent with the ρ tail phase up to $M_{K\bar{K}} = 1.25$ GeV and then rises slowly. This latter phase variation may be an indication of the $\rho'(1600) \rightarrow K\bar{K}$ decay.

The results for $c_P = P_-/P_0^\pi$ and $c_D = D_-/D_0^\pi$ do not show any systematic $M_{K\bar{K}}$ dependence (see Fig. 5.11), and they are not consistent with the Williams model (or the

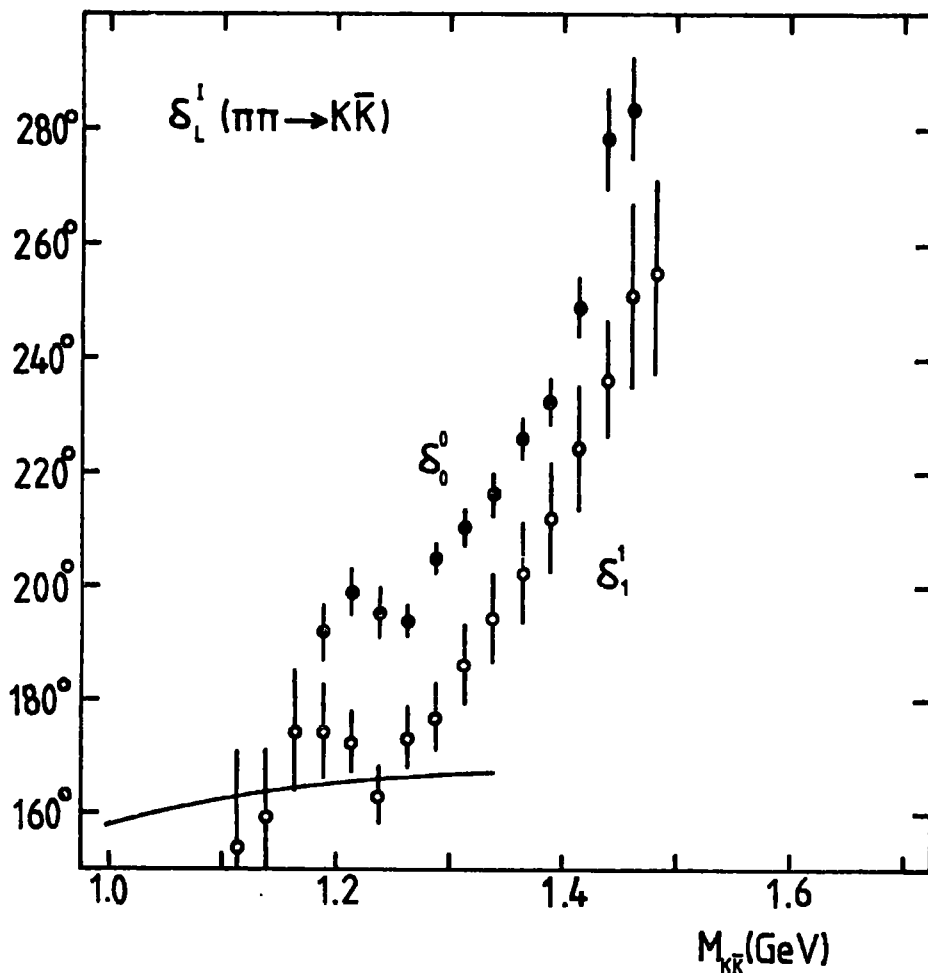


Figure 5.12: The resulting $\delta_0^0(\pi\pi \rightarrow \kappa\bar{\kappa})$ and $\delta_1^1(\pi\pi \rightarrow \kappa\bar{\kappa})$ phases for the favoured solution. The curve is the ρ tail δ_1^1 prediction. These phases are fixed by assuming δ_2^0 is given as in Fig. 5.3.

"Poor Man Absorption") prediction (c.f. eq. (2.41)). In the analysis we assumed that the L_- amplitudes are produced by OPE absorptive effects and ignored possible L_- contributions from B or Z exchange. This could be the reason why the c_p and c_D values are not consistent with simple OPE absorption model predictions. However the sign is consistent with a OPE absorptive effect.

We are able to obtain an accurate determination of $|A_0^0|$ up to $M_{K\bar{K}} = 1.45$ GeV. The resulting values of $|A_0^0|$ show a strong S^* peak, reaching the unitarity limit at $M_{K\bar{K}} = 1.02$ GeV.

Beyond 1.15 GeV, $|A_0^0|$ does not continue to fall off as the tail of an S^* resonance, but stays flat on average value of 0.325 throughout the mass region $1.15 < M_{K\bar{K}} < 1.4$ GeV (see Fig. 5.10). This information can help to determine the size of the poorly known $I = 0$ $\pi\pi \rightarrow \pi\pi$ S wave in this mass region (see Ref. (78) for a recent review). If we ignore the effects of the channels other than $\pi\pi$ and $K\bar{K}$, then $\eta_{L=0}^{I=0}(\pi\pi)$ should be about 0.76 in the region $M_{\pi\pi} = 1.15 - 1.4$ GeV. The behaviour of $S^{I=0}(\pi\pi \rightarrow \pi\pi)$ and $S^{I=0}(\pi\pi \rightarrow K\bar{K})$ cannot lead to an unambiguous solution, since we do not have any information about the phase of the $S^{I=0}(K\bar{K} \rightarrow K\bar{K})$ amplitude. However the resulting δ_0^0 , in Fig. 5.12, seems to be consistent with the phase of $I = 0$, $\pi\pi \rightarrow \pi\pi$ S wave.

5.5 Conclusions

The complexity of the exchange mechanisms for the reactions (5.1) and (5.2) means that the (K^+K^-) data can only be reliably analysed if we have further information on contributing amplitudes. However using the results of Chapter IV for (K^-K^0) production to determine the $I = 1$ S and D waves, and inputting this information we were able to perform an $I = 0$ S,D and $I = 1$ P,F partial wave analysis of the (K^+K^-) data. In this way we obtained rather accurate information about $\pi\pi \rightarrow K\bar{K}$ scattering. The main results of this chapter are following:

- 1) We first determined the $I = 0$, $\pi\pi \rightarrow K\bar{K}$ D wave, in terms of overlapping f_0 and f_0' resonances. We described the $f_0 - f_0'$ interference effect by the mass-matrix formalism and found the f_0' meson parameters

$$m_{\rho'} = 1.513 \pm 0.003 \text{ GeV}$$

$$\Gamma_{\rho'}^{++} = 43 \pm 9 \text{ MeV}$$

$$B(\rho' \rightarrow \pi\pi) = 1.6 \pm 0.6\%$$

2) We analysed the threshold region in terms of S^* and δ resonances, relating the B to the π exchange amplitudes by π -B EXD. We found that the data are compatible with the phases of the amplitudes as predicted by π -B EXD and determined the δ meson parameters as

$$m_{\delta} = 974 \pm 5 \text{ MeV},$$

$$\Gamma_{\delta}^{\pi\eta} = 49.2 \pm 3.6 \text{ MeV}.$$

We were able to determine the S wave ($K\bar{K}$) production amplitudes, S^{π} and S^R , and found $|S^{\pi}|/|S^R| \sim 10$ at $-t = 0.05 \text{ GeV}^2$. We did not find any evidence of an S^Z amplitude in the threshold region. We explicitly calculated the effect of K^+ , K^- and K^0 , \bar{K}^0 mass difference and found that it was unimportant.

3) We fitted the $|S_{\rho}|$ extracted from (K^-K^0) data, both as function of $M_{K\bar{K}}$ and t , in terms of S^Z and S^R amplitudes. We determined the δ' meson parameters as

$$m_{\delta'} = 1.302 \pm 0.023 \text{ GeV}$$

$$\Gamma_{\delta'}^{++} = 220 \pm 44 \text{ MeV}$$

We then used the resulting S^Z and S^R in the (K^+K^-) production data analysis by extrapolating them $p_L = 10 \text{ GeV}/c$ to $p_L = 6 \text{ GeV}/c$.

4) We found that the $\pi\bar{\pi} \rightarrow K\bar{K}$ P wave is given by ρ -tail by fitting $\Delta\langle Y^3 \rangle$ in terms of ρ - ω interference. We also found that the $\pi\bar{\pi} \rightarrow K\bar{K}$ F wave is given by the ρ meson tail with $B(\rho \rightarrow \pi\bar{\pi}) = 24\%$, $B(\rho \rightarrow K\bar{K}) = 1.3\%$.

5) We performed a $\pi\bar{\pi} \rightarrow K\bar{K}$ phase shift analysis to determine the $I = 0$ $\pi\bar{\pi} \rightarrow K\bar{K}$ S wave. We determined its magnitude and phase accurately up to $M_{K\bar{K}} = 1.4$ GeV. The magnitude of $\pi\bar{\pi} \rightarrow K\bar{K}$ S wave shows the strong S^* peak in the threshold region and stays flat at about 0.325 in the region of $M_{K\bar{K}} = 1.15 - 1.4$ GeV. We found two possible solutions, one of which gives $S(\pi\bar{\pi} \rightarrow K\bar{K})$ with a rapid counter clockwise phase movement, while the other gives a slow phase variation. We favour the solution with slow phase.

CHAPTER VI

Classification of $J^{PC} = 0^{++}$ Mesons

In the last three chapters of this thesis we have obtained a lot of information about the non-strange 0^{++} mesons. We have seen that the S^* is a normal Breit-Wigner resonance with $m_{S^*} = 980$ MeV and $(g_{S^*}^{\pi\pi})^2 / (g_{S^*}^{K\bar{K}})^2 \approx 0.25$. There could be a very broad elastic $I = 0$ $\pi\pi$ resonance, called ξ . The $I = 1$ $\delta(970)$ is observed clearly in the $(\pi\eta)$ mass spectrum and its $\pi\eta$ and $K\bar{K}$ couplings ratio is consistent with the SU(3) predicted value. In addition to the $\delta(970)$, there is another $I = 1$, 0^{++} resonance with mass 1.3 GeV and width 220 MeV. The existence of two $I = 1$, 0^{++} resonances, $\delta(970)$, $\delta'(1300)$, makes the problem of classifying the 0^{++} mesons a very delicate job. However one may question the existence of these $I = 1$, 0^{++} mesons. The $\delta(970)$ is clearly evident in the $(\pi\eta)$ mass spectrum^(76,79). We have also observed the $\delta(970)$ production in the (K^+K^-) system in the Section 5.3. The $\delta'(1300)$ is observed as a pronounced peak in the (K^-K^0) S wave mass spectrum (see Figs. 4.9 and 5.8). Also the t-dependence of $|S_0|$ extracted from (K^-K^0) production data in the region $M_{K\bar{K}} = 1.2 - 1.4$ GeV shows very clear indication of $\delta'(1300)$ production (see Fig. 4.2). Further evidence for $\delta'(1300)$ production can be obtained from the (K^+K^-) production data⁽¹⁹⁾. In

Fig. 6.1 we use the (K^+K^-) data to plot $\sum \langle Y_0^0 \rangle \approx 2 |S|^2$ and $\Delta \langle Y_0^0 \rangle \approx 4 \operatorname{Re} (S^{J=0} S^{J=1*})$ at $M_{K\bar{K}} = 1.045$ GeV; and also $2 |S|^2$ and $\Delta \langle Y_0^0 \rangle$ (which is again $S^{J=0} - S^{J=1}$ interference effect since $\Delta \langle Y_0^0 \rangle$ is small indicating that $D^{I=0} - D^{I=1}$ interference effect is negligible) at $M_{K\bar{K}} = 1.275$ GeV, as functions of t . The figure shows that the exchange mechanism for S wave production at $M_{K\bar{K}} = 1.045$ and 1.275 GeV are entirely different. We know that in the threshold region S^{π} is the dominant amplitude, and that $\Delta \langle Y_0^0 \rangle$ can be explained by including a small S^B amplitude (see Section 5.3, Fig. 5.4). The t -dependence of $|S|^2$ at $M_{K\bar{K}} = 1.275$ GeV is shallower than that at $M_{K\bar{K}} = 1.045$ GeV, indicating the presence of other exchanges besides S^{π} . Also $\Delta \langle Y_0^0 \rangle$ has a very different t -dependence in the two mass regions. $\Delta \langle Y_0^0 \rangle$, at $M_{K\bar{K}} = 1.275$ GeV, cannot be described without introducing a large S^Z amplitude. The shallow t -dependence of $|S|^2$ around $M_{K\bar{K}} = 1.3$ GeV has been also observed in the reaction $\pi p \rightarrow (K_S^0 K_S^0) n$ (9).

Before the discovery of the $\delta'(1300)$ Morgan was able to accommodate the 0^{++} mesons in a non-ideally mixed (mixing angle about 70°) $L = 1$ ($q\bar{q}$) nonet, provided the states were taken to be $\delta(970)$, $\kappa(1200)$, $S^*(980)$ and $\xi(1300)$ (11). There are some outstanding problems with this classification scheme. The 1^{--} and 2^{++} nonets, which are the well-established nonets, are ideally mixed, therefore one might have expected an ideally mixed 0^{++} nonet. The other problem is the uncertainty about the mass of the κ and ξ mesons. For instance, a recent analysis of the $(K\pi)$ system (13) has shown the mass of the κ resonance could be as high as 1.45 GeV, which

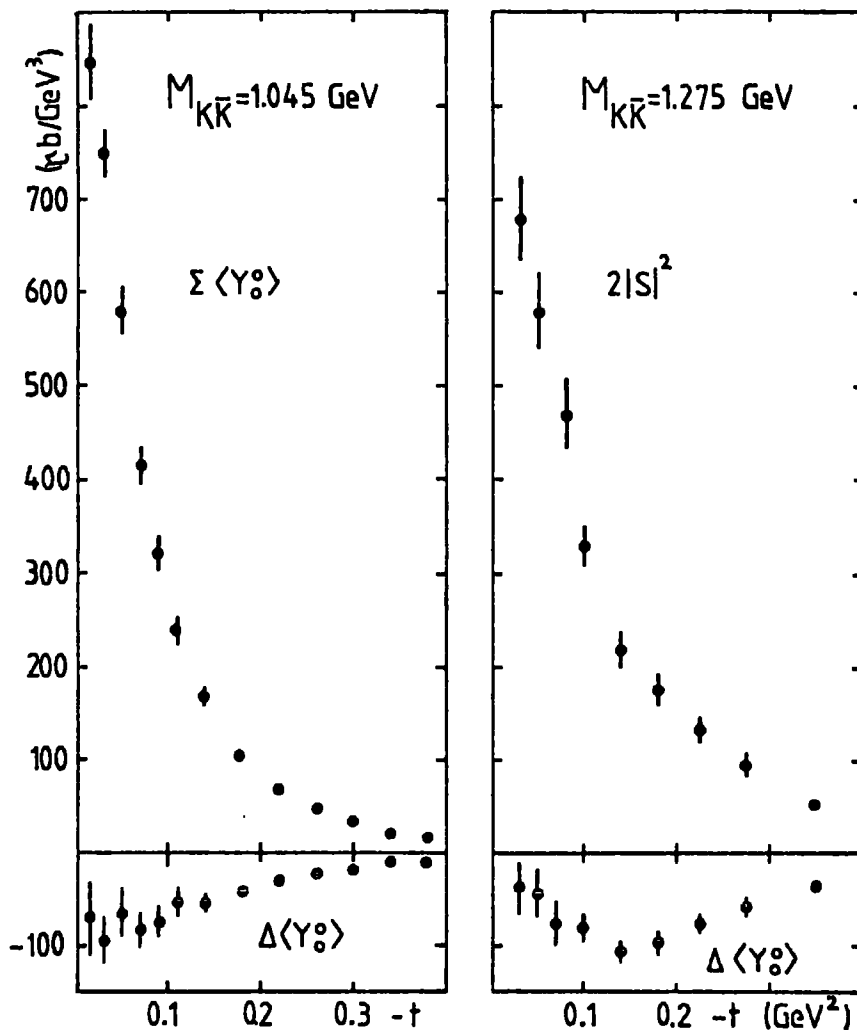


Figure 6.1: The t -dependence of $\Sigma\langle\Upsilon_0\rangle \sim 2|S|^2$ and $\Delta\langle\Upsilon_0\rangle = 4\text{Re}(S^{I=0}S^{I=1*})$ at $M_{K\bar{K}} = 1.045$ GeV; and of $2|S|^2$ and $\Delta\langle\Upsilon_0\rangle$ at $M_{K\bar{K}} = 1.275$ GeV. At $M_{K\bar{K}} = 1.275$ GeV we use $\Sigma\langle\Upsilon_0\rangle$, $\Sigma\langle\Upsilon_1\rangle$, $\Sigma\langle\Upsilon_2\rangle$ and $\Sigma\langle\Upsilon_3\rangle$ to isolate $2|S|^2$.

will violate the Gell-Mann, Okubo mass formulae for the 0^{++} nonet. Also the ξ mass could vary from 800 MeV up to 1.3 GeV.

The $\delta'(1300)$ has $I = 1$. Thus it cannot belong to an SU(3) singlet, (that means it cannot be a glueball or a dilaton). The simplest assumption is that there are two 0^{++} nonets. If we assume that the δ , ν , S^* and ξ are members of the $L = 1$ ($q\bar{q}$) nonet, then the δ' could be a

member of the radially excited $L = 1$ ($q\bar{q}$) nonet. However this is very unlikely, because the mass difference of the $\delta'(1300)$ and the $\delta(970)$, about 300 MeV, is small. We do not expect to see the first radial excitation of the $\delta(970)$ below 1.45 GeV.

A possible way out of the dilemma has been given by Jaffe⁽⁷⁾. He has studied the $L = 0$ ($qq\bar{q}\bar{q}$) states, using a simple magnetic gluon interaction to estimate the mass splitting⁽⁸⁰⁾, and found that the lowest lying ($qq\bar{q}\bar{q}$) states belong to a O^{++} nonet. Interestingly an explicit quark-bag model calculation⁽⁷⁾ estimates the mass of such states to be about 1 GeV or less. So if the ($qq\bar{q}\bar{q}$) states exist, we would expect to observe two O^{++} nonets with masses below 1.4 GeV. Jaffe has identified the δ , κ , S^* and ξ as the members of ($qq\bar{q}\bar{q}$) O^{++} nonet and claimed the existence of ($q\bar{q}$) O^{++} nonet with masses around 1.3 GeV. However De Rujula et al. has predicted the masses of ($q\bar{q}$) O^{++} mesons less than that⁽⁸⁰⁾.

To discuss the problem in detail let us establish notation for the members of a O^{++} nonet; we denote the $I = 1$ member by δ , the $I = \frac{1}{2}$ member by κ and the $I = 0$ members by S and ξ . If the nonet is ideally mixed we take S to contain an ($s\bar{s}$) pair and ξ to be built entirely of non-strange quarks. For the ($qq\bar{q}\bar{q}$) states the quark contents of the members would be⁽⁷⁾

$$\begin{aligned}
 \xi &= (u\bar{u}d\bar{d}) \\
 S &= \frac{1}{\sqrt{2}} s\bar{s}(u\bar{u} + d\bar{d}) \\
 \delta &= u\bar{d}s\bar{s} \text{ etc.} \\
 \kappa &= u\bar{s}d\bar{d} \text{ etc.}
 \end{aligned}
 \tag{6.1}$$

For the ideally mixed ($q\bar{q}$) nonet, ξ and δ will be degenerate

in mass with the S state at a higher mass. On the other hand, for the ideally mixed $(qq\bar{q}\bar{q})$ nonet, the δ and S are degenerate in mass and the ξ lies at lower mass. The resulting mass spectrum for the two nonets is sketched in Fig. 6.2. It was the approximate degeneracy of the observed $S^*(980)$ and $\delta(970)$ which prompted Jaffe to assign these states to the $(qq\bar{q}\bar{q})$ nonet, together with broad ξ and κ states. This assignment seems to be in good agreement with the observed properties of the δ , κ , S^* and ξ . Indeed the only obvious problem with this identification is the

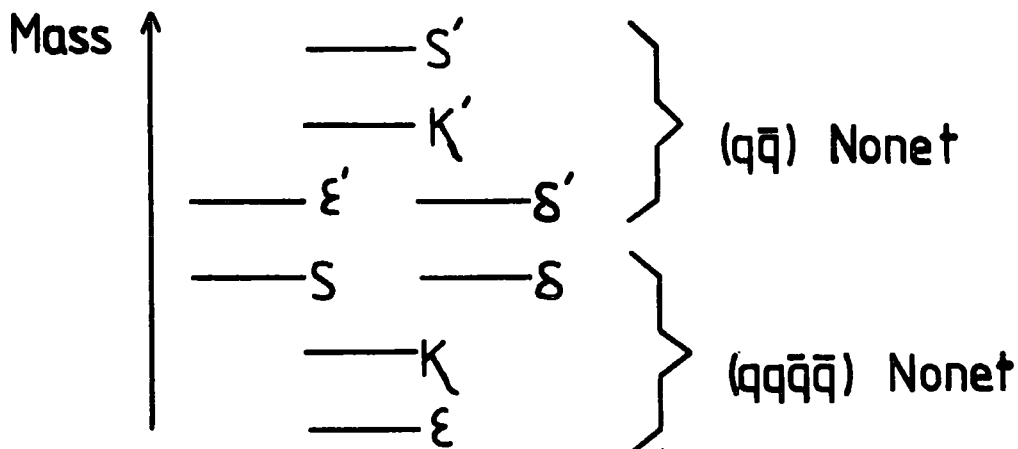


Figure 6.2: The mass spectrum of the $(q\bar{q})$ and $(qq\bar{q}\bar{q})$ nonets. The quark content of $(qq\bar{q}\bar{q})$ states are shown in (6.1). The members of the other nonet have the usual quark content of an ideally mixed $(q\bar{q})$ nonet.

observed narrow width of the $\delta \rightarrow \pi\eta$ decay; since this is a $(qq\bar{q}\bar{q}) \rightarrow (q\bar{q}) + (q\bar{q})$ "fall apart" type of decay, it should be much broader. Of course the problem of the masses of the κ and ξ still remains. In Jaffe's scheme the mass of the ξ should be about 700 MeV and the mass of κ would be about 900 MeV. The most important evidence, which supports this assignment, is the existence of the $\delta'(1300)$. As we have discussed above, to identify the $\delta'(1300)$ as the

radial excitation of the $\delta(970)$, although it is possible, seems an unlikely explanation.

Having established the existence of second 0^{++} nonet, we should look for the other members of this nonet. We expect to observe the $\xi' \rightarrow \pi\bar{\pi}, K\bar{K}, \eta' \rightarrow K\bar{\pi}, S' \rightarrow K\bar{K}$ decays. In the previous Chapter, we have found that the $I = 0 \pi\bar{\pi} \rightarrow K\bar{K}$ S wave magnitude does not fall off as the tail of S^* with increasing $M_{K\bar{K}}$ and there is a broad structure in the region of $M_{K\bar{K}} = 1.15 - 1.4$ GeV, which could be attributed to the ξ' . The $I = 0 \pi\bar{\pi} \rightarrow \pi\bar{\pi}$ S wave is not known very well, but the results of all the analyses⁽⁷⁸⁾ agree that the $I = 0 \pi\bar{\pi} \rightarrow \pi\bar{\pi}$ S wave goes around counter-clockwise in the Argand diagram more than two full turns by $M_{\pi\bar{\pi}} \sim 1.7$ GeV. This means that $\sum_{\pi\bar{\pi}}^{I=0}$ has more phase than that produced by two resonances. Therefore it is conceivable that there are three overlapping resonances, ξ, S^*, ξ' , in the $I = 0 \pi\bar{\pi} \rightarrow \pi\bar{\pi}$ S wave, but it is not possible to determine the parameters of the ξ and ξ' from the presently available data. The situation is similar in the $I = \frac{1}{2} K\bar{\pi} \rightarrow K\bar{\pi}$ S wave (without, of course, the S^* effect)⁽¹³⁾. It is again possible to accommodate a broad η and η' states in the $I = \frac{1}{2} K\bar{\pi} \rightarrow K\bar{\pi}$ S wave, though without definitive identification.

The discussion given above represents an idealized situation. There will be several complications. First the members of the two nonets can mix by gluon exchange. Second we expect some violation of ideal mixing. For example, in a $(qq\bar{q}\bar{q})$ state one $(q\bar{q})$ pair spends a fraction of the time in a colour octet state⁽⁷⁾ or in a 0^{-+} state. In either

case this will lead to violations of ideal mixing. Also from a phenomenological point of view, we have to face the problem of determining the properties of several overlapping resonances within a given partial wave.

The discovery of the $\delta'(1300)$ has led us to classify the O^{++} mesons in terms of two nonets. The only possible solution of this problem within the conventional quark model, in which the mesons are always $(q\bar{q})$ states, is to assign the $\delta'(1300)$ as a radial excitation of the $\delta(970)$. This explanation seems unreasonable, because of the small mass difference of the δ and δ' . An alternative solution has been proposed by Jaffe⁽⁷⁾ in which there are two nonets with $(q\bar{q})$ and $(qq\bar{q}\bar{q})$ states. An explicit calculation has predicted⁽⁷⁾ the mass of the $(qq\bar{q}\bar{q})$ O^{++} mesons about 1 GeV or less; which means we should expect to observe two O^{++} nonets with masses below 1.4 GeV. There are some indications for the existence of the members of the second nonet besides δ' , but with the available data, it is hard to draw any firm conclusions.

CHAPTER VII

Conclusions

We have studied properties of some mesons, which decay into the $(\pi\pi)$ and $(K\bar{K})$ channels, using high statistics (meson-meson) production data for reactions of the type

$$\pi N \rightarrow (\pi\pi) N$$

$$\pi N \rightarrow (K\bar{K}) N$$

with a primary interest in the $J^{PC} = 0^{++}$ mesons. We have obtained several other new results as by products of our line of enquiry.

We have studied the properties of the S^* effect in Chapter III. We have found that the data favour the two-pole description of the S^* ; that is the S^* is a normal Breit-Wigner resonance. We have determined

$$m_{S^*} = 978 \pm 7 \text{ MeV}$$

$$(g_{S^*}^{\pi\pi} / g_{S^*}^{K\bar{K}})^2 \approx \frac{1}{4}$$

We have been unable to calculate reliable parameters for the ξ meson. We have seen that the S^* pole positions are determined by the data accurately, independent of the way of parametrization. We have proposed forms of parametrization of the coupled channel $(\pi\pi, K\bar{K})$ $I = 0$ S wave which permit an investigation of the nature of the S^* and ξ .

We have seen that it is not possible to explain these mesons simply as $(q\bar{q})$ states and that forces in the meson-meson $(qq\bar{q}\bar{q})$ sector are also important.

We have analyzed the data for the reaction $\pi^- p \rightarrow (K^- K^0) p$ in Chapter IV. We have found that A_2 production proceeds dominantly by NPE, and that the UPE A_2 production amplitude is consistent with that found in CEX A_2^0 production. We determined the A_2 meson parameters as

$$m_{A_2} = 1.318 \pm 0.001 \text{ GeV}$$

$$\Gamma_{A_2} = 0.113 \pm 0.004 \text{ GeV.}$$

We have seen that there is an $I = 1$ S wave resonance in the A_2 mass region, called $\delta'(1300)$, with the parameters

$$m_{\delta'} = 1.302 \pm 0.023 \text{ GeV}$$

$$\Gamma_{\delta'} = 0.220 \pm 0.044 \text{ GeV.}$$

The t -dependence of the S wave amplitude shows that the $\delta'(1300)$ is produced by B and more strongly Z exchanges.

We have related A_2 and $K^*(1420)^+$ production using the ρ, ρ' dominated scheme for the pomeron. We have estimated the pomeron relative to ρ exchange and found, for example, at $-t \sim 0.2 \text{ GeV}^2$ a ratio 1:1 in $\pi^- p \rightarrow A_2^- p$ at 10 GeV/c.

We have seen that the g meson production proceeds dominantly by UPE (π exchange), and found

$$B(g \rightarrow K\bar{K}) = 1.3 \pm 0.4\% .$$

We have compared the NPE (ω exchange) g production amplitude with NPE (ω exchange) ρ production data and estimated

$B(g \rightarrow K\bar{K}) \simeq 1.5\%$. We have determined the g meson parameters to be

$$m_g = 1.698 \pm 0.012 \text{ GeV}$$

$$\Gamma_g = 0.199 \pm 0.040 \text{ GeV.}$$

We have observed the emergence of $L = 4$ (K^-K^0) production above $M_{K^-K^0} = 1.6$ GeV. The t -structure of G_+ shows that $1 + 4$ (K^-K^0) system is produced by NPE (\mathbb{P} , f exchanges). The data do not allow the determination of the mass and the width of this resonance, but D_+G_+ interference term suggests that the G_+ amplitude is resonating.

We have analysed the data for the reactions

$$\pi^- p \rightarrow (K^+ K^-) n$$

$$\pi^+ n \rightarrow (K^+ K^-) p$$

in Chapter V. We have fitted the combinations of $N < \gamma_M^4 >$ moments, employing a mass-matrix parametrization to describe the f, f' interference. We have determined the f' resonance parameters to be

$$m_{f'} = 1513 \pm 3 \text{ MeV}$$

$$\Gamma_{f'} = 43 \pm 9 \text{ MeV}$$

$$B(f' \rightarrow \pi\pi) = 1.6 \pm 0.6\% .$$

We have analysed the data with $M_{KR} < 1.1$ GeV in terms of S^* and δ resonances, relating the B exchange amplitudes to the π exchange amplitudes by π - B EXD. The data are compatible with π - B EXD as far as the phases are concerned. We have determined the δ meson parameters to be

$$m_\delta = 974 \pm 5 \text{ MeV}$$

$$\Gamma_\delta^{\pi\eta} = 49.2 \pm 3.6 \text{ MeV.}$$

We have calculated the effect of the K^+K^- and K^0, \bar{K}^0 mass difference and found that this effect does not change the

results appreciable. We have found that the $\pi\bar{\pi} \rightarrow K\bar{K}$ p wave is given by the ρ tail, and that the F wave is compatible with the g meson tail with $B(g \rightarrow K\bar{K}) = 1.3\%$ and $B(g \rightarrow \pi\bar{\pi}) = 24\%$. We have determined the $I = 0$ $\pi\bar{\pi} \rightarrow K\bar{K}$ S wave by performing an energy-independent analysis of the data in the forward scattering region. The magnitude of the $\pi\bar{\pi} \rightarrow K\bar{K}$ S wave shows the strong S^* peak near the $K\bar{K}$ threshold and stays flat at about 0.325 in the region of $M_{K\bar{K}} = 1.15 - 1.4$ GeV. We have found two possible solutions, one of which gives the S wave with fast phase variation. We have favoured the solution with slow phase.

We have explored the possible classification schemes of the known O^{++} mesons. The existence of two $I = 1$ O^{++} mesons has suggested the existence of two O^{++} nonets. A possible classification scheme has been proposed by Jaffe, in which there are two O^{++} nonets composed of $(q\bar{q})$ and $(qq\bar{q}\bar{q})$ states. The $\delta'(1300)$, in addition to $\delta(970)$, is good evidence for such a scheme.

This thesis contains a remarkable amount of information about the O^{++} mesons. Although we know quite a lot about these mesons we still have a long way to go to reach the final picture. The most important problem is to discover the missing members of the two O^{++} nonets. Investigation of $\pi\bar{\pi}$, $K\bar{K}$ channels in other charge configurations or of the $\eta\eta$ channel, would be invaluable in this respect. When we have enough information about all the members of the O^{++} nonets, a quantitative analysis of the properties of these mesons will answer many of the present questions, the most

important of which is the possible existence of multi-quark states among the 0^{++} mesons.

APPENDIX I

Moments in Terms of Density Matrix Elements

Here we give the relations between the moments defined in (2.15), and the spin density matrix elements $\rho_{\lambda_{R1} \lambda_{R2}}^{L_1 L_2}$ (2.21) for $L_1, L_2 \leq 4$ and $|\lambda_{R1}|, |\lambda_{R2}| \leq 1$. We use eq. (2.22) to calculate the appropriate coefficients. A given moment only contains terms with $L_1 + L_2 \geq J$ and $|\lambda_{R1} - \lambda_{R2}| = M$. $L_1 + L_2$ must be even (odd) if J is even (odd). These restrictions are embodied in the Clebsch-Gordan coefficients in eq. (2.22). Here $\rho_{\lambda_{R1} \lambda_{R2}}^{L_1 L_2} \equiv \text{Re}(\rho_{\lambda_{R1} \lambda_{R2}}^{L_1 L_2})$.

$$\begin{aligned} \sqrt{4\pi} \langle Y_0^0 \rangle &= 1.000 \rho_{00}^{00} + 1.000 \rho_{00}^{11} + 2.000 \rho_{11}^{11} + 1.000 \rho_{00}^{22} \\ &+ 2.000 \rho_{11}^{22} + 1.000 \rho_{00}^{33} + 2.000 \rho_{11}^{33} + 1.000 \rho_{00}^{44} \\ &+ 2.000 \rho_{11}^{44} \end{aligned}$$

$$\begin{aligned} \sqrt{4\pi} \langle Y_0^1 \rangle &= 2.000 \rho_{00}^{10} + 1.789 \rho_{00}^{21} + 3.098 \rho_{11}^{21} + 1.757 \rho_{00}^{32} \\ &+ 3.312 \rho_{11}^{32} + 1.746 \rho_{00}^{43} + 3.381 \rho_{11}^{43} \end{aligned}$$

$$\begin{aligned} \sqrt{4\pi} \langle Y_1^1 \rangle &= 2.000 \rho_{10}^{10} - 0.894 \rho_{01}^{21} + 1.549 \rho_{10}^{21} - 1.014 \rho_{01}^{32} \\ &+ 1.434 \rho_{10}^{32} - 1.069 \rho_{01}^{43} + 1.380 \rho_{10}^{43} \end{aligned}$$

$$\begin{aligned}\sqrt{4\pi} \langle Y_0^2 \rangle &= 0.894 \rho_{00}^{11} - 0.894 \rho_{11}^{11} + 2.000 \rho_{00}^{20} + 0.639 \rho_{00}^{22} \\ &+ 0.639 \rho_{11}^{22} + 1.757 \rho_{00}^{31} + 0.596 \rho_{00}^{33} + 2.869 \rho_{11}^{31} \\ &+ 0.894 \rho_{11}^{33} + 1.714 \rho_{00}^{42} + 0.581 \rho_{00}^{44} + 3.130 \rho_{11}^{42} \\ &+ 0.987 \rho_{11}^{44}\end{aligned}$$

$$\begin{aligned}\sqrt{4\pi} \langle Y_1^2 \rangle &= 1.549 \rho_{10}^{11} + 2.000 \rho_{10}^{20} + 0.639 \rho_{10}^{22} - 1.014 \rho_{01}^{31} \\ &+ 1.656 \rho_{10}^{31} + 0.422 \rho_{10}^{33} - 1.143 \rho_{01}^{42} + 1.565 \rho_{10}^{42} \\ &+ 0.318 \rho_{10}^{44}\end{aligned}$$

$$\begin{aligned}\sqrt{4\pi} \langle Y_2^2 \rangle &= -1.095 \rho_{11}^{11} - 0.782 \rho_{11}^{22} + 0.586 \rho_{11}^{31} - 0.730 \rho_{11}^{33} \\ &+ 0.639 \rho_{11}^{42} - 0.711 \rho_{11}^{44}\end{aligned}$$

$$\begin{aligned}\sqrt{4\pi} \langle Y_0^3 \rangle &= 1.757 \rho_{00}^{21} - 2.028 \rho_{11}^{21} + 2.000 \rho_{00}^{30} + 1.193 \rho_{00}^{32} \\ &+ 0.843 \rho_{11}^{32} + 1.746 \rho_{00}^{41} + 1.091 \rho_{00}^{43} + 2.760 \rho_{11}^{41} \\ &+ 1.408 \rho_{11}^{43}\end{aligned}$$

$$\begin{aligned}\sqrt{4\pi} \langle Y_1^3 \rangle &= 1.434 \rho_{01}^{21} + 1.656 \rho_{10}^{21} + 0.422 \rho_{01}^{32} + 2.000 \rho_{10}^{30} \\ &+ 0.894 \rho_{10}^{32} - 1.069 \rho_{01}^{41} + 0.182 \rho_{01}^{43} + 1.690 \rho_{10}^{41} \\ &+ 0.704 \rho_{10}^{43}\end{aligned}$$

$$\sqrt{4\pi} \langle Y_2^3 \rangle = -1.852 \rho_{11}^{21} - 1.155 \rho_{11}^{32} + 0.756 \rho_{11}^{41} - 1.029 \rho_{11}^{43}$$

$$\begin{aligned} \sqrt{4\pi} \langle Y_0^4 \rangle &= 0.857 \varphi_{00}^{22} - 1.143 \varphi_{11}^{22} + 1.746 \varphi_{00}^{31} + 0.545 \varphi_{00}^{33} \\ &\quad - 2.138 \varphi_{11}^{31} + 0.182 \varphi_{11}^{33} + 2.000 \varphi_{00}^{40} + 1.162 \varphi_{00}^{42} \\ &\quad + 0.486 \varphi_{00}^{44} + 0.636 \varphi_{11}^{42} + 0.486 \varphi_{11}^{44} \end{aligned}$$

$$\begin{aligned} \sqrt{4\pi} \langle Y_1^4 \rangle &= 1.565 \varphi_{10}^{22} + 1.380 \varphi_{01}^{31} + 1.690 \varphi_{10}^{31} + 0.704 \varphi_{10}^{33} \\ &\quad + 0.318 \varphi_{01}^{42} + 2.000 \varphi_{10}^{40} + 0.987 \varphi_{10}^{42} + 0.486 \varphi_{10}^{44} \end{aligned}$$

$$\begin{aligned} \sqrt{4\pi} \langle Y_2^4 \rangle &= -0.904 \varphi_{1-1}^{22} - 1.690 \varphi_{1-1}^{31} - 0.575 \varphi_{1-1}^{33} - 0.905 \varphi_{1-1}^{42} \\ &\quad - 0.512 \varphi_{1-1}^{44} \end{aligned}$$

$$\begin{aligned} \sqrt{4\pi} \langle Y_0^5 \rangle &= 1.699 \varphi_{00}^{32} - 2.402 \varphi_{11}^{32} + 1.741 \varphi_{00}^{41} + 1.052 \varphi_{00}^{43} \\ &\quad - 2.202 \varphi_{11}^{41} + 0.136 \varphi_{11}^{43} \end{aligned}$$

$$\begin{aligned} \sqrt{4\pi} \langle Y_1^5 \rangle &= 1.519 \varphi_{01}^{32} + 1.612 \varphi_{10}^{32} + 1.348 \varphi_{01}^{41} + 0.610 \varphi_{01}^{43} \\ &\quad + 1.706 \varphi_{10}^{41} + 0.816 \varphi_{10}^{43} \end{aligned}$$

$$\sqrt{4\pi} \langle Y_2^5 \rangle = -1.741 \varphi_{1-1}^{32} - 1.595 \varphi_{1-1}^{41} - 1.050 \varphi_{1-1}^{43}$$

$$\begin{aligned} \sqrt{4\pi} \langle Y_0^6 \rangle &= 0.840 \varphi_{00}^{33} - 1.261 \varphi_{11}^{33} + 1.691 \varphi_{00}^{42} + 0.504 \varphi_{00}^{44} \\ &\quad - 2.470 \varphi_{11}^{42} - 0.050 \varphi_{11}^{44} \end{aligned}$$

$$\sqrt{4\pi} \langle Y_1^6 \rangle = 1.572 \varphi_{10}^{33} + 1.492 \varphi_{01}^{42} + 1.634 \varphi_{10}^{42} + 0.731 \varphi_{10}^{44}$$

$$\sqrt{4\pi} \langle Y_2^6 \rangle = -0.861 \begin{Bmatrix} 33 \\ 11 \end{Bmatrix} - 1.688 \begin{Bmatrix} 42 \\ 11 \end{Bmatrix} - 0.517 \begin{Bmatrix} 44 \\ 11 \end{Bmatrix}$$

$$\sqrt{4\pi} \langle Y_0^7 \rangle = 1.672 \begin{Bmatrix} 43 \\ 00 \end{Bmatrix} - 2.590 \begin{Bmatrix} 43 \\ 11 \end{Bmatrix}$$

$$\sqrt{4\pi} \langle Y_1^7 \rangle = 1.548 \begin{Bmatrix} 43 \\ 01 \end{Bmatrix} + 1.599 \begin{Bmatrix} 43 \\ 10 \end{Bmatrix}$$

$$\sqrt{4\pi} \langle Y_2^7 \rangle = -1.696 \begin{Bmatrix} 43 \\ 11 \end{Bmatrix}$$

$$\sqrt{4\pi} \langle Y_0^8 \rangle = 0.831 \begin{Bmatrix} 44 \\ 00 \end{Bmatrix} - 1.330 \begin{Bmatrix} 44 \\ 11 \end{Bmatrix}$$

$$\sqrt{4\pi} \langle Y_1^8 \rangle = 1.577 \begin{Bmatrix} 44 \\ 10 \end{Bmatrix}$$

$$\sqrt{4\pi} \langle Y_2^8 \rangle = -0.843 \begin{Bmatrix} 44 \\ 11 \end{Bmatrix}$$

APPENDIX II

S-Matrix, State Normalization, Phase Space
Cross Section, Partial Wave Expansion

We use the units such that

$$\hbar = c = 1. \quad (\text{A.II.1})$$

In these units

$$(\text{GeV})^{-2} = 0.38935 \text{ mb}. \quad (\text{A.II.2})$$

We define the metric such that the four momentum

$$P = (E, p_x, p_y, p_z) \quad (\text{A.II.3})$$

satisfies

$$p^2 = E^2 - p^2 = m^2 \quad (\text{A.II.4})$$

where E is total energy of a particle of rest mass m . That is the metric tensor is

$$g_{\mu\nu} = \begin{pmatrix} 1 & 0 & 0 & 0 \\ 0 & -1 & 0 & 0 \\ 0 & 0 & -1 & 0 \\ 0 & 0 & 0 & -1 \end{pmatrix}. \quad (\text{A.II.5})$$

We define the S-matrix elements so that

$$S_{ij} = \langle f|i \rangle + i(2\pi)^4 \delta^4(P_i - P_f) T_{ij}. \quad (\text{A.II.6})$$

We normalize the single particle states

$$\langle P_a, \lambda_a | P_b, \lambda_b \rangle = (2\pi)^3 2E_a \delta^4(P_a - P_b) \delta_{\lambda_a, \lambda_b} \quad (\text{A.II.7})$$

where P_i and λ_i are the particle four momentum and the helicity respectively.

For a system consisting of n particles with four-momenta $P_1 \dots P_n$, the Lorentz invariant phase space element is given by

$$dLips(P_1 \dots P_n) = (2\pi)^{-3n} \prod_{i=1}^n \frac{d^3 p_i}{2E_i} \quad (\text{A.II.8})$$

For the states with a given total four momentum P , we define the restricted phase space element

$$dLips(s; P_1 \dots P_n) = (2\pi)^4 \delta^4(P - \sum P_i) dLips(P_1 \dots P_n) \quad (\text{A.II.9})$$

where

$$s = (\sum P_i)^2 \quad (\text{A.II.10})$$

We define the cross-section for the process

$$a + b \longrightarrow 1+2+\dots+n$$

$$\sigma = \frac{1/TV}{2[\lambda(s; m_a^2, m_b^2)]^{1/2}} \int dLips(P_1 \dots P_n) |S(a+b \rightarrow 1+\dots+n)|^2 \quad (\text{A.II.11})$$

in the limit of infinite space-time volume TV , where

$$\begin{aligned} \lambda(s; m_a^2, m_b^2) &= [s - (m_a + m_b)^2][s - (m_a - m_b)^2] \\ &= 4 q^2 s \\ &= (2 p_a^{\mu\nu} m_b)^2 \end{aligned} \quad (\text{A.II.12})$$

The second formulae in (A.II.12) is written in the centre-of-mass frame of particles a,b, where q is the three-momenta. The third one is written in the laboratory frame of particle b, with particle a moving with three momenta p_a^{lab} .

The cross-section is given in terms of T , defined in (A.II.6), and the restricted phase space element (A.II.9):

$$\sigma = \frac{1}{2[\lambda(s; m_a^2, m_b^2)]^{1/2}} \int dL: p_3(s; p_1, \dots, p_n) |T_{i_f}|^2. \quad (\text{A.II.13})$$

We define the partial wave expansion of T_{i_f} of (A.II.6), in terms of Legendre polynomials $P_L(x)$, as

$$T(\theta) = 2\pi s^{1/2} \sum_{L=0}^{\infty} (2L+1) P_L(x) T_L \quad (\text{A.II.14})$$

where $x = \cos \theta$, θ is the scattering angle. Note that T_L have no θ dependence. They are called partial waves. We can define the partial wave S-matrix such that

$$S_{i_f, L} = S_{i_f} + 2i T_{i_f, L} \sqrt{k_i k_f} \quad (\text{A.II.15})$$

where k_i, k_f are the initial and final three-momenta respectively in the centre of mass frame.

APPENDIX III

The π Coupling at the Nucleon Vertex

Since we study OPE processes we wish to study the form of the π exchange coupling at the nucleon vertex. The Dirac equation for a spin $\frac{1}{2}$ nucleon of mass m has the form

$$(\not{p} - m)U_{1,2}(p) = 0 \text{ (Positive Energy)} \quad (\text{A.III.1})$$

where

$$\not{p} \equiv \gamma^\mu p_\mu . \quad (\text{A.III.2})$$

We use the representation of γ^μ

$$\gamma_0 = \begin{pmatrix} 1 & 0 \\ 0 & -1 \end{pmatrix}, \quad \underline{\gamma} = \begin{pmatrix} 0 & \underline{\sigma} \\ -\underline{\sigma} & 0 \end{pmatrix}, \quad \gamma_5 = \begin{pmatrix} 0 & 1 \\ 1 & 0 \end{pmatrix}$$

$$\gamma_5 = i \gamma_0 \gamma_1 \gamma_2 \gamma_3 \quad (\text{A.III.3})$$

where $\underline{\sigma}$ are the Pauli matrices.

The Dirac spinors for a spin $\frac{1}{2}$ particle of momentum p , with polar angles θ and ϕ , rest mass m , and energy E are

$$U_+(p) = \sqrt{E+m} \begin{pmatrix} \cos(\theta/2) \\ \sin(\theta/2)e^{-i\phi} \\ \frac{P \cos(\theta/2)}{E+m} \\ \frac{P \sin(\theta/2)}{E+m} e^{-i\phi} \end{pmatrix}$$

$$(\text{A.III.4})$$

$$U_{\pm}(p) = \sqrt{E+m} \begin{pmatrix} -\sin(\theta/2) e^{i\phi} \\ \cos(\theta/2) \\ \frac{P \sin(\theta/2)}{E+m} e^{i\phi} \\ -\frac{P \cos(\theta/2)}{E+m} \end{pmatrix}. \quad (\text{A.III.4})$$

Here U_{\pm} correspond to nucleons with helicity of $\pm \frac{1}{2}$ respectively.

For the vertex $N_i \rightarrow \pi N_f$, we choose the coordinates as shown in Fig. A.III.1. The spinors of N_f and N_i in this frame are given by relation (A.III.4). For N_i we have $\theta = 0, \phi = 0, p_z = p_i$, and for N_f we have $\theta, \phi = 0, p_f$.

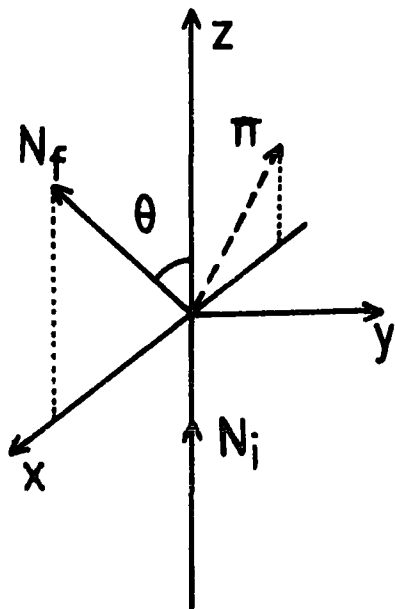


Figure A.III.1

Using the Feynman rules, the vertex function is:

$$V_{\lambda_f \lambda_i} \sim G U_{\lambda_f}^{\dagger}(p_f, \lambda_f) \gamma^0 \gamma^5 U_{\lambda_i}(p_i, \lambda_i) \quad (\text{A.III.5})$$

where λ_f and λ_i are the helicities of the final and initial nucleons respectively. Using the spinors of eq. (A.III.4) we find

$$V_{++} \sim G \cos \theta/2 \left[\sqrt{(E_f+m)(E_i-m)} - \sqrt{(E_i+m)(E_f-m)} \right]$$

where m is the nucleon mass. Similarly

arily

$$V_{+-} \sim G \sin \theta/2 \left[\sqrt{(E_f+m)(E_i-m)} - \sqrt{(E_i+m)(E_f-m)} \right].$$

Thus the contribution to the cross section is

$$|V_{++}|^2 + |V_{+-}|^2 = -2 G^2 [p_f p_i \cos \theta + m^2 - E_i E_f]. \quad (\text{A.III.6})$$

Defining the square of the four-momentum transfer to be

$$t = (P_i - P_f)^2 = 2(m^2 - E_i E_f + p_i p_f \cos \theta),$$

and averaging over the initial nucleon helicities and summing over the final nucleon helicities, we find

$$\frac{1}{2} \sum_{\lambda_i, \lambda_f} |V_{\lambda_i, \lambda_f}|^2 = -G^2 t. \quad (\text{A.III.7})$$

APPENDIX IV

Phase Space Calculation

The Lorentz invariant phase space element occurring in the expression for the cross-section for the reaction $q_1 + q_2 \longrightarrow p_1 + p_2 + p_3$ is given in (2.32). Suppose p_1 and p_2 form a system R of mass M, then

$$p_R = p_1 + p_2, \quad p_R^2 = M^2$$

We multiply the right-hand side of eq. (2.32) by

$$d^4 p_R \delta(p_R - p_1 - p_2) \equiv 1,$$

and re-write in the form

$$\begin{aligned} d\text{Lips}(s; p_1 p_2 p_3) &= d\text{Lips}(M^2; p_1 p_2) \delta^4(q_1 + q_2 - p_R - p_3) \\ &\quad \times d\text{Lips}(p_3) d^4 p_R. \end{aligned} \tag{A.IV.1}$$

Using

$$d^4 p_R = (2\pi)^3 d\text{Lips}(p_R) dM^2, \tag{A.IV.2}$$

we find eq. (A.IV.1) becomes:

$$d\text{Lips}(s; p_1, p_2, p_3) = \frac{1}{2\pi} d\text{Lips}(s; p_R, p_3) d\text{Lips}(M^2; p_1, p_2) dM^2. \tag{A.IV.3}$$

We calculate $d\text{Lips}(s; p_R, p_3)$ in the centre-of-mass frame of the reaction $\pi N \rightarrow RN$, shown in Fig. A.IV.1; we find

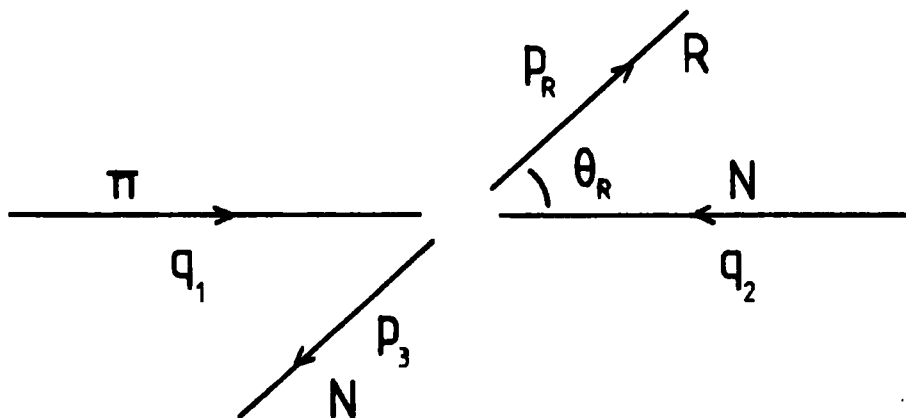


Figure A.IV.1

$$d\text{Lips}(s; p_R, p_3) = \frac{p_R dE d\Omega}{(2\pi)^2 4E} \delta(s^{\frac{1}{2}} - E),$$

where three-momenta part of p_R is

$$|p_R| = |p_3| = \left[\lambda(s; m_N^2, M^2) / 4s \right]^{1/2}.$$

Performing the ϕ integration of $d\Omega = d\phi d\cos \theta_R$

$$d\text{Lips}(s; p_R, p_3) = \frac{p_R d\cos \theta_R}{8\pi s^{\frac{1}{2}}}. \quad (\text{A.IV.4})$$

Now

$$t = (q_1 - p_R)^2 = (E_1 - E_R)^2 - q_1^2 - p_R^2 + 2q_1 p_R \cos \theta_R$$

$$dt = 2 q_1 p_R d \cos \theta_R, \quad (\text{A.IV.5})$$

and so eq. (A.IV.4) becomes (c.f. eq. (A.II.12))

$$d\text{Lips}(s; p_R, p_3) = \frac{dt}{16\pi q_1 s^{\frac{1}{2}}} = \frac{dt}{8\pi [\lambda(s; m^2, m_N^2)]^{\frac{1}{2}}}. \quad (\text{A.IV.6})$$

We have calculated $\int_{\phi} dLips(s; p_R, p_3)$ in terms of Lorentz invariants, therefore we can use the result in any Lorentz frame. Substituting (A.IV.6) into (A.IV.3) we obtain:

$$\int_{\phi} dLips(s; p_1, p_2, p_3) = \frac{dt dM^2}{(4\pi)^2 [\lambda(s; m^2, m_N^2)]^{\frac{1}{2}}} dLips(M^2; p_1, p_2) .$$

(A.IV.7)

APPENDIX V

$\pi\pi \rightarrow \pi\bar{\pi}, (K\bar{K})$ Scattering

Here we evaluate

$$\int_{\Omega} dL: p_5(M^2; p_1, p_2) |T|^2$$

where

$$T = T(\pi\bar{\pi} \rightarrow \pi\bar{\pi}(K\bar{K})),$$

p_1 are the momenta of the produced mesons, and M is the mass of the di-meson system. We calculate $dLips(M^2; p_1, p_2)$ in the rest frame of the produced resonance, R . It is also the centre-of-mass frame of the produced di-meson system.

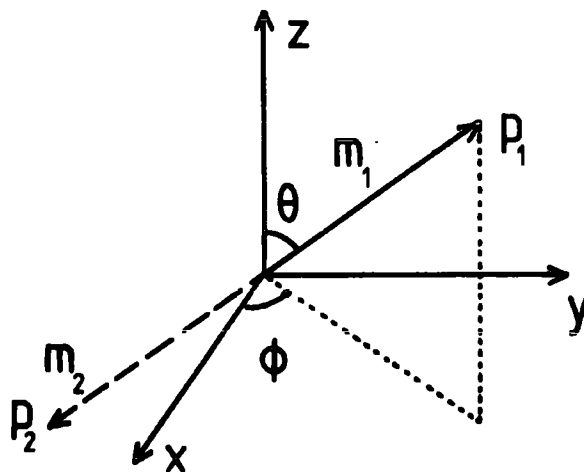


Figure A.V.1

In the rest frame of the produced resonance

$$p_2 \equiv 0$$

$$d^3 p_2 \delta^3(p_1 + p_2) = 1$$

$$E_2 = \sqrt{m_m^2 + p_1^2}$$

where $m_m = m_\pi$ or m_K according as the produced system is $\pi\pi$ or KK . Also we have

$$p_1 = p_2 = (M^2/4 - m_m^2)^{1/2} \equiv p$$

$$d^3 p_1 = p^2 dp d\cos\theta d\phi$$

$$E = E_1 + E_2 = 2\sqrt{m_m^2 + p^2}$$

$$dE = \frac{2p dp}{E}$$

(A.V.2)

Therefore, performing the integration of $d\phi$

$$\int_{\phi} d\text{Lips}(M^2; p_1, p_2) = \frac{p d\cos\theta}{8\pi M} . \quad (\text{A.V.3})$$

It is convenient to express \mathcal{Z} in terms of partial waves using eq. (A.II.14):

$$\mathcal{Z} = 8\pi M \sum_{L=0}^{\infty} (2L+1) T_L(\pi\pi \rightarrow \pi\pi, (K\bar{K})) P_L(\cos\theta) . \quad (\text{A.V.4})$$

Substituting (A.V.3) and (A.V.4) into eq. (2.35) we find

$$\int_{\phi} d\text{Lips}(M^2; p_1, p_2) |\mathcal{Z}|^2 = 8\pi p M d\cos\theta \left| \sum_{L=0}^{\infty} (2L+1) T_L(\pi\pi \rightarrow \pi\pi, (K\bar{K})) P_L(\cos\theta) \right|^2 . \quad (\text{A.V.5})$$

Using the orthogonality relation of $P_L(\cos\theta)$

$$\int_{-1}^1 d\cos\theta (L+1/2) P_L(\cos\theta) P_{L'}(\cos\theta) = \delta_{LL'} ,$$

we find

$$\int_{\Omega} dL: \rho_s(M^2; \rho_1, \rho_2) |\mathcal{Z}|^2 = 16\pi M_p \sum_{L=0}^{\infty} (2L+1) |T_L(\pi\bar{\pi} \rightarrow \pi\bar{\pi}, (K\bar{K}))|^2 \quad (\text{A.V.6})$$

where $T_L(\pi\bar{\pi} \rightarrow \pi\bar{\pi}, (K\bar{K}))$ can be written in terms of the phase shift and inelasticity as

$$T_L(\pi\bar{\pi} \rightarrow \pi\bar{\pi}) = \frac{\eta_L e^{2i\delta_{\pi\bar{\pi}}^L}}{2 k_{\pi\bar{\pi}}}$$

and

$$T_L(\pi\bar{\pi} \rightarrow K\bar{K}) = \frac{\sqrt{1-\eta_L} e^{i(\delta_{\pi\bar{\pi}}^L + \delta_{K\bar{K}}^L)}}{2 (k_{\pi\bar{\pi}} k_{K\bar{K}})^{1/2}}$$

for two open channel ($\pi\bar{\pi}$ and $K\bar{K}$).

APPENDIX VI

Density Matrix Elements In Terms
of Di-Meson Production Amplitudes

Here we give the relations between density matrix elements and the definite exchanged parity amplitudes, $L_{0,\pm} = H_{\lambda\lambda}^{L\pm}$, with $L \leq 4$, $|\lambda_R| \leq 1$. We use the spectroscopic notation for the amplitudes; that is: $L = S, P, D, F, G$ for $L = 0, 1, 2, 3, 4$, respectively. The definition of the density matrix elements is given in eq. (2.21). Using eq. (2.21), (2.22) and (2.23) we see that:

$$N \operatorname{Re} \rho_{00}^{L L} = \operatorname{Re} (L_0^* L_0)$$

$$N \operatorname{Re} \rho_{01}^{L L} = \operatorname{Re} (L_0^* L_-) / \sqrt{2}$$

$$N \operatorname{Re} \rho_{11}^{L L} = \operatorname{Re} (L_+^* L_+ + L_-^* L_-) / 2$$

$$N \operatorname{Re} \rho_{1-1}^{L L} = \operatorname{Re} (L_+^* L_- - L_-^* L_+) / 2.$$

For instance, with only $L = 0, 1$ present, the density matrix elements are:

$$N \operatorname{Re} \rho_{00}^{00} = |S|^2$$

$$N \operatorname{Re} \rho_{00}^{01} = \operatorname{Re} (S P_0^*)$$

$$N \operatorname{Re} \rho_{01}^{01} = \operatorname{Re} (S P_-^*) / \sqrt{2}$$

$$N \operatorname{Re} \rho_{00}^{11} = |P_0|^2$$

$$N \operatorname{Re} \rho_{01}^{11} = \operatorname{Re} (P_0 P_-^*) / \sqrt{2}$$

$$N \operatorname{Re} \rho_{11}^{11} = (|P_+|^2 + |P_-|^2) / 2$$

$$N \operatorname{Re} \rho_{1-1}^{11} = (|P_+|^2 - |P_-|^2) / 2.$$

APPENDIX VII

Classification of Phase Shift Solutions

Barrelet zeros⁽⁶⁷⁾ provide a convenient way of finding and classifying all possible phase shift solutions. Consider a case where only partial waves with $L \leq \mathcal{L}$ contribute. Then, using the spectroscopic notation,

$$L_{\lambda_R}^{\lambda_L} = H_{\lambda_L \lambda_R}^L,$$

where $H_{\lambda_L \lambda_R}^L$ are defined in eq. (2.19), the scattering amplitude can be written as

$$H \sim \sum_{L=0}^{\mathcal{L}} L_{\lambda_R} Y_L^{\lambda_R}(\theta, \phi), \quad (\text{A.VII.1})$$

where we use eq. (2.19) and

$$d_{\lambda_R, 0}^L = \sqrt{\frac{L! \pi}{2L+1}} Y_L^{\lambda_R}(\theta, \phi) e^{-i\lambda_R \phi},$$

and omit the nucleon helicities. The amplitude H in eq. (A.VII.1) can be re-written in terms of the definite exchanged parity amplitudes L_0, L_-, L_+ , with $|\lambda_R| \leq 1$ as:

$$H \sim \sum_{L=0}^{\mathcal{L}} (2L+1)^{1/2} \left[L_0 P_L(z) + \left(\frac{(L-1)!}{(L+1)!} \right)^{1/2} (1-z^2)^{1/2} \frac{e^{i\phi} - e^{-i\phi}}{\sqrt{2}} L_+ + \frac{d}{dz} P_L(z) \right] \quad (\text{A.VII.2})$$

where $z = \cos \theta$ and we use eq. (2.23) and we set $L_- \equiv 0$. We also use the relations between $Y_L^{\lambda R}$ and $\rho_L^{\lambda R}$. Therefore for UPE and NPE sectors we can write:

$$H(\text{UPE}) = H' \left[z^3 + \frac{3D_0}{\sqrt{35} F_0} z^2 + \left(\frac{2\sqrt{3} P_0}{5\sqrt{7} F_0} - \frac{3}{5} \right) z + \left(\frac{2S_0}{5\sqrt{7} F_0} - \frac{D_0}{\sqrt{35} F_0} \right) \right] \\ = H' \prod_{i=1}^{\mathcal{L}} (z - z_i) \quad (\text{A.VII.3})$$

where $\mathcal{L} = 3^{\dagger)}$, and

$$H(\text{NPE}) = H'' \left[z^3 + \frac{\sqrt{5} F_+}{\sqrt{21} G_+} z^2 + \left(\frac{\sqrt{8} D_+}{7\sqrt{3} G_+} - \frac{3}{7} \right) z + \left(\frac{2\sqrt{10} P_+}{35\sqrt{3} G_+} - \frac{F_+}{\sqrt{105} G_+} \right) \right] \sin \phi \sin \theta \\ = H'' \sin \phi \sin \theta \prod_{i=1}^{\mathcal{L}-1} (z - z'_i) \quad (\text{A.VII.4})$$

where $\mathcal{L} = 4$. Here we assume that the amplitudes in NPE(UPE) sector are all nucleon spin coherent.

Since the amplitudes are complex, the "Barrelet" zeros, Z_i ; Z'_i are complex. The ambiguities arise because the data do not determine the signs of the $\text{Im } Z_i$ or the $\text{Im } Z'_i$. Thus there is a $2^{\mathcal{L}}$ -fold ambiguity within the UPE sector and a $2^{\mathcal{L}-1}$ -fold ambiguity within the NPE sector. From a given solution we generate the other solutions by first determining the $Z_i (Z'_i)$ and then making substitutions $Z_i \rightarrow Z_i^*$, ($Z'_i \rightarrow Z_i'^*$) for the various combinations of the zeros.

$\dagger)$ In the analysis we take $G_0 \equiv 0$.

APPENDIX VIII

The Effect of the K^+, K^- and K^0, \bar{K}^0 Mass Difference

Consider the $\underline{M} = \underline{K}^{-1}$ matrix parametrization of $L = 0$ S wave Argand amplitude (see eq. (3.45)):

$$\underline{A} = \underline{k}^{1/2} (\underline{M} - i \underline{k})^{-1} \underline{k}^{1/2} \quad (\text{A.VIII.1})$$

To describe $\pi\eta \rightarrow K^+ K^-$ and $\pi\bar{\pi} \rightarrow K^+ K^-$ we may define two bases:

$$\text{Basis I: } \{ |\pi\eta; I=1\rangle, |\pi\bar{\pi}; I=0\rangle, |K^+ K^-\rangle, |K^0 \bar{K}^0\rangle \}$$

$$\text{Basis II: } \{ |\pi\eta; I=1\rangle, |K\bar{K}; I=1\rangle, |\pi\bar{\pi}; I=0\rangle, |K\bar{K}; I=0\rangle \}. \quad (\text{A.VIII.2})$$

The momentum matrix \underline{k} , can be written in diagonal form in Basis I:

$$\underline{k} = \begin{pmatrix} k_\eta & 0 & 0 & 0 \\ 0 & k_{\bar{\pi}} & 0 & 0 \\ 0 & 0 & k_+ & 0 \\ 0 & 0 & 0 & k_0 \end{pmatrix} \quad (\text{A.VIII.3})$$

where k_η and $k_{\bar{\pi}}$ are the $(\pi\eta)$ and $(\pi\bar{\pi})$ centre of mass momenta; and k_+ and k_0 are given by eqs. (5.22). On the other hand \underline{M} matrix has the block diagonal form in Basis II:

$$\underset{\sim}{M}_{\text{II}} = \begin{pmatrix} M_{11} & M_{12} & 0 & 0 \\ M_{12} & M_{22} & 0 & 0 \\ 0 & 0 & N_{11} & N_{12} \\ 0 & 0 & N_{12} & N_{22} \end{pmatrix}$$

(A.VIII.4)

where M_{ij} describe $\pi\eta \rightarrow \pi\eta$, $\pi\eta \rightarrow K\bar{K}$ and $K\bar{K} \rightarrow K\bar{K}$ ($I = 1$) processes; and N_{ij} describe $\pi\pi \rightarrow \pi\pi$, $\pi\pi \rightarrow K\bar{K}$ and $K\bar{K} \rightarrow K\bar{K}$ ($I = 0$) processes with $L = 0$. In order to determine $\pi\eta \rightarrow K^+K^-$ and $\pi\pi \rightarrow K^+K^-$ amplitudes, we transform $\underset{\sim}{M}_{\text{II}}$ to the Basis I. For this procedure we need to know the (II) \rightarrow (I) transformation matrix

$$(I) = \underset{\sim}{G} (II).$$

Using eqs. (5.23) we find:

$$\underset{\sim}{G} = \begin{pmatrix} 1 & 0 & 0 & 0 \\ 0 & 0 & 1 & 0 \\ 0 & 1/\sqrt{2} & 0 & -1/\sqrt{2} \\ 0 & 1/\sqrt{2} & 0 & 1/\sqrt{2} \end{pmatrix}$$

(A.VIII.5)

Then the $\underset{\sim}{M}_{\text{I}}$ in Basis I is given by

$$\underset{\sim}{M}_{\text{I}} = \underset{\sim}{G} \underset{\sim}{M}_{\text{II}} \underset{\sim}{G}^{-1}$$

$$\underset{\sim}{M}_{\text{I}} = \begin{pmatrix} M_{11} & 0 & 1/\sqrt{2} M_{12} & 1/\sqrt{2} M_{12} \\ 0 & N_{11} & -1/\sqrt{2} N_{12} & 1/\sqrt{2} N_{12} \\ 1/\sqrt{2} M_{12} & -1/\sqrt{2} M_{12} & \frac{1}{2}(M_{22} + N_{22}) & \frac{1}{2}(M_{22} - N_{22}) \\ 1/\sqrt{2} M_{12} & 1/\sqrt{2} N_{12} & \frac{1}{2}(M_{22} - N_{22}) & \frac{1}{2}(M_{22} + N_{22}) \end{pmatrix} \quad (\text{A.VIII.6})$$

In order to calculate $\underset{\sim}{A}$ matrix elements we need

$$\det(\underset{\sim}{M} - ik):$$

$$\det(\underline{M}_J - i \underline{k}) = \left[(M_{11} - i k_\gamma)(M_{22} - i \bar{k}) - M_{12}^2 \right] \times$$

$$\left[(N_{11} - i k_\pi)(N_{22} - i \bar{k}) - N_{12}^2 \right] + \frac{1}{4} (k_c - k_o)^2 (M_{11} - i k_\gamma)(N_{11} - i k_\pi),$$

(A.VIII.7)

where

$$\bar{k} = \frac{1}{2}(k_c + k_o).$$

The $A(\pi\pi \rightarrow K^+K^-)$ and $A(\pi\eta \rightarrow K^+K^-)$ amplitudes are

$$A(\pi\pi \rightarrow K^+K^-) = \frac{-\frac{1}{\sqrt{2}} (k_\pi k_c)^{1/2} N_{12}}{\det(\underline{M}_J - i \underline{k})} \left[(M_{11} - i k_\gamma)(M_{22} - i k_o) - M_{12}^2 \right]$$

(A.VIII.8)

$$A(\pi\eta \rightarrow K^+K^-) = \frac{\frac{1}{\sqrt{2}} (k_\eta k_c)^{1/2} M_{12}}{\det(\underline{M}_J - i \underline{k})} \left[(N_{11} - i k_\pi)(N_{22} - i k_o) - N_{12}^2 \right].$$

(A.VIII.9)

In our problem we have $I = 1, \delta$ and $I = 0, S^*$ resonances decaying into the (K^+K^-) final state. In this case the M_{ij} and N_{ij} elements are given in terms of resonance parameters by:

$$\underline{M} = \underline{K}^{-1}; \quad K_{11} = \frac{(g_{S^*}^{\pi\eta})^2}{m_{S^*}^2 - s}, \quad K_{22} = \frac{(g_{S^*}^{K\bar{K}})^2}{m_{S^*}^2 - s}, \quad K_{12} = \frac{g_{S^*}^{\pi\eta} g_{S^*}^{K\bar{K}}}{m_{S^*}^2 - s},$$

$$\underline{N} = \underline{L}^{-1}; \quad L_{11} = \frac{(g_{S^*}^{\pi\pi})^2}{m_{S^*}^2 - s}, \quad L_{22} = \frac{(g_{S^*}^{K\bar{K}})^2}{m_{S^*}^2 - s}, \quad L_{12} = \frac{g_{S^*}^{\pi\pi} g_{S^*}^{K\bar{K}}}{m_{S^*}^2 - s}.$$

Then $\det(\underline{M}_J - i \underline{k})$ becomes:

$$\det(\underline{M}_J - i \underline{k}) = \left\{ m_{S^*}^2 - s - i \left[(g_{S^*}^{\pi\pi})^2 k_\pi + (g_{S^*}^{K\bar{K}})^2 \bar{k} \right] \right\} \times$$

$$\left\{ m_{S^*}^2 - s - i \left[(g_{S^*}^{\pi\eta})^2 k_\gamma + (g_{S^*}^{K\bar{K}})^2 \bar{k} \right] \right\} + \frac{1}{4} (k_c - k_o)^2 (g_{S^*}^{K\bar{K}})^2 (g_{S^*}^{K\bar{K}})^2.$$

(A.VIII.10)

The $A(\pi\bar{\pi} \rightarrow K^+K^-)$ and $A(\pi\eta \rightarrow K^+K^-)$ amplitudes becomes:

$$A(\pi\bar{\pi} \rightarrow K\bar{K}) = \frac{\frac{1}{\sqrt{2}}(k_{\pi}k_c)^{1/2} g_{s^0}^{\pi\bar{\pi}} g_{s^*}^{K\bar{K}}}{\det(M_I - i\epsilon)} \left\{ m_s^2 - s - i \left[(g_{s^*}^{\pi\eta})^2 k_{\eta} + (g_{s^*}^{K\bar{K}})^2 k_0 \right] \right\}$$

(A.VIII.11)

$$A(\pi\eta \rightarrow K\bar{K}) = \frac{\frac{1}{\sqrt{2}}(k_{\eta}k_c)^{1/2} g_{s^*}^{\pi\eta} g_{s^*}^{K\bar{K}}}{\det(M_I - i\epsilon)} \left\{ m_{s^*}^2 - s - i \left[(g_{s^*}^{\pi\bar{\pi}})^2 k_{\pi} + (g_{s^*}^{K\bar{K}})^2 k_0 \right] \right\}$$

(A.VIII.12)

where $\det(M_I - i\epsilon)$ is given by eq. (A.VIII.10). Note that for $k_c = k_0$, $A(\pi\bar{\pi} \rightarrow K^+K^-)$ and $A(\pi\eta \rightarrow K^+K^-)$ reduce to normal Breit-Wigner forms.

REFERENCES

- (1) M. Gell-Mann, Phys. Rev. 92 (1953) 833
M. Gell-Mann, Suppl. Nuovo Cim. 4 (1956) 848
K. Nishijima, Progr. Th. Phys. 13 (1955) 285
- (2) J. D. Jackson, "New Particle Spectroscopy". CERN Report, Ref. TH.2351 - CERN
- (3) F. E. Close, "How High are Higher Symmetries? and Ψ chology For J-Walkers". Rutherford Lab. Report RL.75.091
- (4) H. J. Lipkin, Phys. Reports 8C (1973) 175
- (5) J. L. Rosner, Phys. Reports 11C (1974) 191
- (6) R. L. Jaffe et al., Phys. Lett. 60B (1976) 201
- (7) R. L. Jaffe, Phys. Rev. D15 (1977) 267
- (8) D. Robson, Nucl. Phys. B130 (1977) 328
- (9) N. M. Cason et al., Phys. Rev. Lett. 36 (1976) 1485
- (10) A. J. Pawlicki et al., Phys. Rev. Lett. 37 (1976) 1666
- (11) D. Morgan, Proceeding of the Summer Symposium held at Argonne National Laboratory ANL-HEP-CP-75-58, page 45
- (12) D. W. G. S. Leith, SLAC Preprint SLAC-PUB-1980, July 1977
- (13) P. Estabrooks et al., SLAC Preprint SLAC-PUB-2004, August 1977
- (14) J. P. Baton et al., Phys. Lett. 33B (1970) 525, 528
- (15) S. D. Protopopescu et al., Phys. Rev. D7 (1973) 1279
- (16) G. Grayer et al., Nucl. Phys. B75 (1974) 189
- (17) B. R. Martin, D. Morgan, G. Shaw, Pion-Pion Interactions in Particle Physics, Academic Press, 1976
- (18) J. L. Petersen, The $\pi\bar{\pi}$ Interaction, CERN Yellow Report, CERN 77-04
- (19) A. J. Pawlicki et al., Phys. Rev. D15 (1977) 3196

- (20) W. Wetzel et al., Nucl. Phys. B115 (1976) 208
- (21) R. Baldi et al., Uni. of Geneva preprint, presented at the European Conference on Particle Physics, Budapest, Hungary, July 1977
- (22) A. D. Martin, T. D. Spearman, Elementary Particle Theory, North-Holland Pub. Co. 1970, Chapter 5
- (23) G. Cohen-Tannoudji et al., Nuovo Cim. 55 (1968) 412
- (24) C. Goebel, Phys. Rev. Lett. 1 (1958) 337
G. F. Chew, F. E. Low, Phys. Rev. 113 (1959) 1640
- (25) E. Ferrari, F. Selleri, Nuovo Cim. Suppl. 24 (1962) 453
- (26) H. Pilkuhn, The Interactions of Hadrons, North-Holland Pub. Co., 1967
- (27) M. M. Nagels et al., Nucl. Phys. B109 (1976) 1
- (28) P. K. Williams, Phys. Rev. D1 (1970) 1312
- (29) G. C. Fox, Proc. Conf. on Phenomenology in Particle Physics, Pasadena, 19, California Institute of Technology, 1971, page 703
- (30) P. Estabrooks et al., Phys. Lett. 41B (1972) 350
- (31) W. Ochs et al., Phys. Lett. 44B (1973) 1271
- (32) B. Hyams et al., Nucl. Phys. B64 (1973) 134
- (33) P. Estabrooks et al., Nucl. Phys. B95 (1975) 322
- (34) A. C. Irving et al., Nucl. Phys. B82 (1974) 282
- (35) A. C. Irving, Nucl. Phys. B105 (1976) 491
- (36) C. Micheal, Springer Tracts in Modern Physics 55 (1970) 174
- (37) "Review of Particle Properties", Rev. of Mod. Phys. 48 (1976) No. 2, Part II
- (38) R. I. Hess et al., Phys. Rev. Lett. 17 (1966) 1109
- (39) D. J. Crennel et al., Phys. Rev. Lett. 16 (1966) 1025
- (40) S. Margulies et al., Nuovo Cim. 63A (1969) 1124
- (41) B. D. Hyams et al., Nucl. Phys. B22 (1970) 189
- (42) B. Y. Oh et al., Phys. Rev. D1 (1970) 2494
- (43) M. Alston-Garnjost et al., Phys. Lett. 36B (1971) 152
- (44) S. M. Flatté' et al., Phys. Lett. 38B (1972) 232
- (45) A. D. Martin et al., Proc. of the Pion Exchange Meeting, Daresbury Study Weekend Series No. 6, page 77

- (46) D. Morgan, Phys. Lett. 51B (1974) 71
- (47) A. J. Pawlicki et al., Phys Rev. D12 (1975) 631
- (48) W. R. Frazer et al., Phys. Rev. 134B (1964) 1307
- (49) Y. Fujii et al., Progr. Theor. Phys. Suppl. 21
(1963) 138
Y. Fujii, Phys. Rev. 139B (1965) 472
- (50) M. Kato, Ann. of Phys. 31 (1965) 130
- (51) K. J. Le Couteur, Proc. Roy. Soc. A256 (1960) 115
R. G. Newton, J. Math. Phys. 2 (1961) 188
- (52) Y. Fujii et al., Nuovo Cim. 13 (1973) 311
- (53) Y. Fujii et al., Nucl. Phys. B85 (1975) 179
- (54) M. H. Ross et al., Ann. of Phys. 13 (1961) 147
- (55) G. Gustafson et al., Nordita preprint 76/5
- (56) G. Heuschel, Thesis, Uni. of Munich (1976)
E. Lorenz, private communication
- (57) J. D. Kimel et al., Nucl. Phys. B122 (1977) 464
- (58) G. W. Brandenburg et al., Nucl. Phys. B104 (1976) 413
- (59) R. Baldi et al., Phys. Letters 70B (1977) 377
- (60) A. D. Martin et al., Amplitude and natural-parity-exchange analysis of $K^+p \rightarrow (K\pi)^+ p$ data at 10 GeV/c submitted to Nuclear Phys. B, October 1977
- (61) P. Estabrooks et al., SLAC-PUB-2011, 1977
- (62) M. J. Emms et al., Phys. Lett. 58B (1975) 117
- (63) M. J. Corden et al., Rutherford Lab. preprint RL-77-697/A September 1977
- (64) R. Carlitz et al., Phys. Rev. Lett. 26 (1971) 1515;
Phys. Rev. D4 (1971) 3439
P.G.O. Freund et al., Phys. Lett. 36B (1971) 89
- (65) A. C. Irving, Nucl. Phys. B121 (1977) 176
- (66) P. D. B. Collins et al., J. Phys. G. 4 (1978) 471
- (67) E. Barrelet, Nuovo Cimento 8A (1972) 331,
A. Gersten, Nucl. Phys. B12 (1969) 537
- (68) P. Hoyer et al., Nucl. Phys. B56 (1973) 173
- (69) H. A. Gordon et al., Phys. Rev. D8 (1973) 779
- (70) J. Bartsch et al., Nucl. Phys. B46 (1972) 46

- (71) N. P. Samios et al., Rev. Mod. Phys. 46 (1974) 49
- (72) R. Baldi et al., Observation of a spin 4, $I = 1$, meson resonance, submitted to Phys. Lett. B
- (73) W. Beusch et al., Phys. Lett. 60B (1975) 101
- (74) A. J. Pawlicki et al., Phys. Rev. Lett. 37 (1976) 971
- (75) V. Ruuskanen et al., Uni. of Helsinki preprint No. 3-77
- (76) J. B. Gay et al., Phys. Lett. 63B (1976) 220
- (77) D. Cohen, $K\bar{K}$ Amplitude Analysis, ANL-HEP-CP-77-37 and Proc. 5th Exp. Meson Spec. Conf., Boston (1977)
- (78) W. Ochs, Results on $\pi\bar{u}$ -Scattering, Max-Planck Ins. preprint, MPI - PAE/P.Th 32/77
- (79) H. Grässler et al., Nucl. Phys. B121 (1977) 189
- (80) A. De Rujula et al., Phys. Rev. D12 (1975) 147

